國立臺灣大學工學院機械工程學系

博士論文

Department of Mechanical Engineering

College of Engineering

National Taiwan University

Doctoral Dissertation

基於延展實境及可視化有限元素分析的手工電弧銲接實作訓練
及教學系統

An extended reality-based training and tutorial system for
hands-on practice of manual metal arc welding and finite
element analysis visualization

柯帕娜

Kalpana Shankhwar

指導教授：陳湘鳳 博士

Advisor: Shana Smith, Ph.D.

中華民國 111 年 11 月

November, 2022

國立臺灣大學博士學位論文
口試委員會審定書
PhD DISSERTATION ACCEPTANCE CERTIFICATE
NATIONAL TAIWAN UNIVERSITY

基於延展實境及可視化有限元素分析的手工電弧銲接實作訓練及教學系統

An extended reality-based training and tutorial system for hands-on practice of manual metal arc welding and finite element analysis visualization

本論文係 Kalpana Shankhwar (D06522022)在國立臺灣大學機械工程學系設計組完成之博士學位論文，於民國 111 年 9 月 29 日承下列考試委員審查通過及口試及格，特此證明。

The undersigned, appointed by the Department of Mechanical Engineering on 29/09/2022 have examined a PhD dissertation entitled above presented by Kalpana Shankhwar (D06522022) candidate and hereby certify that it is worthy of acceptance.
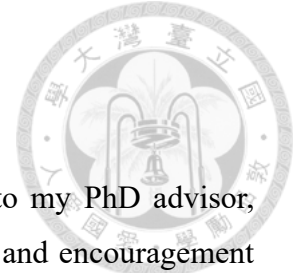
口試委員 Oral examination committee：

Shana Smith　　　*R. Tiwari*

（指導教授 Advisor）

Jiajang Luang　　*Jyhjone Lee*　　*Yanjay Fan*

系主任/所長 Director：

Acknowledgment

I feel honored to express my deepest and most sincere gratitude to my PhD advisor, Professor Shana Smith, for her invaluable guidance, kind suggestions, and encouragement throughout the progress of this research work. I am highly grateful to her for providing me with the freedom to do my research work. Apart from guiding me in my research, my advisor has been very kind and understanding, who always emotionally and morally supported me during my difficult times and guided me in the right direction.

I would also like to take this opportunity to express my sense of gratitude to the defense committee members for saving time from their busy schedules to attend my oral thesis defense and generously providing their invaluable remarks on my research to help me improve my work. I would also like to thank the other faculty members for their kind help and encouragement, and to all the non-teaching staff of the department, without whose help, I would not have completed this project work.

I would like to acknowledge the support of my lab members Mr. Liyea Chuang, Ms. Zi-Ying Li, Mr. Wu, Bing-Ruei, Mr. Wu, Hong-Sheng, and Mr. Lin, Yu-Tingq for being always keen and helpful in my research work and other daily life issues. I would like to thank every lab member throughout all the years of my PhD for being so helpful and kind in every step of my research. I am extremely grateful to be a part of this laboratory with the wonderful advisor and lab mates.

Also, I would like to express thankfulness to my dear friends Ayush Goyal, Amali Gitanjali, Ankit Das, Suyash Wagh, Zhan Minghui, Lynn, and Rona for their good company, care, and emotional support during my stay at National Taiwan University.

Last but not the least, I wish to express my gratitude to my father Mr. Shivkumar Shankhwar, my mother Mrs. Meera Devi Shankhwar, my brother Suraj Kumar Shankhwar and my relatives for their love, patience, and support during the period of my study. Without their support, this endeavor would not have been possible. I deeply thank my parents for their belief in me, for encouraging me to achieve my goals, and for celebrating the small steps of my research success with me during all the years of my PhD. I wish everyone who helped me great health, joy, and happiness.

摘要

由於焊接具備簡單及高度的可靠性，因此常成為製造業於各種應用中最受歡迎的連接工藝之一。在各式不同的焊接工藝中，手工金屬電弧焊(Manual Metal Arc Welding，MMAW)具備方便攜帶、可由操作人員親自進行操作等特點，因此成為受歡迎的焊接工藝手法。而為新手焊工提供 MMAW 之培訓成為工業中的一項重要任務。然而，此項工藝很難通過傳統課堂教學來描述複雜的概念；焊接過程會產生高溫及有害紫外線(Ultraviolet，UV))，使危險度大幅增加；焊接培訓也常耗費大量能源和材料。因此，提供具備高效率、高成本效益，且並無風險的焊接培訓環境進行尤為重要。

在焊接過程中，焊板溫度分佈不均勻會產生殘留應力，將對焊板的疲勞強度產生負面影響。焊板不均勻熱脹冷縮也會產生結構變形，影響最終產品品質。因此，使用有限元素法（Finite Element Method，FEM）進行殘留應力和熱變形分析有其必要性。

為了解決上述焊接培訓的當前不足和挑戰，本研究利用延展實境(Extended Reality，XR)技術開發了一種互動式焊接教學系統，其包含三項與 XR 技術應用相關的研究。首先，開發用於基本手工金屬電弧焊培訓的 XR 互動式教學系統，提供使用者在 VR 環境中學習基礎焊接基知識。其次，開發具備視覺及觸覺的 XR 手工金屬電弧焊培訓系統，在焊接培訓期間提供真實的磁力和熱量，以用來模擬真實焊接過程中的觸覺回饋。最後，開發了具備混合實境(Mixed Reality，MR)的使用者介面，將有限元素分析其殘餘應力和變形進行可視化，在 MR 環境中進行實時渲染。本研究透過將 XR 技術用於焊接教育、培訓及設計，透過使用者測試，驗證了本系統的完整度及可行性。

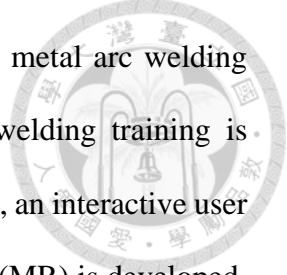關鍵字：延展實境, 虛擬實境, 混合實境, 手工金屬電弧焊, 焊接訓練, 視覺觸覺, 有限元素法

Abstract

Welding is one of the most popular joining processes in manufacturing industries for a variety of applications due to its simplicity and reliability. Among the wide range of welding processes, manual metal arc welding (MMAW) is preferred the most, which is portable and can be performed by human operators. Therefore, providing MMAW welding training to novice welders is an important task in industry. However, it is difficult to describe complex welding concepts through the traditional classroom teaching method. Welding is also a dangerous process involving high temperature and harmful ultraviolet (UV) radiation. In addition, welding training causes a significant amount of wastage of energy and material. Therefore, it is necessary to find an efficient and cost-effective way to provide welding training in a risk-free environment.

During the welding process, the non-uniform distribution of temperature on the weld plates causes residual stress, which negatively affects the fatigue strength of the weld plates. The non-uniform thermal expansion and contraction of the weld plates also produce structural deformation, affecting the final product quality. Therefore, it is necessary to conduct the residual stress and deformation analysis using finite element method (FEM).

In order to resolve the aforementioned challenges and shortcomings of the current welding training, this study utilizes XR technology to develop an interactive XR-based welding tutorial system with hands-on practice. This thesis involves three studies related to the applications of extended reality (XR) technologies. First, an interactive XR-based tutorial system for fundamental manual metal arc welding training is developed. The XR-based tutorial system provides users with fundamental knowledge of welding in a VR environment.
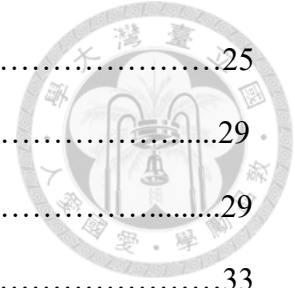
Second, a visuo-haptic XR-based training system for hands-on manual metal arc welding training is developed. Realistic magnetic force and heat during the welding training is provided to simulate the haptic feedback in a real welding process. Lastly, an interactive user interface for the visualization of finite element analysis in mixed reality (MR) is developed. The residual stress and deformation can be rendered in an MR environment in real time. In this dissertation, the XR technologies were employed in welding application for education, training and design purposes. The developed systems were validated for their performance and feasibility by conducting the user studies.

Keywords: Extended reality, virtual reality, mixed reality, manual metal arc welding, welding training, visuo-haptic, finite element analysis.
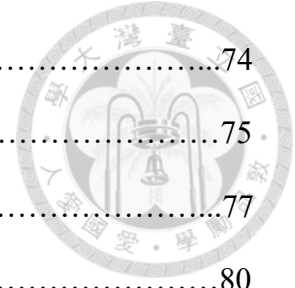
Table of Contents

List of Figures

xi

List of Tables

Chapter 1   Introduction

Among various types of mechanical joining techniques including bolting, riveting, brazing, and soldering, welding is the most commonly used joining process. Modern industries mostly rely on robots or machinery-based welding for mass production. However, manual welding processes are still very important in several manufacturing sectors such as ship building, small part fabrication, maintenance and repair work. In the manual welding processes, manual metal arc welding (MMAW) is one of the most frequently used processes. The quality of the welded structure produced critically depends on the skills of the welders, which can be improved by continuous welding practice. Besides industries, MMAW is also a discipline in the engineering and technology education, which is explained through the traditional classroom instructions and practical welding performed in the mechanical workshop. However, the conventional methods of education and training for the welding process are inefficient and dangerous. Therefore, it is essential to adopt advanced technologies to build an efficient and risk-free tutorial and training system. Extended reality (XR) technologies which include, virtual reality (VR), augmented reality (AR) and mixed reality (MR) are increasingly gaining importance in advanced manufacturing and education. To overcome the limitations of conventional education and training methods, the XR technologies can be employed to build a training and tutorial system for the MMAW process.

Consequently, the thesis is composed of three parts. The first part focuses on developing an interactive XR-based welding tutorial system to facilitate the novice welder with the fundamental welding knowledge and skill development with hands-on practice. Users can

perform hands-on welding to observe the effects of welding process parameters on weld bead geometry in an MR environment. The developed welding tutorial system was validated for its learnability, workload, and usability by conducting a user study. The user study results revealed that the XR-based welding training system provided significantly better results than the conventional classroom training method. This work has been published in Virtual Reality in January, 2022 and is introduced in Chapter 2 (Shankhwar and Smith, 2022).

The second part of this dissertation presents a visuo-haptic extended reality (VHXR)-based welding training system for the MMAW process. The real welding process produces a strong magnetic force and intense heat. In order to provide realistic haptic feedback, the study utilizes a visuo-haptic technology to build the welding training system. The trainees are guided to maintain a constant arc length, travel speed, and electrode angle by providing realistic force and visual feedback. The user study results deduced that users trained through the VHXR-system performed significantly better than the users who were trained by traditional video training. This work is presented in Chapter 3 and has been published in the International Journal of Advanced Manufacturing Technology in May, 2022 (Shankhwar et al., 2022).

The third part of this dissertation aims to utilize a machine learning (ML) algorithm to visually display the FEM analysis results in an MR environment in real time with enhanced comprehension and visualization. The gradient boosted regression tree (GBRT) algorithm is employed to predict the residual stress and deformation in the MR environment. A total number of 216 FEM simulations are conducted to train the GBRT model with three inputs (welding current, voltage, and speed) for predicting two output parameters (residual stress and displacement). With the integrated MR-FEM system, the user can interactively choose

the welding process parameters using virtual sliders and visualize the FEM results superimposed directly on the real weld plate. This work is introduced in Chapter 4.
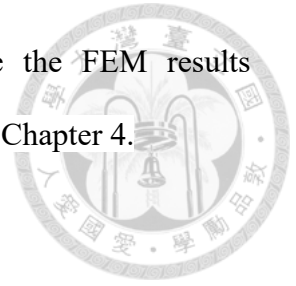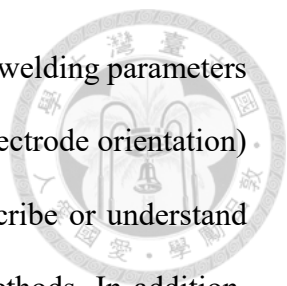
Chapter 2   An interactive extended reality-based tutorial system for fundamental manual metal arc welding training
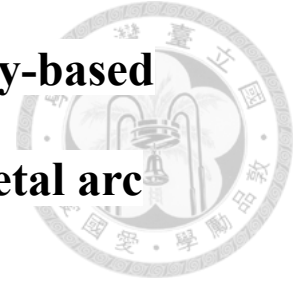
Extended reality (XR) technology has been proven an effective human-computer interaction tool to increase the perception of presence. The purpose of this study is to develop an interactive XR-based welding tutorial system to enhance the learning and hands-on skills of novice welders. This study is comprised of two parts: (1) fundamental manual metal arc welding (MMAW) science and technology tutoring in a virtual reality (VR)-based environment, and (2) hands-on welding training in a mixed reality (MR)-based environment. Using the developed tutorial system, complicated welding process and the effects of welding process parameters on weld bead geometry can be clearly observed and comprehended by using a 3D interactive user interface. Visual aids and quantitative guidance are displayed in real time to guide novice welders through the correct welding procedure and help them to maintain a proper welding position. A user study was conducted to evaluate the learnability, workload, and usability of the system. Results show that users obtained significantly better performance by using the XR-based welding tutorial system, compared to those who were trained using the conventional classroom training method. This abstract and the following subchapters are from Shankhwar and Smith (2022).

2.1 Introduction
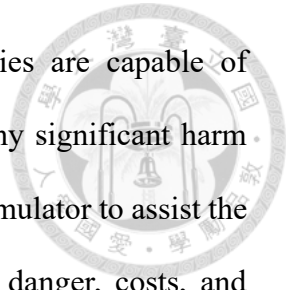
Welding is a dangerous manufacturing process that involves high temperature and

harmful ultraviolet radiation. Welding process involves various complex welding parameters (i.e., welding current, arc length, travel speed, electrode diameter, and electrode orientation) and requires high-level hands-on skills. Therefore, it is difficult to describe or understand some welding processes using the conventional classroom teaching methods. In addition, during welding training, sample disposal often causes material and energy waste. Therefore, it is necessary to find an efficient and cost-effective way to teach students about professional welding skills.

With the rapid growth of information technology, extended reality (XR) has gained a growing amount of attention in the past two decades due to its innovative human-computer interaction technique. The XR is based on computer vision and computer graphics technology, which can visually simulate real interactions between the user and the virtual environment application in a natural and efficient way by using hand gestures, eye tracking, handheld controller and speech recognition. XR is an umbrella term which refers to different reality technologies, e.g., virtual reality (VR), augmented reality (AR) and mixed reality (MR) (Doolani et al., 2020). VR is often referred to as immersive computing technology that enables people to immersively experience a virtual world beyond reality (Berg and Vance, 2017). AR is a technology which augments the real world by superimposing virtual objects on it (Thomas and David, 1992). MR is similar to AR, which also combined the digital elements with real world. However, in MR, physical objects and virtual objects can interact with each other, and users can interact with and manipulate physical and virtual objects (Doolani et al., 2020).

XR technologies have the capacity to be employed in different types of domains by facilitating immersion, presence, and interaction to enhance users' perception and
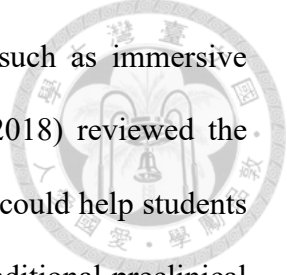
performance (Kaplan et al., 2020; Pomerantz, 2019). XR technologies are capable of providing safe, engaging, and effective training with reduced risk of any significant harm (Doolani et al., 2020). For example, Heirman et al. (2020) used an XR simulator to assist the Navy's firefighting training program to alleviate the issues related to danger, costs, and environmental pollution in the conventional training.

Therefore, by taking the advantages of XR technologies, it is possible to teach dangerous welding process and complex welding parameters in a harmless and intuitive way. The purpose of this study is to develop an interactive XR-based welding tutorial system to equip novice welders with basic welding knowledge and hands-on skills, in a safe and economic environment. The following of this chapter is structured as follows. Section 2 provides related work. Section 3 gives an overview of the software and hardware used in the study. Section 4 introduces the VR module for fundamental welding science and technology tutoring. Section 5 describes the design and implementation of the MR module for hands-on welding training. Section 6 describes the user test. Section 7 gives the user test results. Section 8 provides a discussion. Finally, Section 9 offers conclusions and future work.

2.2 Related work

2.2.1   XR in education

Traditional classroom instruction is difficult for students to learn and understand critical and complex knowledge due to the lack of 3D visualization of the objects or the processes. Prior research has proven that the 3D visualization and immersive perception of AR could enhance teaching and learning (Wu et al., 2013). The application of AR allows learners to visualize complex spatial relationships and experience the hands-on practices of real world (Arvanitis et al., 2009). Milovanovic et al. (2017) surveyed the applications of VR and AR
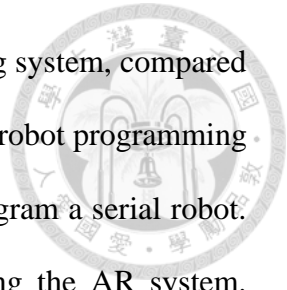
in architectural education, showing the multiplicity of possible uses such as immersive design, on-site simulations, and remote collaboration. Huang et al. (2018) reviewed the applications of VR and AR in dentistry. They indicated that AR and VR could help students to learn by themselves and reduce instructors' load, compared to the traditional preclinical teaching methods. Cardoso et al. (2019) presented a design-based approach using VR and AR to support the teaching and learning of technical drawing. Macariu et al. (2020) applied AR in chemistry education. The evaluation results showed that both professors and students appreciated the "overall look and feel experience" provided by the AR learning tool.

Some extensive reviews of the state-of-the-art of XR applications in K-12 and higher education have also been carried out. For example, Loureiro et al. (2021) reviewed the usage of VR and gamification in higher education. Students were found to be more focused on the tasks that were demonstrated and learned in an immersive environment. Di Natale et al. (2020) surveyed the applications of immersive VR (IVR) on K-12 and higher education. They revealed that the performance of the IVR group outperformed significantly over the control group. Maas and Hughes (2020) reviewed the use of VR, AR, and MR technologies in K-12 education. The study found that students became more competitive with their peers when using AR simulations. Middle school students also reported positive attitude towards learning by using MR systems.

2.2.2 XR in manufacturing

XR technologies have also been applied to workshop to enhance learners' hands-on skills in manufacturing. For example, Matsas et al. (2018) demonstrated how VR could be used for a safe human-robot collaboration in assembly, cleaning, welding and punching. Roldán et al. (2019) presented a VR training system for industrial operators in an assembly task of building

7

blocks. A user study revealed significant better results of the VR training system, compared to the conventional method. Ong et al. (2020) developed an AR assisted robot programming system, which allowed users with little programming knowledge to program a serial robot. The results showed significant higher speed of programming by using the AR system. Gonzalez-Franco et al. (2017) presented an MR setup for assisting a manufacturing procedure of an aircraft maintenance door. A knowledge retention test was conducted to evaluate the effectiveness of the training. The study indicated that the MR setup produced as effective results as the conventional face-to-face training.

2.2.3 XR in welding training

XR-based welding simulators have also been drawn a lot of attention recently (Lavrentieva et al., 2020). Mavrikios et al. (2006) developed a VR-based prototype demonstrator for manual welding. Since everything was virtual in the prototype demonstrator, users lacked the realistic sensation of holding a welding gun. In addition, no user study was conducted to prove the functionality and usability of the system. Byrd et al. (2015) used a commercial VR welding simulator, VRTEX 360, to assess existing skill levels in welders. The results show that although the VR simulator could evaluate welding skills, it could not accurately identify an individual as an experienced welder or a novice welder. Okimoto et al. (2015) used a commercial AR-based welding training tool, called Soldamatic, to conduct a user study in welding education. However, difficulties were reported in visual accommodation. In addition, no comparative study was carried out between the AR-based training system and conventional ones. Feier and Banciu (2021) conducted an ergonomics comparison between the real torches and Soldamatic torches. It was found that the weight of the Soldamatic torches was much lighter than the real ones. No educational or training aspect

8

was mentioned in this study. In addition, Lavrentieva et al. (2020) mentioned that most commercial welding simulators were too costly.

Prior studies have demonstrated the benefits and challenges of using XR technologies in welding training. However, most welding simulators are meant for assessing existing welding skills. They do not provide real-time visual aids or quantitative guidance to guide novice welders step by step through the correct welding procedure or help them to maintain a proper welding position. Therefore, they lack fundamental educational instructions for novice welders. Real-time simulation of the effects of welding process parameters on welding bead geometry is also lacking. In addition, most simulators still need an experienced welder to help novice welders to perform a quality welding simulation. For some marker-based AR welding simulators, users have to be very close to the weld plates to obtain correct tracking in the AR environment, which is contrary to the real-world practices.

3D representations with stereoscopic visions of the topics and the simulation of a process can tremendously enhance the learning and hands-on practices (Andrews et al., 2019). Learning with hands-on practices can be an efficient way to retain knowledge. The purpose of this study is to develop a realistic XR-based welding tutorial system to help novice welders to equip fundamental manual metal arc welding (MMAW) knowledge and hands-on skills in an immersive environment. Visual aids and quantitative guidance are displayed in real time to guide novice welders through the correct welding procedure and help them to maintain a proper welding position. The complicated welding process and the effects of welding process parameters on weld bead geometry can be clearly observed and comprehended by using a 3D interactive user interface (UI).

9
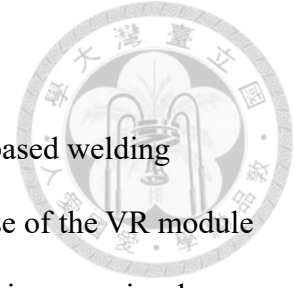
2.3 System overview

The flowchart of the training process is shown in Fig. 2.1. The XR-based welding tutorial system consists of a VR module and an MR module. The purpose of the VR module is to deliver the fundamentals of welding science and technology, which is more visual related. However, the purpose of the MR module is to provide realistic welding exercises, which is more hands-on practice related.

The tutorial begins from the VR module, in which the fundamental knowledge about MMAW is presented using 3D models along with audio output for the elaboration of the contents. After receiving basic MMAW training, users can choose any welding process parameter in the VR room and enter into the MR room to acquire hands-on welding experiences and observe the effects of the chosen parameter on weld bead geometry in real time.

In the MR room, users first choose a joint geometry (i.e. butt, tee, corner or lap joint) and then pick an electrode. Then, users set the value of the chosen parameter to the minimum and perform the welding. Users can increase the parameter value and observe the changes in bead geometry. The same hands-on practice is repeated until all welding process parameters are tested. In order to replicate the real welding environment, the visual effects of the MMAW process, including weld bead, sparkling particles, electrode and workpiece, are displayed in the MR environment.

The system architecture of the XR system is shown in Fig. 2.2. HTC Vive Pro is used to display the VR and MR scenes. The HTC Vive Pro headset includes a head-mounted display (HMD), one handheld controller, one Vive tracker, and two lighthouses. The Vive tracker is used to track the electrode, which has a distance sensor attached to it. The distance sensor

10

readings are handled by the Arduino integrated development environment (IDE). The handheld controller is used to interact with the graphical user interface (UI). Users can press the trigger button on the handheld controller to click a virtual button or drag a virtual slider.

The VR and MR modules are developed using the C# programming language on the Unity3D game engine and ran on a 3.00 GHz Intel Core i7-9700F processor, 64 GB RAM and 6.0 GB dedicated GPU memory. The VR module includes three sub-modules: VR rendering, UI, and fundamentals of welding. The VR rendering module displays the virtual contents to the users in the VR scene with the help of Vive Input Utility (VIU). The UI module provides text and image instructions to the users and allows them to interact with the UI elements in the VR scene with the help of the handheld controller. The module of fundamentals of welding provides the basic fundamental MMAW science and technology in the VR room.

11
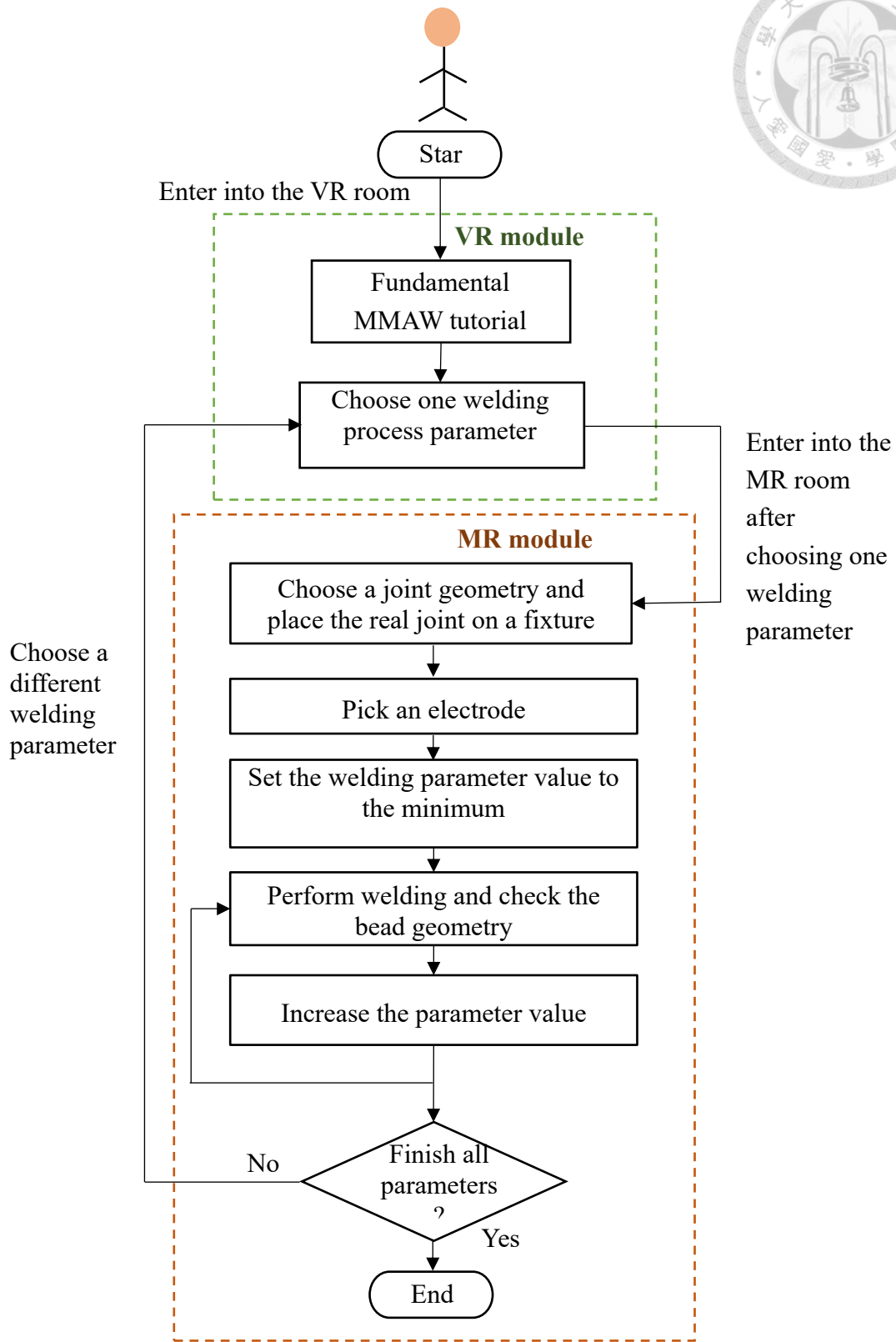
Fig. 2.1. Flowchart of the MMAW training process.

12
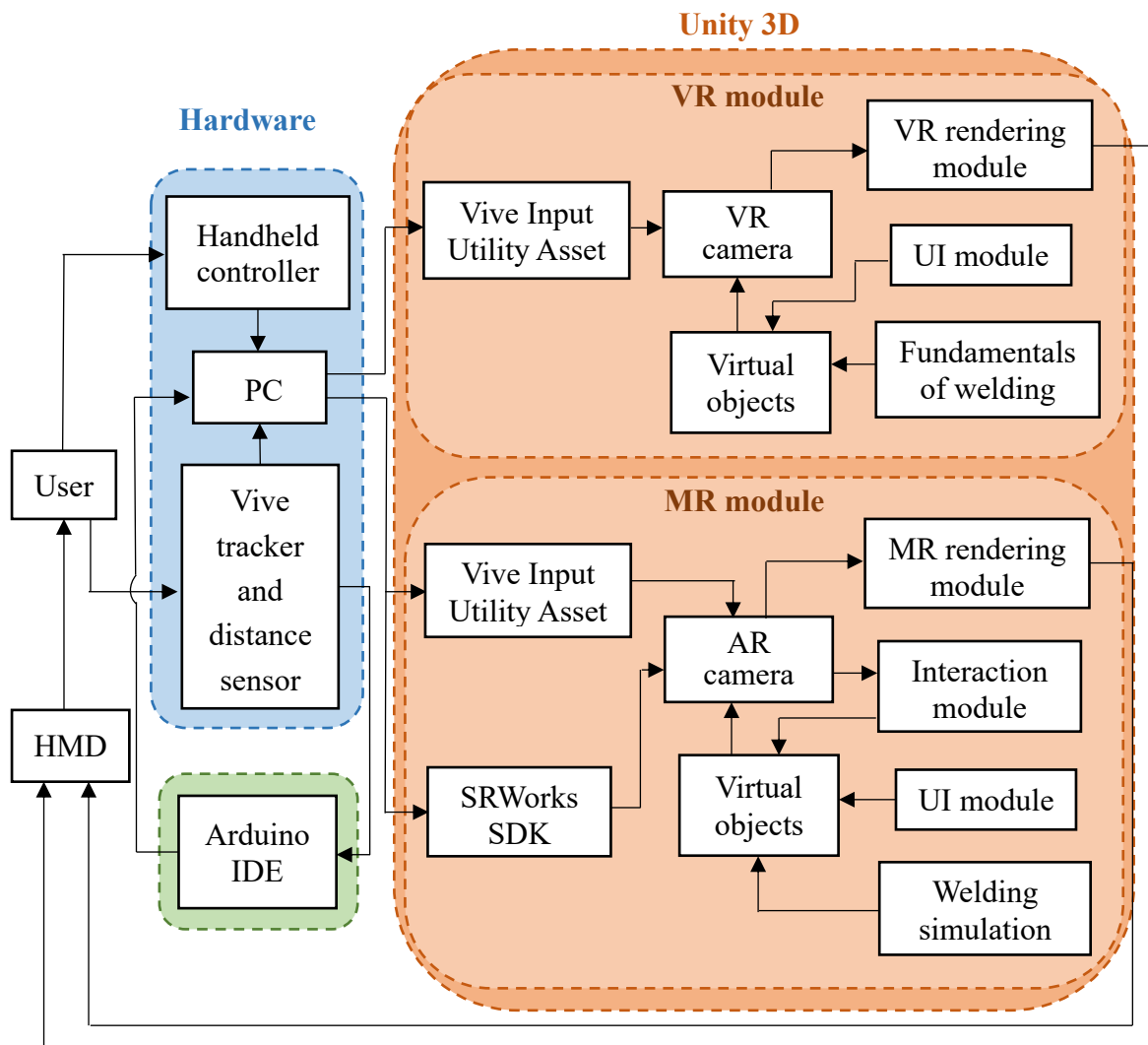
Fig. 2.2. System architecture.

The MR module includes four sub-modules: MR rendering, interaction, UI, and welding simulation. The MR rendering module integrates the virtual objects with the real world scene with the help of SRWorks software development toolkit (SDK) and VIU. The interaction module provides access for the users to interact with virtual objects in the MR scene. The UI module provides text and image instructions to the users and allows them to interact with the UI elements in the MR scene with the help of the handheld controller. The welding simulation module provides hands-on welding practice in the MR room.

13
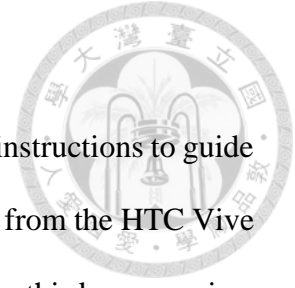
2.4 VR module

The VR welding tutorial starts from an immersive virtual room with instructions to guide the users to follow the steps. Fig. 2.3(a) shows a user's first-person view from the HTC Vive Pro HMD in the beginning of the welding tutorial. Fig. 2.3(b) shows the third-person view of the training. Fig. 2.3(c) shows the content of the tutorial, from which users can select different MMAW topics using an interactive 3D UI. Fig. 2.3(d) is an example of using 3D virtual representations to demonstrate the nomenclatures of butt weld and fillet weld.

Fig. 2.3(e) shows the interface to choose a welding process parameter. When users press the trigger button on the handheld controller, a cyan light beam will be emitting from the handheld controller for users to interact with the UI elements. The explanations for each chosen process parameter will be presented. After that, in order to practically visualize the effects of each process parameter on weld beads, users can click the MR scene button, as shown in Fig. 2.3(f), and enter into the MR room to conduct a hands-on welding practice. Users can observe the effects of welding process parameter on weld bead geometry in real time by interactively changing the value of the parameter.

2.5 MR Module

The MR module aims to provide interactive experience and hands-on practice about the complex effects of welding process parameters on weld bead geometry. SRWorks SDK provides an access to the front facing camera of the HTC Vive Pro HMD to overlay the virtual objects on the real scene. Fig. 2.4 shows an example of a virtual weld joint being augmented on a real weld joint, being viewed from the HTC Vive Pro HMD. Visual aids and quantitative guidance are augmented in the MR scene to guide novice welders to follow

a correct welding procedure.

(a)

(b)

(c)

(d)

Light beam emitting from the handheld controller
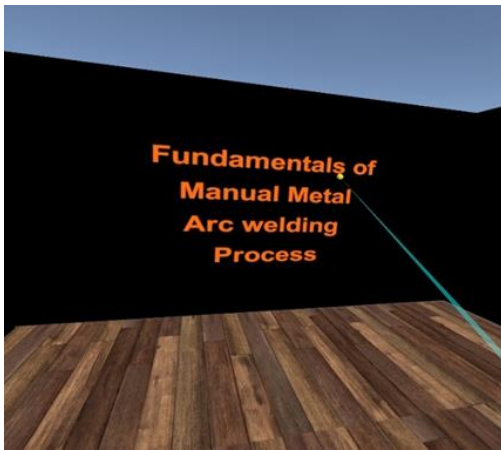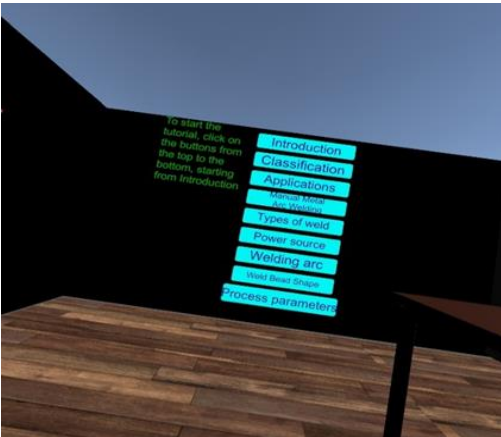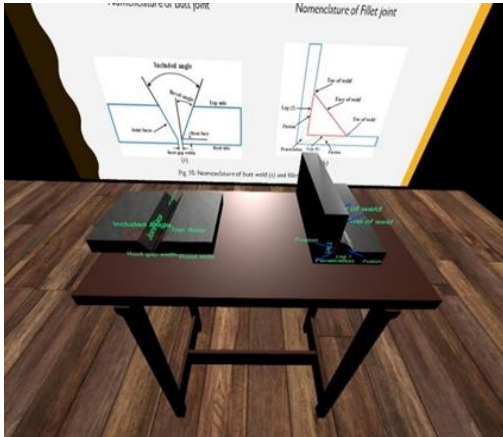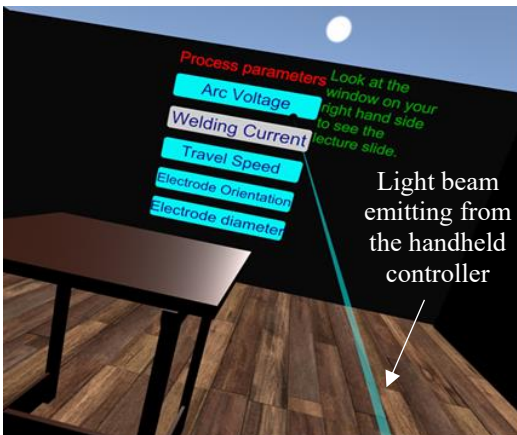
(e)
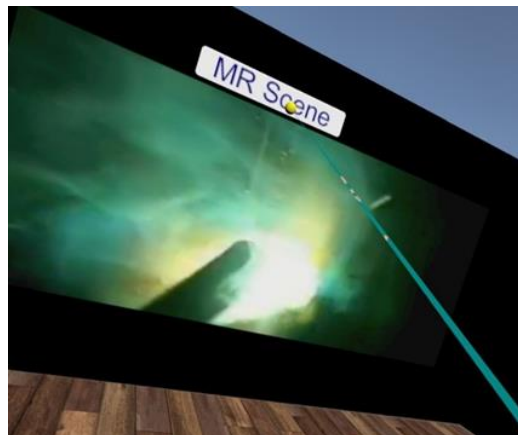
(f)

Fig. 3. Fundamental welding science and technology tutorial in the VR room.

15

<div align="center">

(a)   (b)

(c)   (d)

</div>
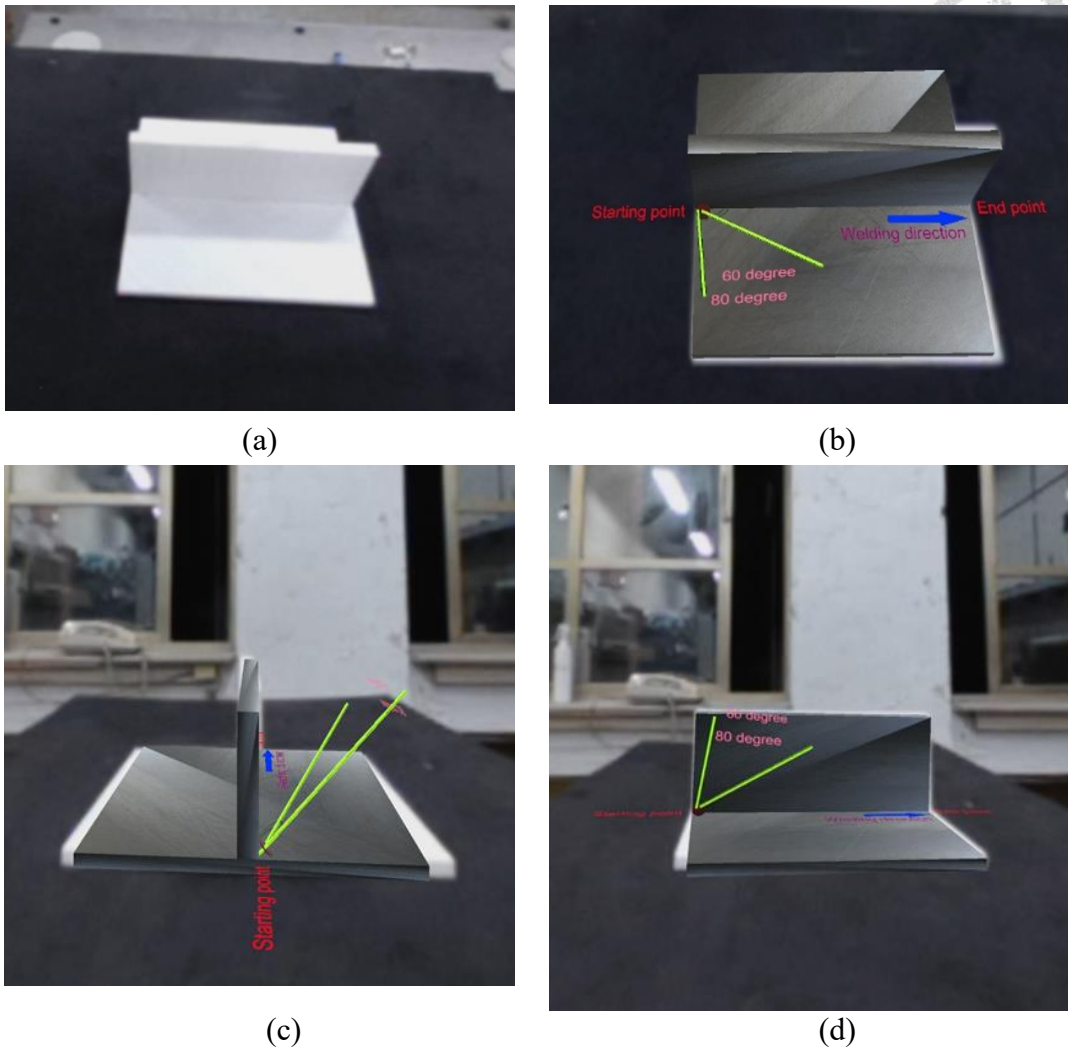
Fig. 4. MR scene being viewed from the Vive Pro HMD. (a) a real tee joint, (b) virtual tee joint augmented on the real tee joint, (c) side view of the augmented tee joint and (d) front view of the augmented tee joint.

2.5.1 Welding process parameters

There are various welding parameters such as arc voltage, welding current, travel speed, electrode orientation and electrode diameter. Based on the prior research, in this study, the range of the welding current is set between 90 A and 210 A, arc voltage is set between 27 V and 45 V, travel speed is set between 0.38 m/min and 1.5 m/min and electrode diameter is set

16

between 3.2 mm and 5.5 mm (Ahmed et al., 2018; Clark, 1985; Karadeniz et al., 2007; Lenin et al., 2010; Nagesh and Datta, 2002; Saha and Mondal, 2017; Tewari et al., 2010). Three types of electrode orientations are considered: pulling, perpendicular and pushing, as shown in Fig. 2.5.

(a) Pulling technique (b) Perpendicular technique   (c) Pushing technique
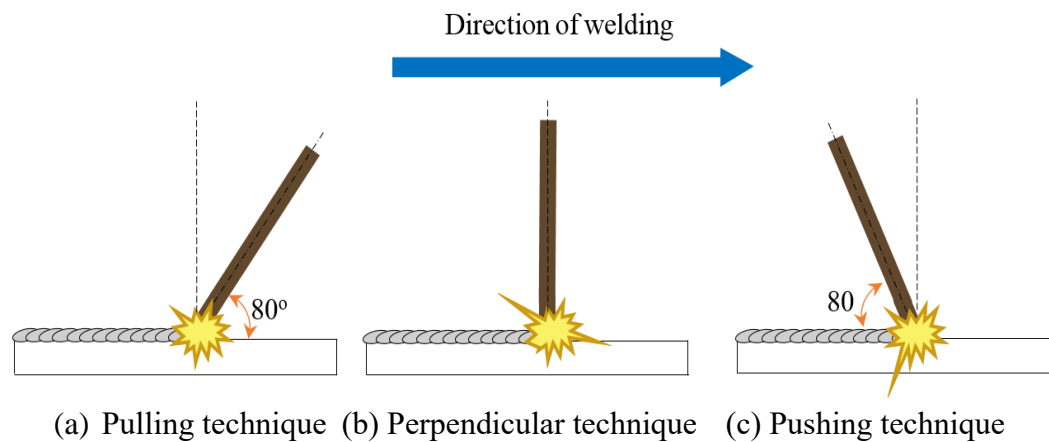
Fig. 2.5. Electrode orientations.
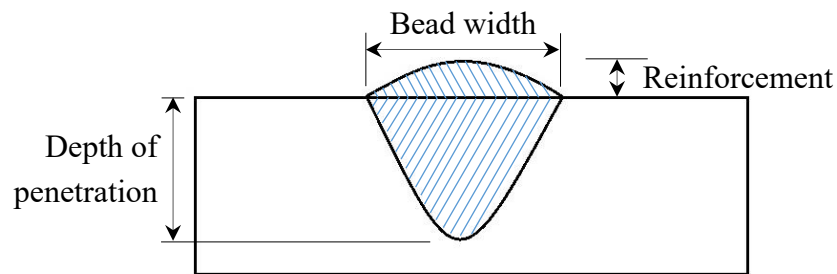
Fig. 2.6. Geometry of weld bead.

Usually, the weld bead geometry is specified by bead width, reinforcement and depth of penetration, as shown in Fig. 2.6. Five welding process parameters, welding current, arc voltage, travel speed, electrode diameter and electrode orientation, are considered in the MR welding training. It is necessary to study the effects of these parameters on the weld bead geometry to obtain good quality of weld (Omajene et al., 2014). Since the effects of the

17

reinforcement are the same as the depth of penetration, the simulation is focused on the depth of penetration and the width of beads. In this study, four different physical welding joints, butt joint, tee joint, corner joint, and lap joint, are created using a 3D printer for the hands-on practice in the MR environment, as shown in Fig. 2.7.

| (a) Butt joint | (b) Tee joint |
| (c) Corner joint | (d) Lap joint |
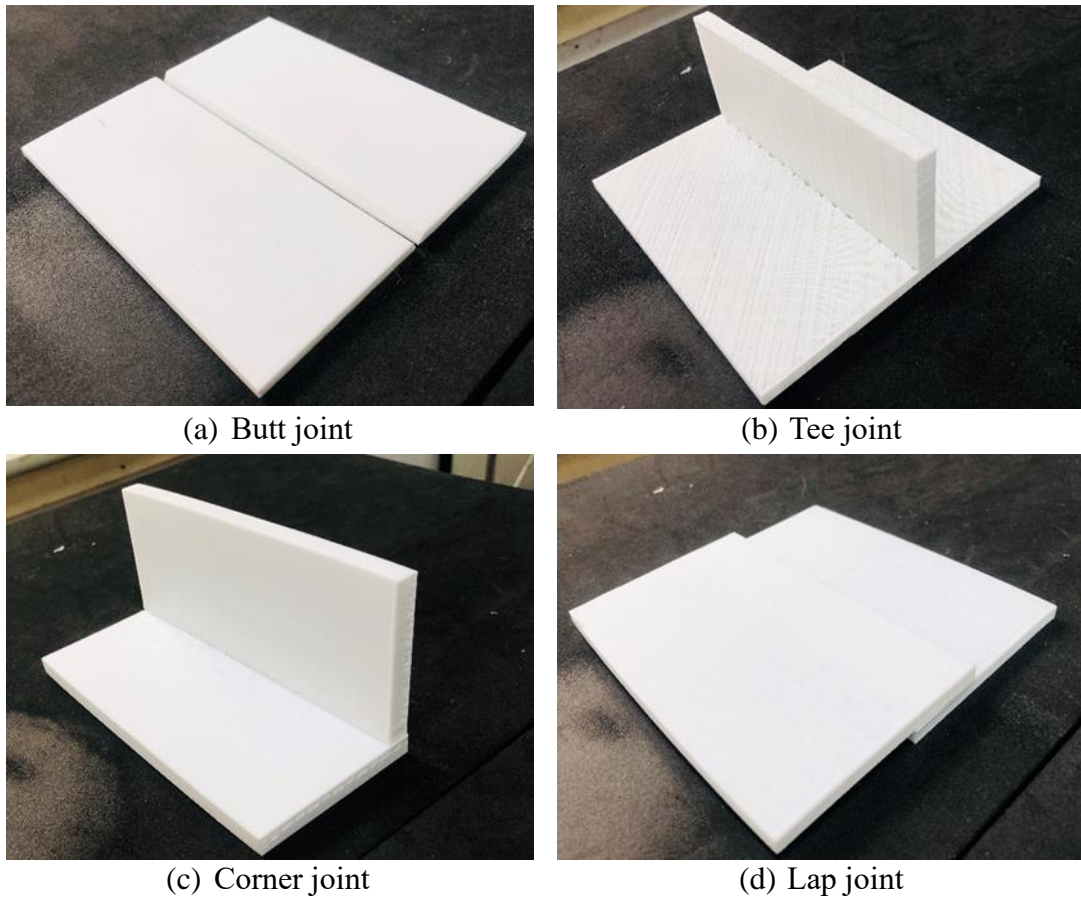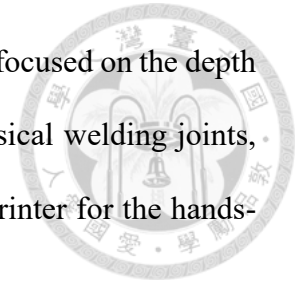
Fig. 2.7. Welding joints used in the MR room.

In order to realistically simulate a weld bead geometry, the physics relationship between the welding process parameters and the weld bead geometry needs to be considered. The amount of molten metal, deposition rate and depth of penetration are proportional to the heat input rate when the arc voltage keeps constant. Heat input rate is a relative measure of energy transfer per unit length of the weld plates (Boob and Gattani, 2013). The relationship between

18
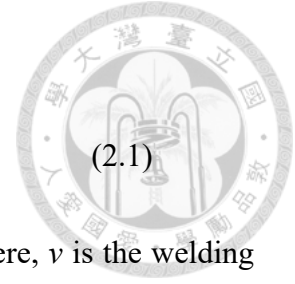
the heat input rate and the welding process parameters is as follows.

$$\text{Heat input rate } Q = \frac{IV \times 60}{v} \text{ J/mm} \tag{2.1}$$

Where V is the arc voltage in volts, I is the welding current in ampere, v is the welding speed in m/sec. Therefore, if the current increases by keeping the arc voltage constant, the penetration depth will increase, but the bead width will increase only a little.

The arc voltage is a voltage drop at the arc, which is directly proportional to the arc length (distance between the weld plates and the tip of the electrode). The relationship of the arc voltage and the welding process parameters can be described as follows.

$$\text{Arc voltage } V = IR \tag{2.2}$$

Where arc resistance $R = \frac{\rho l}{A}$, ρ = resistivity; l = arc length; A = arc cone cross-sectional area. If the arc length increases by keeping the welding current constant, the arc cone cross-sectional area will increase, which causes wider bead width, as shown in Fig. 2.8, but the penetration will reduce a little.

When the electrode moves, the heat source also moves. If the moving speed reduces, the heat dissipation rate will increase, which leads to a deeper penetration and larger bead width (Omajene et al., 2014). When the electrode diameter increases, the current density will decrease, which reduces the penetration but increases the bead width, and vice versa.
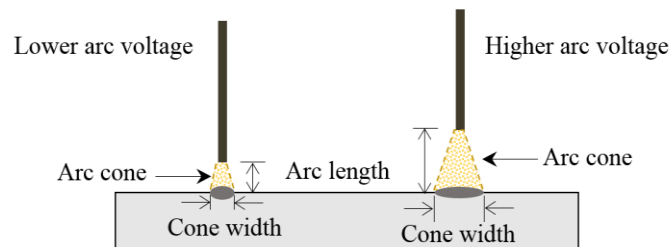
Fig. 2.8. Effect of arc length on the weld bead width.

19

(a) Pulling technique (top view)
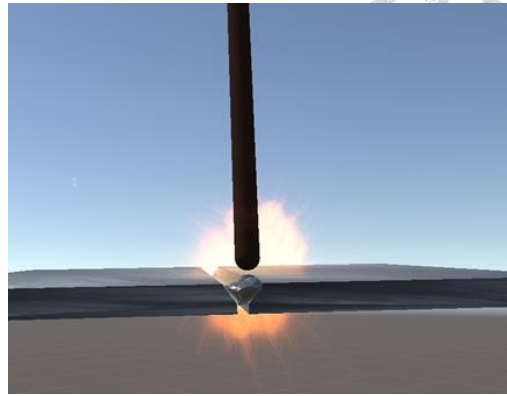
(b) Pulling technique (side view)
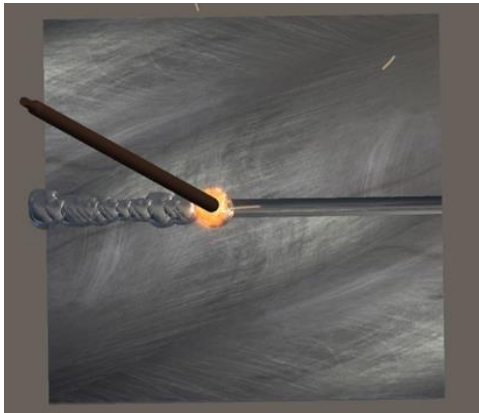
(c) Pushing technique (top view)
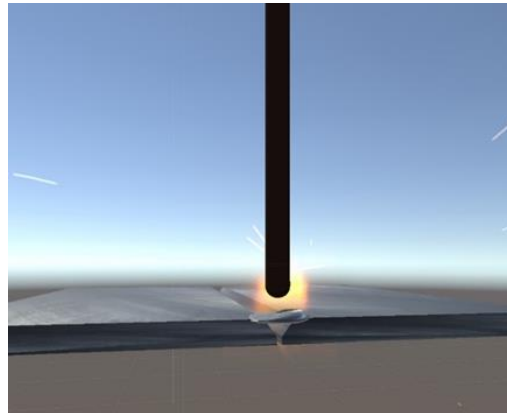
(d) Pushing technique (side view)
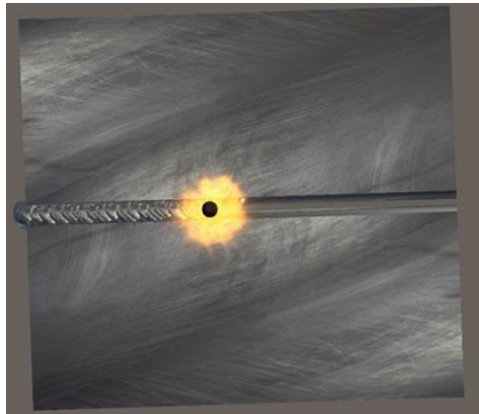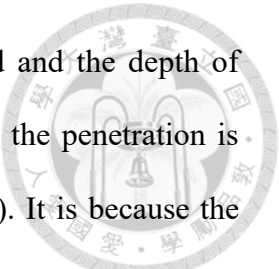
(e) Perpendicular technique (top view)
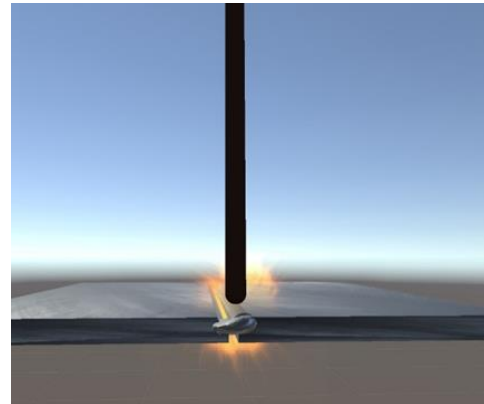
(f) Perpendicular technique (side view)

Fig. 2.9. (a) and (b): Pulling technique causes deeper penetration but narrower bead width;

(c) and (d): Pushing technique causes smaller penetration but wider bead width; (e) and

(f): Perpendicular technique causes moderate penetration and moderate bead width.

In addition, electrode orientations also affect the width of the bead and the depth of penetration. When the electrode is dragged in the direction of welding, the penetration is deeper, but the bead width is narrower, as shown in Figs. 2.9(a) and (b). It is because the pulling technique will cause more heat flow along the thickness of the weld plates but less heat at the top surface of the weld plates, which results in deeper penetration but narrower bead width. On the other hand, if the electrode is pushed in the direction of welding, the penetration is smaller, but the bead width is wider, as shown in Figs. 2.9(c) and (d). The perpendicular orientation of the electrode provides moderate penetration depth and bead width, as shown in Figs. 2.9(e) and (f) (Eyres and Bruce, 2012; Mandal, 2001; Mandal, 2009; Taggart et al., 1980).

2.5.2 Tracking

There are two tracking devices, one is the HTC Vive tracker for tracking the electrode, and the other one is the handheld controller for interacting with the UI elements. The HTC Vive tracker is attached to the electrode holder to track the electrode position, as shown in Fig. 2.10. In the real world, the MMAW process begins when the electrical arc of the desired length (2 mm to 8 mm) is established between the electrode tip and the weld plates. To simulate this process, a proximity sensor, VL6180X, is mounted at the tip of the electrode to measure the distance between the electrode tip and the weld plates. Based on the measured distance, virtual weld beads and sparkling particles will be simulated in the MR environment.

21
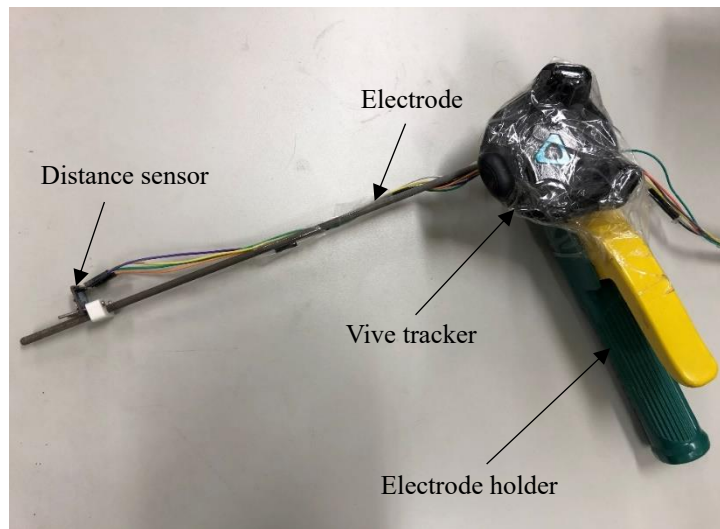
Fig. 2.10. Electrode with distance sensor.

VIU is used to deal with the tracking of the handheld controller. Similar to the VR module, when users press the trigger button on the handheld controller, a cyan light beam will be emitting from the handheld controller for users to interact with the UI elements, as shown in Fig. 2.11(a).

2.5.3 User interface

The usability principles suggested by Regazzoni et al. (2018) and the ergonomics guidelines suggested by Ejaz et al. (2019) are considered in the UI design. In this study, users are free to move around and interact with the virtual and real objects in a space of 1.4 m × 1.4 m.

Fig. 2.11(a) shows a translucent text screen augmented in the real scene with welding process parameters and required welding instructions displayed. A fixture is used to place the 3D printed plates (Fig. 2.11(b)). Next, a virtual welding joint is overlaid on the plates (Fig. 2.11(c)). Users can set the welding speed by dragging the travel speed slider UI using the handheld controller. A red dot starts moving with the specified speed to guide users to

22

perform the welding. Visual aids and quantitative guidance, such as speed guidance, welding direction, electrode angle range, and arc length, are displayed in the MR scene to help novice welders to perform a quality welding. Users have to maintain the arc length in the desired range by holding the electrode holder in the right hand. Fig. 2.11(d) shows a user's first-person view from the HTC Vive Pro HMD while performing welding. Fig. 2.11(e) shows a third-person view of the training environment. When users set the travel speed to the minimum value, wider and deeper weld beads are observed (Figs. 2.11(f) and (g)). When the travel speed is set to the maximum, narrower and smaller penetration are observed (Figs. 2.11(h) and (i)).

Users can use the similar way to vary the current parameter by dragging the current slider UI. The arc length can be changed by changing the distance between the electrode tip and the workpiece. The electrode can be chosen from three different diameters by clicking the electrode button UI.
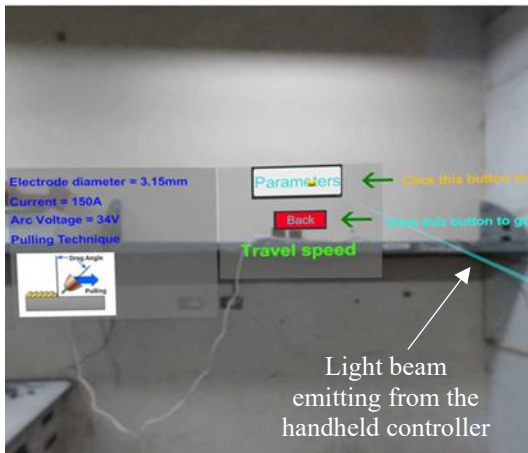
(a) Translucent instructions
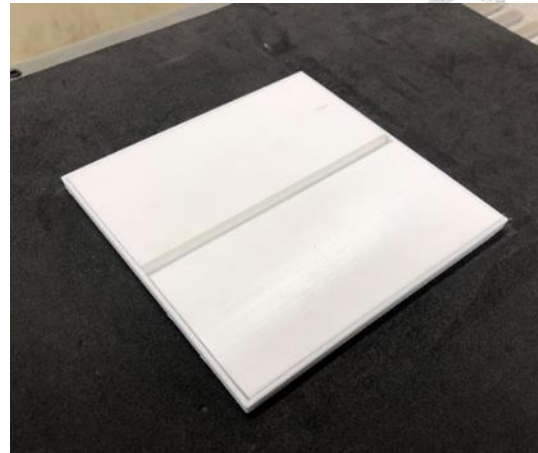
(b) 3D printed weld plate
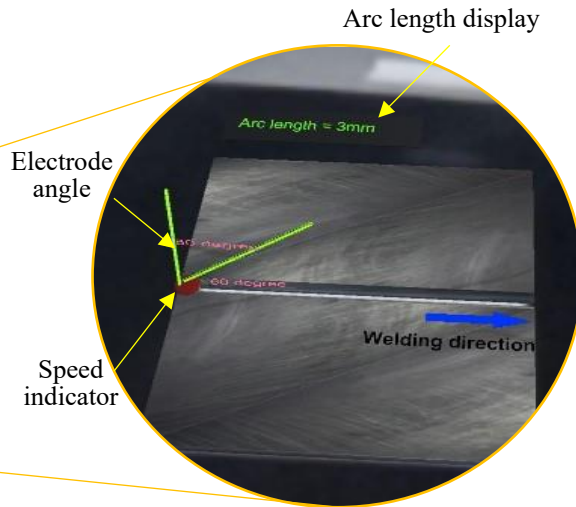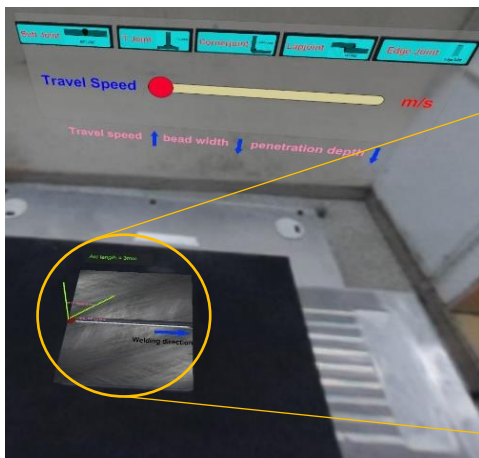
(c) Selecting welding joint
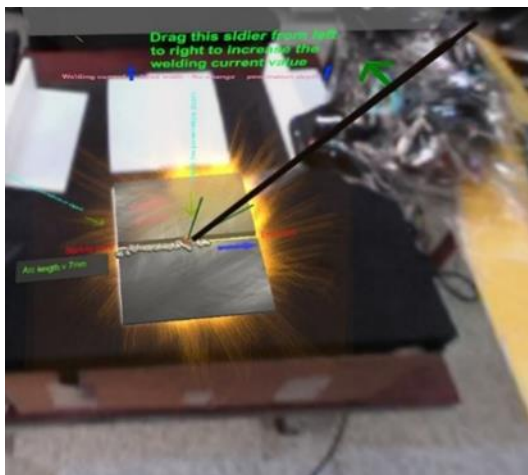
(d) User's first person view

(e) Third person view

24

(f) Wider bead width   (g) Deeper penetration

(h) Narrow bead width   (i) Smaller penetration
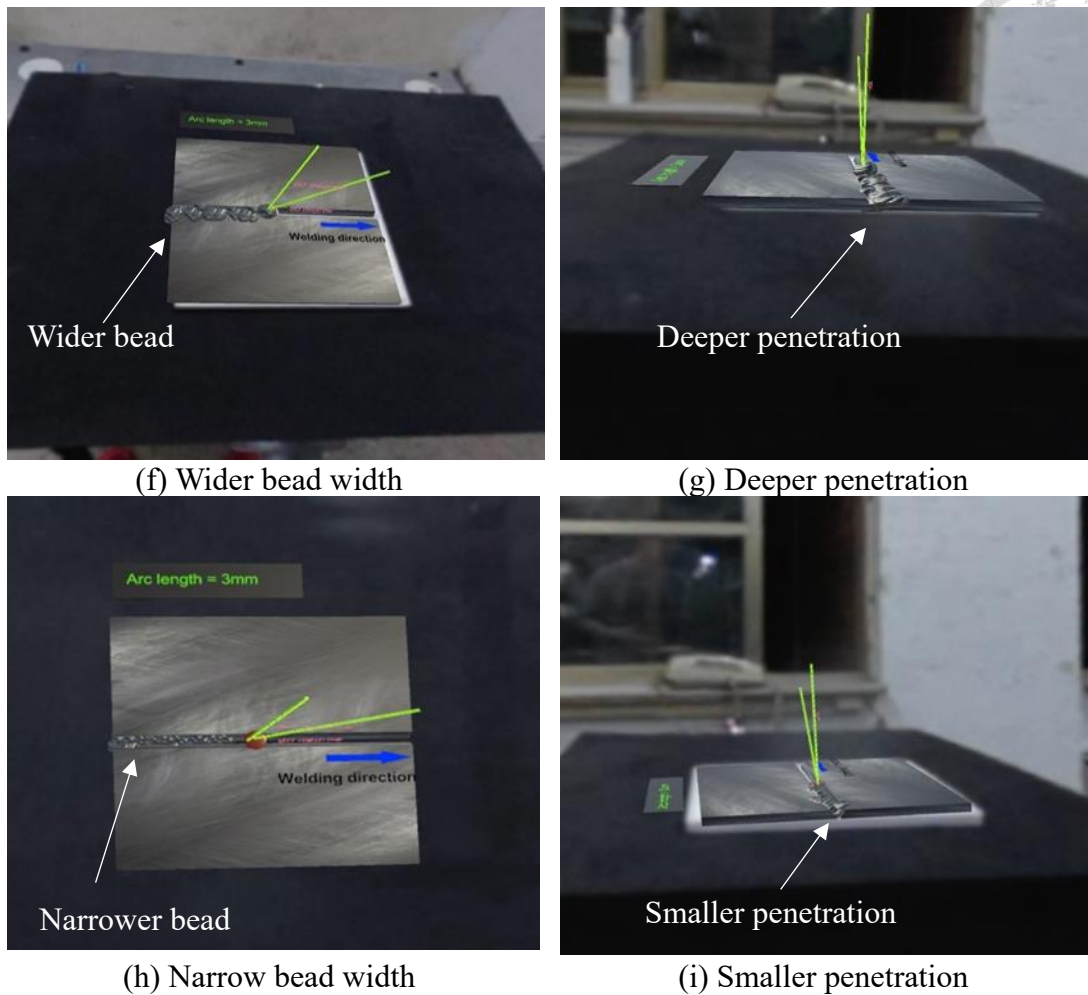
Fig. 2.11. Hands-on welding practice in the MR scene.

2.6 User test

A user test was conducted to evaluate the XR-based welding tutorial system in terms of learnability, workload, and usability. Two groups of participants were recruited. The experimental group was trained using the XR-based method and the control group was trained using the conventional classroom method with the power point presentation. The training performance was evaluated using a written test (for learnability evaluation), the NASA task load index (NASA-TLX) (for workload assessment), the system usability scale

25
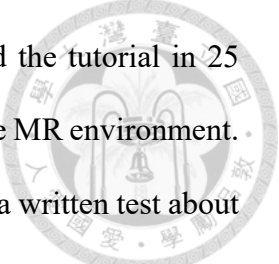
(SUS) (for usability evaluation), and a subjective questionnaire (for general user experience assessment).

For determining an effective sample size (the number of participants) for the experiment to compare their performance, the G*Power tool was used. The sample size of the two groups was calculated with independent mean by considering one tail test. The effect size d was obtain from the following formula (Cohen, 1988):

$$d = \frac{|M_1 - M_2|}{\sigma} \qquad (2.3)$$

where M_1 is the expected mean score of the written test of the experimental group, M_2 is the expected mean score of the written test of the control group, and σ is the standard deviation of the population. The effect size d obtained from Eq. (3) is 1 by assuming the mean percentage score of 60 for the control group and 70 for the XR group with standard deviation of 10. The statistical power P is usually in the range of 0.8 to 0.95 (Cohen, 1988). Here, $P = 0.8$, Type I error $\alpha = 0.05$ and sample size ratio $N_2/N_1 = 1$ are used. The obtained sample size is $N_1 = N_2 = 15$. Therefore, thirty college students were recruited randomly from different engineering and science backgrounds, except mechanical engineering. The people with the mechanical engineering background were not considered because their previous knowledge about welding might affect the results of the user test. Finally, 16 males and 14 females at the age between 21 and 40 (average age = 26.2, $SD = 4.1$) were recruited.

Fig. 2.12 shows the flowchart of the user test. Thirty participants were randomly divided into the XR group and control group. The welding tutorial was delivered to the XR group in the XR-based environment, and to the control group in a traditional classroom. Although the content of the welding tutorial was the same, the participants in the XR group finished the

tutorial in 40 minutes, and the participants in the control group finished the tutorial in 25 minutes. The XR group took longer because of the hands-on practice in the MR environment. Immediately after the tutorial, both groups were given 20 minutes to take a written test about the tutorial contents. After the written test, participants in both groups were asked to fill out the NASA-TLX form to evaluate the workload. The performance of both groups was compared through the objective written test and subjective NASA-TLX questionnaire.

In order to compare the two training methods, the participants in the XR group also attended the tutorial in the traditional classroom. After that, the participants in the XR group filled out the SUS form and a subjective questionnaire to compare their experiences of using the two training methods.
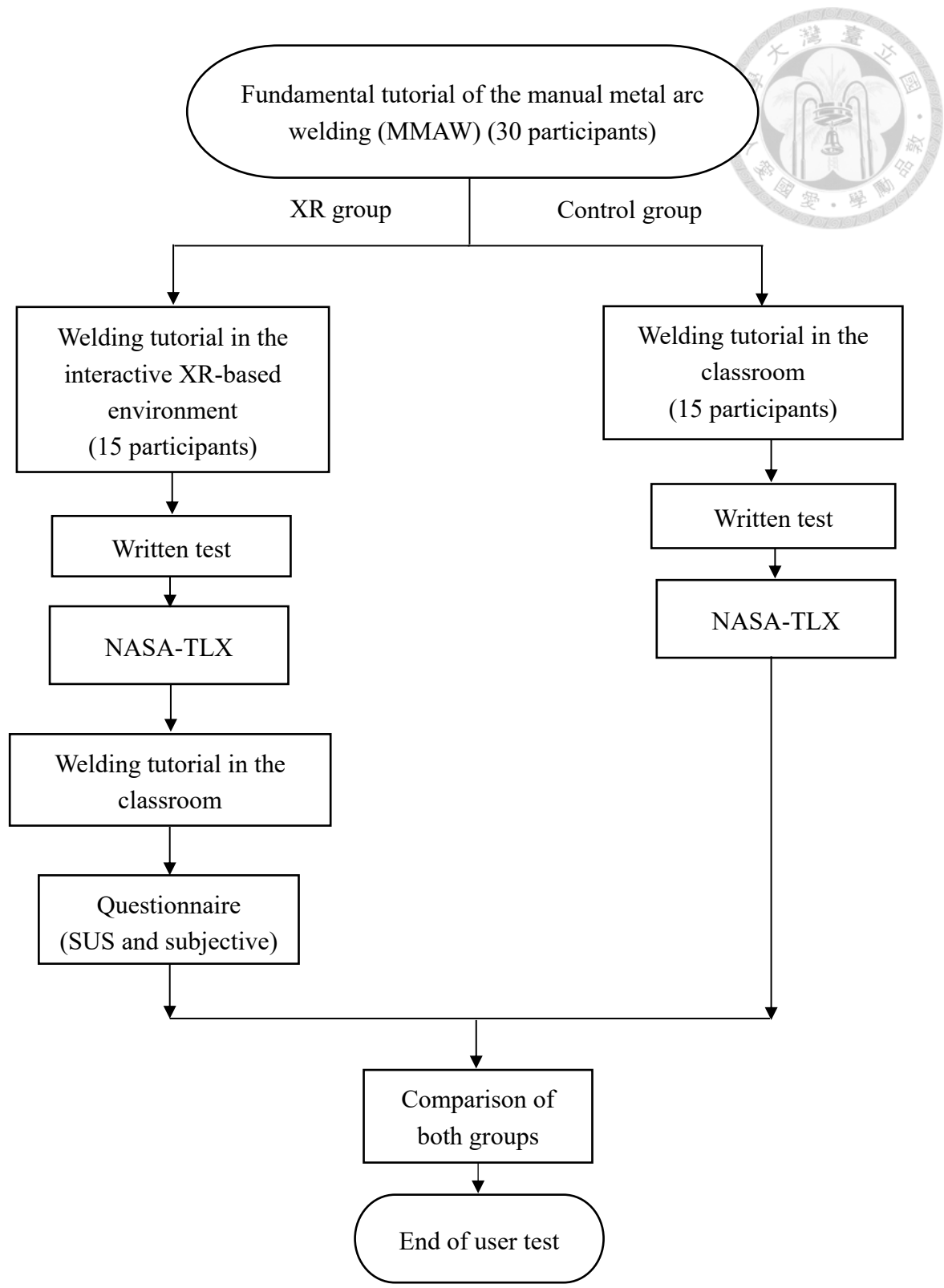
Fig. 2.12. Flowchart of the user test.

2.7 Results

2.7.1 Written test

The written test is used to measure how much knowledge is retained by the participants after the tutorial, and it is used to evaluate the learnability of the system. The written test questions are designed based on the topics in the prior welding books and literature (Clark, 1985; Jeffus, 2020; Mandal, 2001; Mandal, 2009), and they also have been covered in both tutorial sessions. The written test consists of 12 questions with a total score of 32, as shown in Table 2.1.

29

Table 2.1. Written test questions.
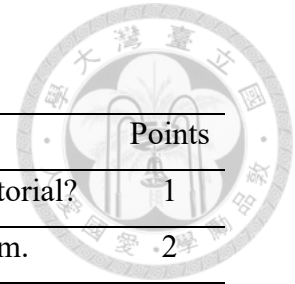
No.	Questions	Points
1	What is the name of the welding process discussed in the tutorial?	1
2	What are the different types of weld joints? Please draw them.	2
3	What are the names of the two types of welds (Weld 1 and Weld 2) shown in Figs. 1 and 2? Please write the nomenclature on the correct locations in the figures.	2

Fig. 1: Weld 1
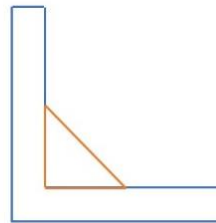
Fig. 2: Weld 2

Weld 1	Weld 2
Included angle	Leg (1)
Root gap width	Leg (2)
Joint faces	Toe of weld
Root face	Face of weld
Top side	
Root side	

No.	Questions	Points
4	Define the arc length and draw it.	2
5	What should be the range of the electrode angle with the normal of the butt weld and fillet weld when it is seen from the side view?	2
6	What should be the range of the electrode angle with the normal of the butt weld and fillet weld when it is seen from the front view?	2
7	What are the welding process parameters and their effects on the weld bead width and depth of penetration?	10
8	What is the difference between the push and pull techniques in terms of electrode orientation? Please draw the diagram.	4
9	What is the minimum value of the arc length required to establish	1
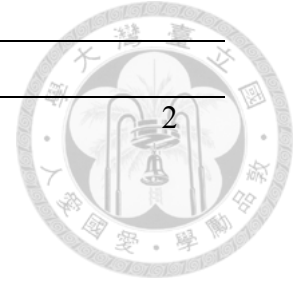
	an arc and start a welding process?	
10	What is the considered range of welding current used in the tutorial?	2
	a. 210 A – 300 A	
	b. 90 A – 210 A	
	c. 300 A – 450 A	
	d. None of above	
11	What are the diameters of the electrodes used in the tutorial?	2
	a. 3 mm, 4.5 mm, 6 mm	
	b. 3.15 mm, 4 mm, 5.5 mm	
	c. 2.5 mm, 4.2 mm, 5 mm	
	d. None	
12	Is it possible to maintain a constant voltage during the welding process? Why?	2

The final scores are normalized between 0 and 100. The average scores obtained by the XR group and the control group are $M_1 = 76.25$ ($SD = 8.84$) and $M_2 = 44.2$ ($SD = 10.63$), respectively. The scores are normally distributed for both groups. Fig. 2.13 shows that most participants in the XR group scored in the range of 71-80, whereas most participants in the control group scored in the range of 41-50. The t-test results reveal that the score in the XR group is significantly higher than the control group ($p < .001$) with $\alpha = 0.05$.

Table 2.2 represents the percentage score of each question by both groups. The XR group scored significantly higher than the control group for most questions, except for questions 4, 5, 6 and 12.

31
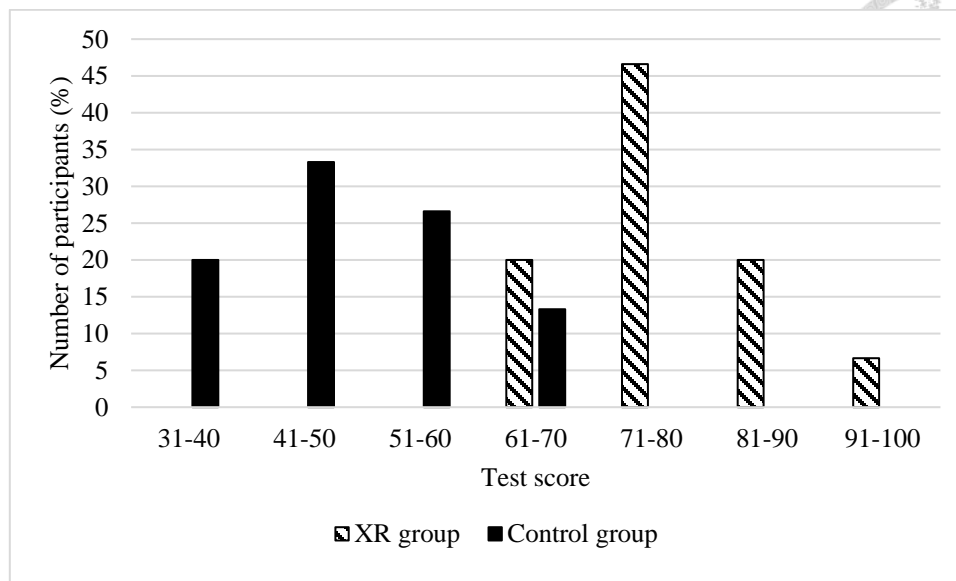
Fig. 2.13. Frequency distribution chart for XR and control groups.

Table 2.2. Written test score results.

	XR group		Control group		
No.	Mean	SD	Mean	SD	*p* value
1	88	21.7	58.3	32.3	(**)
2	89	14.2	43.8	27.2	(***)
3	81	31.1	39.6	25.4	(***)
4	86.6	35.1	72	33.2	(n.s.)
5	68.3	44.7	76	31.2	(n.s.)
6	70	41.4	66.6	40.8	(n.s.)
7	71.2	16.2	29.3	14.9	(***)
8	76.6	38.3	44.1	38.6	(*)
9	85.3	35	40.6	40	(**)
10	80	41.4	43.3	49.5	(*)
11	93.3	25.8	6.6	25.8	(***)
12	53.3	38.8	56.6	40.6	(n.s.)

Note: (*** ≡ $p \leq 0.001$, ** ≡ $p \leq 0.01$, * ≡ $p \leq 0.05$, n.s. ≡ $p > 0.05$).

32

2.7.2 NASA-TLX

After the written test, participants in both groups filled out the NASA-TLX form. The NASA-TLX is an assessment tool for the workload of a task or system. The NASA-TLX is divided into six subjective subscales, mental demand, physical demand, temporal demand, performance, effort, and frustration (Hart, 2006). A higher score represents higher loads. The lower score implies better results. However, in this study, the performance factor is transposed to higher score with higher performance. The NASA-TLX results are shown in Fig. 2.14.

The Kolmogorov-Smirnov test reveals that all six scale ratings are normally distributed. The t-test results show that the performance of the XR group is significantly higher than the control group, and the mental and temporal demands of the XR group are significantly lower than the control group. However, the physical demand, effort, and frustration of the XR group are significantly higher than the control group.
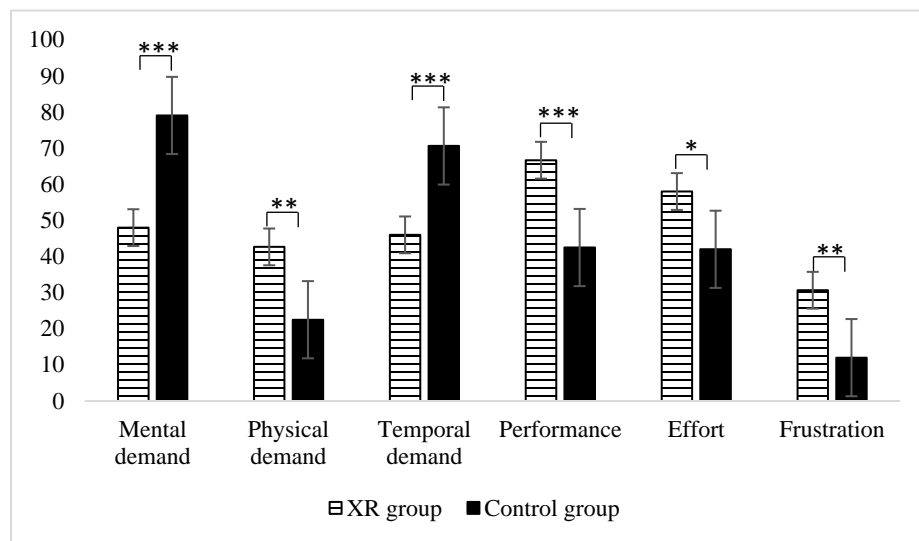
Fig. 2.14. NASA-TLX results for XR group and control group (*** $\equiv p \leq 0.001$, ** $\equiv$ $p \leq 0.01$, * $\equiv p \leq 0.05$).

33

2.7.3 System usability scale

SUS is a reliable tool for measuring the usability of a system. It consists of 10 statements to evaluate the usability of the system (Brooke, 1996). Scoring is based on a 5-point Likert scale (1: strongly disagree; 2: disagree; 3: neutral; 4: agree; 5: strongly agree). Lewis and Sauro (2009) used factor analysis to reveal that SUS actually included two factors: usability and learnability. The overall SUS score can also reveal users' satisfaction towards the system. Table 2.3 shows that in this study, the overall SUS mean score is 72, which is higher than the average score of 70 (Brooke, 1996; Derisma, 2020).

In this study, the Cattell's scree plot indicates that there are three significant factors in the SUS questionnaire, as shown in Fig. 2.15. Table 2.4 presents the varimax rotation matrix of the factor loadings of the 10 SUS statements. The factor loadings indicate that statements 4, 6, 9, and 10 are aligned with the first factor, statements 1, 2, 3, and 5 with the second factor, and statements 7 and 8 with the third factor. A reliability test is also performed to evaluate the consistency of the SUS scale. The Cronbach alpha coefficient of the overall SUS is 0.7, which confirms sufficient reliability of the SUS scale (Lewis and Sauro, 2009).
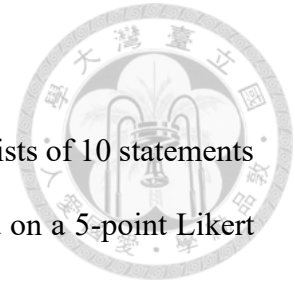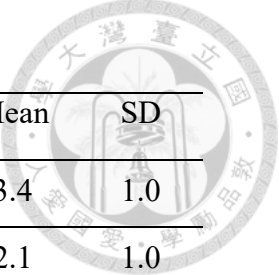
Table 2.3. Questionnaire results for SUS.

	SUS	Mean	SD
1	I think that I would like to use this system frequently.	3.4	1.0
2	I found the system unnecessarily complex.	2.1	1.0
3	I thought the system was easy to use.	4.0	0.7
4	I think that I would need the support of a technical person to be able to use this system.	2.9	1.0
5	I found the various functions in this system were well integrated.	4.4	0.6
6	I thought there was too much inconsistency in this system.	2.5	1.0
7	I would imagine that most people would learn to use this system very quickly.	4.1	0.6
8	I found the system very cumbersome to use.	1.8	0.7
9	I felt very confident using the system.	3.4	0.9
10	I needed to learn a lot of things before I could get going with this system.	1.3	0.4

35
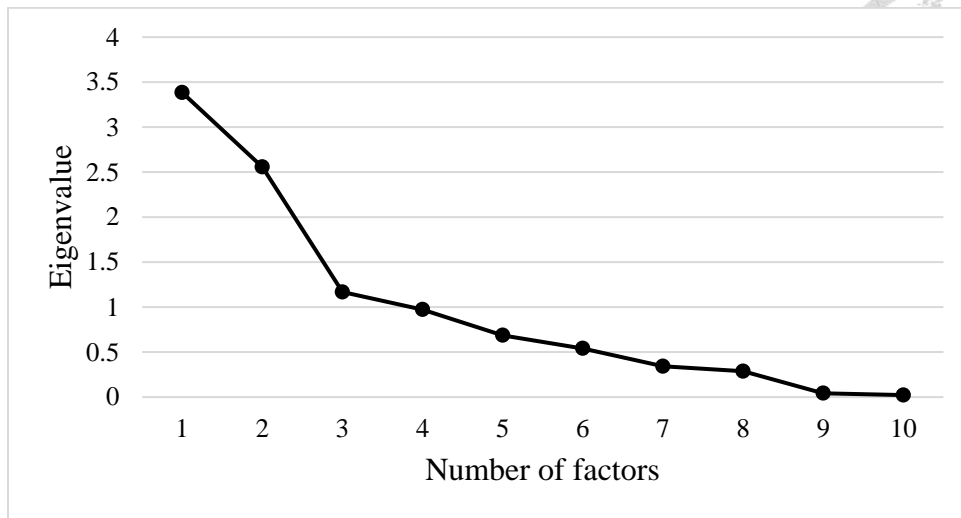
Fig. 2.15. Scree plot of eigenvalues for the SUS results.

Table 2.4. Factor loading matrix for SUS.

	Factors		
Statement	1	2	3
1	-.52	**.69**	.19
2	-.10	**.75**	-.09
3	.26	**.90**	.23
4	**.62**	.14	-.10
5	.28	**.83**	.03
6	**.80**	.04	.04
7	.52	.11	**.59**
8	-.07	.09	**.88**
9	**.60**	-.02	.50
10	**.84**	-.06	.36

36

2.7.4 Subjective questionnaire

The subjective questionnaire is used to evaluate the general experiences of using the XR-based tutorial system. A 5-point Likert scale is used (1: strongly disagree; 2: disagree; 3: neutral; 4: agree; 5: strongly agree). Table 2.5 shows the mean and standard deviation of each question. The Cattell's scree plot indicates that there are six significant factors in the subjective questionnaire, as shown in Fig. 2.16. However, in order to better categorize the statements in a more condense way, only 4 factors are extracted in this study. Table 6 presents the varimax rotation matrix of the factor loadings of the 20 statements. Statements 1, 2, 9, 15, 16, 17, and 18 are aligned with the first factor, statements 3, 5, 10, 11 and 14 with the second factor, statements 4, 6, 7, 8, 19 and 20 with the third factor, and statements 12 and 13 with the fourth factor. The reliability of the subjective questionnaire is confirmed with the Cronbach alpha coefficient of 0.73.
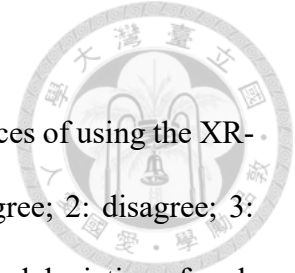
Table 2.5. Subjective questionnaire results.
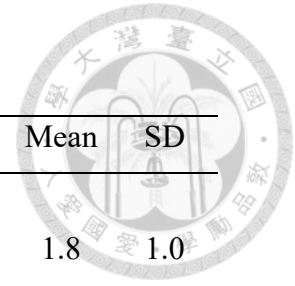
	Subjective	Mean	SD
1	The XR-based training system for the fundamental knowledge of the manual metal arc welding process was not very useful for learning.	1.8	1.0
2	The XR-based training system was easy to operate.	3.8	1.2
3	The XR tutorial is comprehensible.	4.0	0.7
4	The topics in XR tutorial are poorly explained.	1.8	0.6
5	The 3D representations of the objects and processes in the XR tutorial are helpful to understand the welding process.	4.4	0.5
6	The tracking is correct.	3.6	0.9
7	The augmented instructions were adequate and intuitive for user guidance.	4.0	0.7
8	The user interface was appropriate for exploring the tutorial.	4.4	0.6
9	The user interface was complex and difficult to interact.	2.1	1.0
10	XR tutorial was more useful than classroom tutorial.	4.1	0.9
11	XR tutorial was more interesting than the classroom tutorial.	4.4	1.1
12	The graphic interface was complex and intrusive.	2.5	1.1
13	The XR tutorial rapidly enhances the knowledge about the fundamentals of metal arc welding process.	4.4	0.5
14	The XR tutorial is not useful for non-mechanical engineering background.	1.6	0.9
15	The XR training system was helpful for practicing to keep a constant speed of welding.	3.8	1.0
16	The XR training system was helpful for practicing to maintain a desired inclination angle of the electrode.	4.0	1.0
17	The distance sensor is useful for practicing to maintain a desired gap to build an arc.	4.0	1.1

18	The XR training system was useful to learn welding on various welding joints.	4.3	0.6
19	XR tutorial is more useful to understand and remember the effects of various welding process parameters on weld bead geometry.	4.4	0.5
20	I want the XR tutorial more interactive to allow me to ask questions.	3.7	0.7
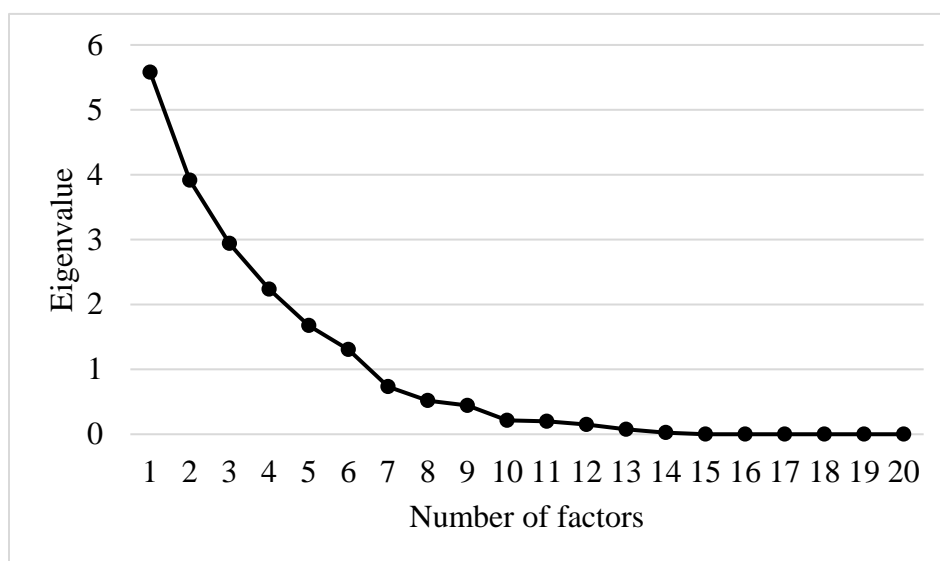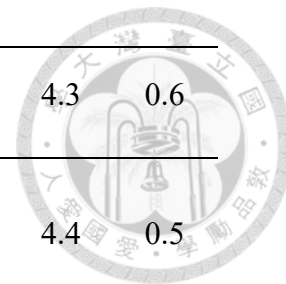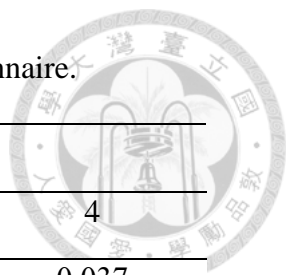
Fig. 2.16. Scree plot of eigenvalues for the subjective questionnaire.

Table 2.6. Factor loading matrix for the subjective questionnaire.

Statement	Factor			
	1	2	3	4
1	**0.666**	0.356	0.001	0.037
2	**0.860**	-0.365	-0.042	-0.165
3	0.405	**0.484**	0.096	-0.063
4	-0.094	0.301	**0.813**	0.070
5	-0.300	**0.315**	-0.257	0.173
6	0.043	-0.528	**0.611**	0.150
7	-0.143	-0.193	**0.744**	-0.440
8	0.446	-0.032	**0.551**	-0.098
9	**0.809**	-0.090	0.357	-0.072
10	0.000	**0.899**	0.123	0.044
11	0.036	**0.834**	-0.139	-0.262
12	0.035	-0.312	0.068	**0.843**
13	0.391	0.260	0.227	**0.730**
14	-0.084	**0.721**	-0.090	-0.128
15	**0.902**	0.282	-0.180	-0.122
16	**0.922**	-0.014	-0.145	0.220
17	**0.678**	-0.359	-0.233	0.175
18	**0.874**	0.015	-0.141	0.338
19	-0.082	0.484	**0.524**	0.352
20	-0.131	-0.063	**0.730**	0.177

40
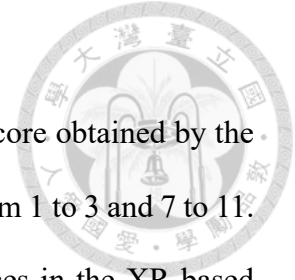
2.8 Discussion

The learnability of the system is validated by the written test. The score obtained by the XR group are significantly higher than the control group in questions from 1 to 3 and 7 to 11. It shows that the 3D representations of the joints and hands-on practices in the XR-based training system help users to remember the effects of process parameters, types of weld joints, welding current range, and electrode diameters. However, 2D texts of the arc length and range of electrode angle in the XR scene do not show any significant difference. It is because the 2D text information in the XR scene is similar to the classroom tutorial, which justifies the results.

The workload of the participants is evaluated using NASA-TLX. Since the XR-based tutorial system simulates the real welding environment, trainees need to stand up to perform the hands-on welding task. Therefore, higher physical demand of the XR-based tutorial system is expected in the study because it reflects the high physical demand in the real welding environment. In addition, since participants in the XR group experience the system for the first time, they have to put more effort to learn the new UI. Compared to the conventional classroom tutorial, they show higher frustration because they might accidently press the wrong button on the handheld controller or select the wrong UI. Therefore, the effort and frustration loadings of the XR group are higher. However, the effort and frustration loadings can be reduced by frequent use of the XR system. The performance factor shows that the XR group perform significantly better than the control group, which justifies the learnability of the system.

The usability of the XR-based training system is evaluated using SUS. Factors analysis indicates that in this study, the SUS statements can actually be categorized into three factors:
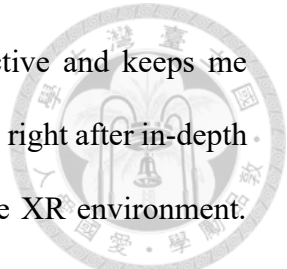
learnability, usability, and easiness, respectively. The mean score of the SUS results is above the average, and the usability of the system is categorized in rank B (Derisma, 2020). It indicates that although the learnability, usability and easiness of the system is good and acceptable, some future improvements are required to enhance the usability.
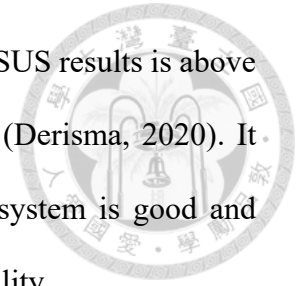
Although based on the SUS responses, the system's learnability, usability, and easiness have been confirmed with mean scores either above 3.5 for most positive statements (odd-numbered) or below 2.5 for most negative statements (even-numbered), some statements received relative neutral responses (3.0). For example, statements 4 and 9 in the learnability factor received means of 2.9 and 3.4, respectively. It indicates that a more self-explanatory environment is needed to explain the training procedure more clearly to increase the confidence of the users and the learnability of the system. Statement 1 in the usability factor received a mean of 3.4. It indicates that a more intriguing UI or contents need to be designed so that users would like to use the system more frequent.

The general experiences for the XR-based training system are evaluated using a subjective questionnaire. Four factors are categorized using the factors analysis: usability, easiness, learnability, and lucidity, respectively. Users' responses show that all of the positive responses are higher than 3.5, and most of the negative responses are below 2.5, except for question 20 in the factor of learnability. It indicates that although the subjective questionnaire confirms the usability, learnability, easiness, and lucidity of the system, a more intelligent and intuitive UI needs to be created to allow users to interactively ask questions and receive relevant answers from the XR system.

Since the participants in the XR group also attended the traditional classroom training, participants in the XR group provided some comparative remarks as follows: "I feel XR

tutorial was a lot better than having a classroom tutorial. It is interactive and keeps me attentive throughout the process. The best part is the hands-on experience right after in-depth exploration of the topics. We cannot ask questions to the teacher in the XR environment. Since the XR system was new to me, I felt uncomfortable while performing welding in the XR environment. The hands-on experience is very useful to understand the effect of process parameters and practice to maintain constant arc length and speed. Distance sensor performance can be improved for better accuracy of the welding. It is an easier and more interesting method to learn complex topics. The 3D representation of the models is more comprehensive and helpful to retain the knowledge. Bright colors on the UI should be avoided for the comfort of eyes."

2. 9 Conclusions

Welding is one of the important engineering and technology topics which need heavy hands-on practices. Welding is also a hazardous manufacturing process due to intense heat and harmful ultraviolet radiation. Most welding tutorials are delivered through the conventional classroom settings. This study developed an interactive XR-based welding tutorial system for fundamental MMAW training for novice welders. 3D interface allows users to perform a hands-on welding task with natural welding behavior, improving the effectiveness of the welding training. Novice welders can follow the visual instructions step by step and maintain a proper welding position. They can change the values of the welding process parameters to observe the effects on weld beads in real time in an immersive environment. The learnability, workload, and usability of the developed system have been validated through a user study. The results show that the XR-based welding training system can help novice welders to retain welding knowledge and enhance hands-on welding skills.

Future work can focus on improving the accuracy of the tracking and arc length measurement.

In addition, a more interactive, interesting, and self-explanatory UI will be created.
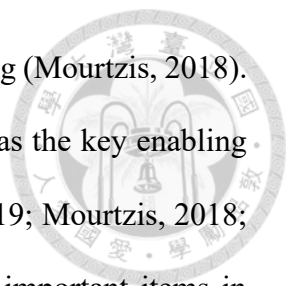
Chapter 3   A visuo-haptic extended reality-based training system for hands-on manual metal arc welding training

Welding training has been an important job training in industry, yet it usually demands a large amount of resources. In real practice, the strong magnetic force and intense heat during welding processes often frighten novice welders. In order to provide safe and effective welding training, this study develops a visuo-haptic extended reality (VHXR)-based hands-on welding training system for training novice welders to perform a real welding task. Novice welders can use the VHXR-based system to perform a hands-on manual arc welding task, without exposure tzo high temperature and intense ultraviolet radiation. Realistic force feedback and visual feedback are provided to help trainees to maintain a constant arc length, travel speed, and electrode angle in real time. Compared to the traditional video training, users trained using the VHXR-based welding training system demonstrated significantly better performance in the real welding tasks. Users were able to produce better-quality joints by performing a smoother welding with lesser number of mistakes, inquiry times, and hints. This abstract and the following subchapters are from Shankhwar et al. (2022).
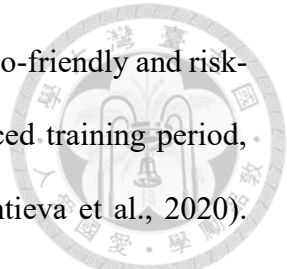
3.1 Introduction

With the advancement of information technology, in order to prepare quality professionals for Industry 4.0, traditional education or training methods should be

45

transformed to Education 4.0, which is digital-based teaching and learning (Mourtzis, 2018). Augmented reality (AR) and virtual reality (VR) have been considered as the key enabling technologies for Industry 4.0 and Education 4.0 (Masood and Egger, 2019; Mourtzis, 2018; Van Lopik et al., 2020). European Union even lists AR as one of the important items in implementing Industry 4.0 (Davies, 2015). Prior research has demonstrated a variety of AR applications in manufacturing, such as maintenance, assembly, logistics, and quality control (Egger and Masood, 2020). AR and VR technologies have also been proven to be an effective teaching and learning tool (Calvert and Abadia, 2020; Di Natale et al., 2020; Loureiro et al., 2021; Maas and Hughes, 2020).

In modern industry, welding can be done by robots or automated machinery. However, in some manufacturing sectors, such as ship building, heavy equipment production, and small part fabrication, most welding jobs are still done manually by human operators, due to complex structures and inaccessibility of robots (Liu and Zhang, 2015). In addition to industry, welding training is also a major program in engineering and technology education. Welding is a skill must be taught correctly and elaborated with practice. However, it is a challenge to teach novice welders with hands-on welding skills because welding usually involves high temperature and harmful ultraviolet radiation. During welding training, repetitive practice of welding often causes wastage of energy and material (Mavrikios et al., 2006). The shortage of skilled welders has become an urgent issue in manufacturing industries due to the problems encountered during welding training. In vocational training, welding is recognized as one of the most expensive training programs (Wu, 1992). Therefore, it is important to transform the traditional welding training into Education 4.0 and take advantage of VR and AR to develop a digital-based, cost-effective, and safe welding training

method to equip novice welders with sufficient welding skills. Such an eco-friendly and risk-free welding training program can prepare certified welders with reduced training period, cost of laboratory work and CO_2 emission to the environment (Lavrentieva et al., 2020). Hence the AR/VR technologies-based welding simulator can provide the hands-on training with a reduced labor, energy, and material cost in a safe and realistic training environment.

In order to achieve high-grade welding joints, welders have to maintain a certain travel speed, arc length, and inclination angle of the electrode, under the influence of strong magnetic force and intense heat. Consequently, an effective AR and VR training tool should provide simulated, but also realistic force, thermal, and visual feedback throughout the welding training. The objective of this research is to develop a risk-free and cost-effective welding training system to allow novice welders to conduct a realistic hands-on welding practice and freely interact with welding components with their natural welding operation behavior as if they are performing a real welding task in the real world. The key contributions of this research are the development and verification of an extended reality (XR)–based welding training system, which provides realistic haptic feedback and real-time visual aids and quantitative guidance in assisting users to correctly perform a welding task using their natural welding behavior.

3.2 Related Work

3.2.1 XR applications

XR is a universal term referring to all immersive learning technologies generated by computer and wearable devices including AR, VR, and mixed reality (MR) (Doolani et al., 2020). The XR technology is an integral part of Industry 4.0 concepts, as it enables operators to access digital information and combine the virtual world with the real world through tools

47

like AR, VR, MR, and haptics. Prior research has provided a variety of AR/VR applications in industries, education, medical, and healthcare (Egger and Masood, 2020; Tang et al., 2021a). One of the industrial applications of AR has been presented by Bottecchia et al. (2009). They proposed a prototype for a collaborative teleassistance system for mechanical repairs based on AR. The operator and expert can collaborate remotely to complete maintenance and repair tasks. The expert can accurately visualize the view of operator and can provide technical information by directly picking, outlining and adding information to an item in an operators' video stream. However, the proposed system is experimented on a predefined maintenance process which can be extended to support non-predefined repairs. Uva et al. (2018) utilized spatial AR to develop technical instruction manual to guide the operators to perform maintenance task on a motorbike engine and evaluated its effectiveness by comparing with paper manual. The AR-based manual proved to be effective for complex tasks. However, the tracking, usability and interface design are yet to be considered for further research. Martín-Gutiérrez et al. (2015) investigated the effect of AR-supported laboratory pratices on education. The evaluation results revealed that students were more comfortable in using AR-based laboratories and felt that the design of the facility and machines were easy to use. However, the study lacks the evaluation of improvement in performance using the AR system. Akçayır et al. (2016) tested an AR-based science laboratory to measure the impact on the university students' skills and attitude towards the physics lab. The user study results showed significantly improved laboratory skills of the students with enhanced science learning capabilities. However, the mobile device can be substituted by head mounted display in further research to build a tangible user interface for the enhanced learning experience. Tang et al. (2021b) presented an interactive VR-based

48

approach to facilitate procedural training for medical practitioners. The conducted survey results for measuring the motivation and enhanced readiness of practitioners indicated good reliability of the learning model. The study provided valuable implications for similar VR training developments in the future. However, the consideration of a few more learning factors such as learnability, system usability, and self-directed learning is still the scope of future research.

3.2.2 XR in welding training

Some prior researchers have used XR technologies to assist real welding operations. For example, Tschirner et al. (2002) applied AR to help welders to recognize the details of the welding environment during real manual gas metal arc welding. Aiteanu et al. (2003) developed an AR welding helmet for manual welding by augmenting visual information before and during the real welding process. Users could see the real environment and correctly position the welding gun. Doshi et al. (2017) used projector-based AR to improve manual spot-welding precision and accuracy for automotive manufacturing. However, their application was only restricted to specific vehicle panels with constraint projector locations.

In addition to assisting real welding operations, XR technologies have also been applied to welding training. Liu and Zhang (2015) proposed a teleoperation-based AR welding training system using machine learning to calculate an optimized welding speed for unskilled workers to follow, during a welding process. The actual welding task still happened at a remote welding station. The remote robot arm would follow the human's movement and perform the real welding task. Mavrikios et al. (2006) developed a prototype demonstrator for simulating metal inert gas welding using VR technology. However, the proposed simulator was incapable to provide realistic sensation of holding a welding gun due to a fully

49

virtual environment.

XR technologies have also been utilized in several commercial welding training simulators. Some of the prior studies have provided insights into the XR-based commercial simulators. For example, Okimoto et al. (2015) studied user perception on a commercial AR-based welding training simulator, called Soldamatic. Although users could experience efficient and fast learning, they needed to stand very close to the workpiece to allow the system to detect the markers. Byrd et al. (2015) assessed the existing skills of welders using a VR-based welding simulator, VRTEX 360. The results showed that the experienced welders performed significantly better than the trained novice welders. Lavrentieva et al. (2020) analyzed the impacts of using commercial VR- and AR-based welding training simulators, such as MIMBUS, Fronius, Soldamatic, etc. They found that simulation-based welding training could reduce training period, cut the cost of laboratory work, diminish CO_2 emission, save resources and materials, and avoid physical risks.

Although prior studies have shown positive outcomes of using XR technologies in welding training, most welding simulators lack realistic haptic feedback, which is an important phenomenon in real metal arc welding tasks. Therefore, in order to provide a high-fidelity simulation, it is necessary to include haptic feedback in welding training. Furthermore, prior studies also lack real-time visual aids and quantitative guidance. Since in the real world, welding is performed by holding a protective helmet in front of the eyes, welding details become unclear to the welders. Thus, welders have to commence the welding with presumed location of the workpiece. However, most existing commercial welding simulators do not provide equivalent visual effects of the real welding helmets. Moreover, most welding simulators also need the presence of an experienced welder to help the novices

50

to correctly operate the welding simulators.
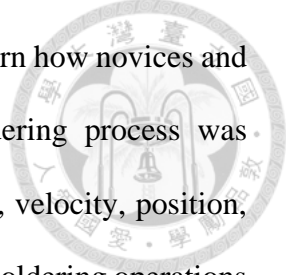
3.2.3 Visuo-haptic applications

It is essential to acquaint novice welders with real welding challenges, e.g., strong magnetic force and intense heat, during hands-on practices in a simulated environment. Haptic feedback can increase training performance, and thus, plays a vital role in industrial and training applications (Cosco et al., 2012). The integration of visual effects and haptic feedback, called visuo-haptic, can enable users to see and touch digital information in a simulated environment (Eck et al., 2015).

Several studies have demonstrated the effectiveness of visuo-haptic in various manufacturing training. Chen and Yang (2004) presented a VR-based machining process using a commercial haptic device, PHANTOM, to provide force feedback during virtual material removal simulation. Crison et al. (2005) designed a haptic device to simulate the milling operation by applying a plastic deformation algorithm. The force feedback varied as a function of tool speed, material type, etc. Fletcher et al. (2013) investigated the usage of VR and PHANTOM Omni for automatic generation of machining process plans, such as operation details and machine and tool selections. He and Chen (2006) presented a haptic virtual turning operation system using PHANTOM to simulate cutting and grinding operations. The shape of the object being produced in the virtual machining process could be seen and felt by the users.

Apart from machining, some of the studies focused on using commercial haptic devices in welding training. Ni et al. (2017) proposed an AR user interface for programming welding robots remotely and defining welding paths using a PHANTOM haptic device. The experimental results proved that using a haptic device could assist users to obtain an accurate

51

welding path. Sung et al. (2011) investigated human hand dexterity to learn how novices and experts operate differently in a soldering process. The manual soldering process was simulated using two PHANTOM Omni devices. By recording the force, velocity, position, and angle of the haptic pen, the skills that required to perform successful soldering operations could be analyzed.

Although the prior studies have shown promising applications of using commercial haptic devices in machining force simulation, the applications were constrained by the mechanism and degrees of freedom of the commercial haptic devices. Therefore, natural machining operation behaviors are not allowed in most manufacturing process simulators. This study develops a visuo-haptic extended reality (VHXR)-based hands-on welding training system for training novice welders to perform a manual metal arc welding (MMAW) task, using their natural welding operation behaviors. Electromagnetic force and thermal feedback are provided to simulate magnetic force and intense heat occurred in the real welding environment. The system also provides real-time visual aids and quantitative guidance to assist users to maintain a constant travel speed, arc length, and inclination angle to correctly perform a welding task.

3.3 Methodology

3.3.1 System overview

In this study, VR is used to graphically introduce basic welding knowledge and tools. However, in order to provide realistic hands-on welding practice, MR is used, so that users could see physical welding components. The training begins with a VR module, in which welding tools are demonstrated on a worktable along with introductions and safety instructions. After the VR module, users enter into the MR module to acquire hands-on

52

welding practices. A real electrode holder is used to help users retain muscle memory. In addition to the force feedback, virtual weld beads, virtual sparkling particles, and virtual electric arc are also displayed in the MR scene.
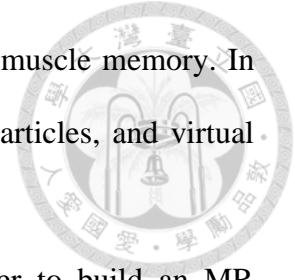
The HTC Vive Pro HMD are used as a display device. In order to build an MR environment, Vive Input Utility (VIU) and SRWorks software development kit (SDK) are used. The VHXR-based welding training system is developed on a PC with a 3.00 GHz Intel Core i7-9700F processor, 64 GB RAM and 6.0 GB dedicated GPU memory. Scripts are written in C# using the Unity3D game engine.

3.3.2 Tracking

In this study, two Vive trackers and two handheld controllers are used. One Vive tracker is mounted on the electrode holder (Fig. 3.1(a)) to track the electrode, while the other Vive tracker is mounted on a 3D printed chipping hammer handle (Fig. 3.1(b)) to track the virtual chipping hammer (Fig. 3.1(c)).

In the real MMAW process, welding begins when the electric arc of the desired length in the range of 2 mm to 8 mm is established between the weld plates and the electrode tip. In order to simulate a real MMAW process, a distance sensor VL6180X is mounted at the tip of the electrode to measure the distance between the weld plates and electrode tip (Fig. 3.1(a)). Virtual weld bead, sparkling particles, and electric arc are rendered if the arc length is maintained within the desired range. However, the best welding results could be achieved when the arc length is between 2 mm and 3 mm.

One handheld controller is used to interact with the user interface (UI) elements, i.e. virtual buttons and sliders, while the other handheld controller is used to track the virtual helmet (Figs. 3.2(a) and (b)).

53
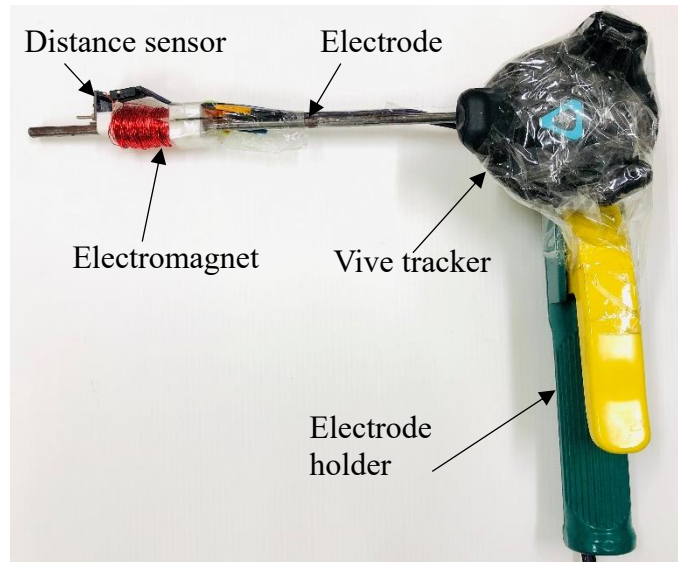
(a) A Vive tracker mounted on the electrode holder.
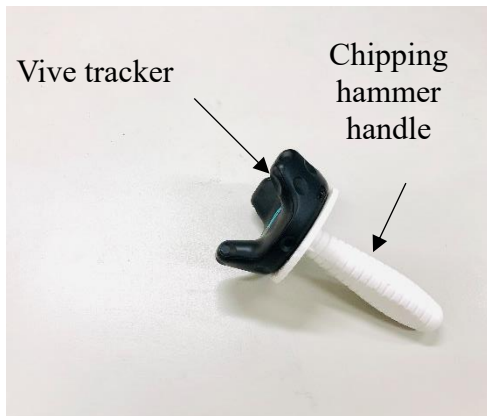
(b) A Vive tracker mounted on the chipping hammer handle.

(c) Virtual chipping hammer.

Fig. 3.1. Vive trackers for tracking the electrode and the virtual chipping hammer.

(a) Handheld controller.　　　　　(b) Virtual helmet.

Fig. 3.2. A handheld controller for tracking the virtual helmet.

3.3.3 Haptic feedback

There are two challenges which might frighten novice welders during the MMAW process. One is a strong magnetic force generated between the electrode tip and the workpiece, and the other is intense heat and hot sparks. It is essential to provide a natural user interface with realistic haptic feedback to help novice welders become more acquainted with the real welding environment.

In the real MMAW process, when the gap between the electrode tip and the workpiece is less than 2 mm, the induction of the longitudinal magnetic field of welding current rapidly increases (Chigarev et al., 2016). This leads the electrode being stuck to the workpiece while performing welding tasks. In order to simulate the magnetic force, an electromagnet is placed at one end of the electrode, which is made of medium carbon steel, as shown in Fig. 3.1(a). The workpiece is made of 10 cm × 4 cm × 1 cm SS41 low-carbon steel. The electromagnet is formed by winding an insulated copper wire around the electrode rod. The magnitude of

55

the induced magnetic force is about 7.6 N. In the real welding process, magnetic force created in a workpiece of the same size is about 22.3 N (Kumar and DebRoy, 2003), which is 2.9 times stronger than the electromagnetic force simulated in this study. Although the simulated magnetic force is smaller than the real one, due to the limitation of the size of the electromagnet, it still provides substantial obstruction in welding practice. Users can practice welding and learn to maintain a constant arc length to avoid the sticking of the electrode to the workpiece, under the influence of magnetic force.

An infrared heat lamp is used to provide thermal feedback during the welding. The infrared lamp can produce heat with temperature of 65°C at a distance of 30 cm (MacCargar, 2006). Since the light of the infrared heat lamp might disturb users, the heat lamp is placed inside a box made of a dark blue translucent plastic foil (Fig. 3.3). The heat lamp is switched on when the arc length is in the range of 2 – 8 mm; otherwise, the heat lamp is switched off.

Fig. 3.3. Infrared heat lamp inside a box made of translucent plastic foil.

3.3.4 Hands-on welding training in MR

It is essential for an effective simulation to replicate the real experience of an application (Howie and Gilardi, 2021). Therefore, each required welding step of a real welding process, from the beginning to the end, is considered in the VHXR-based welding training system. The practical hands-on welding training is provided to the user in the following steps:

56

Step (1): Wearing the safety shoes, hand gloves, and apron

The welding training starts from the VR module, which contains safety instructions and welding equipment introductions. The welding components and tools are demonstrated on a worktable (Fig. 3.4(a)). In addition, videos are provided to show the usage of the welding tools (Fig. 3.4(b)). After that, users enter into the MR module for hands-on welding practice.
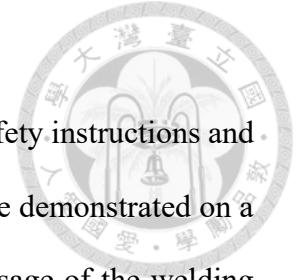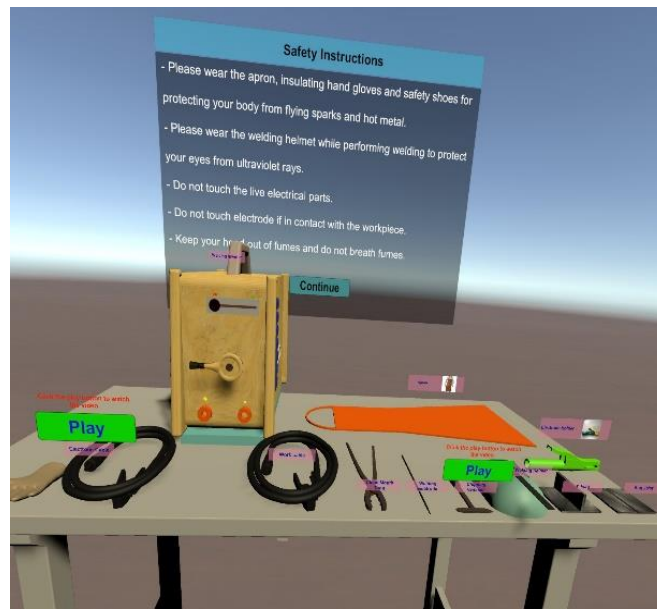
(a) Demonstration of welding components and tools.
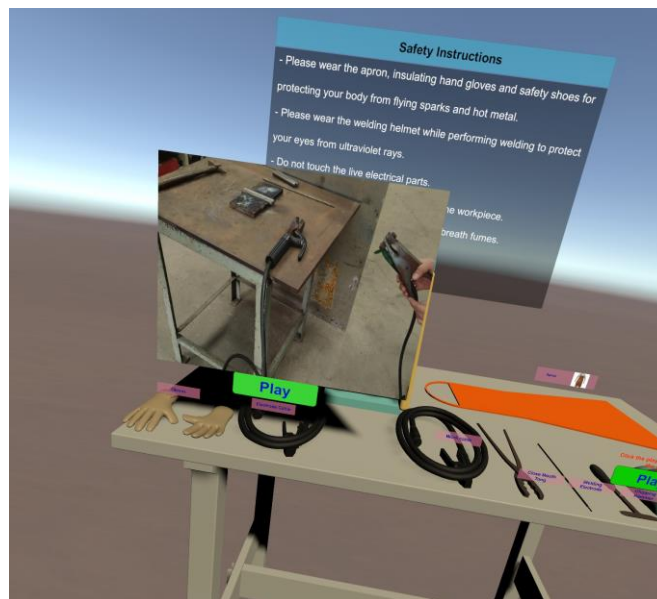
(b) Video showing the usage of the welding tools.

Fig. 3.4. Introduction scene in the VR module.

Step (2): Checking the welding parameters

In this step, users are directed to the parameter page to make sure the values of the welding parameters are correct (Fig. 3.5).

58
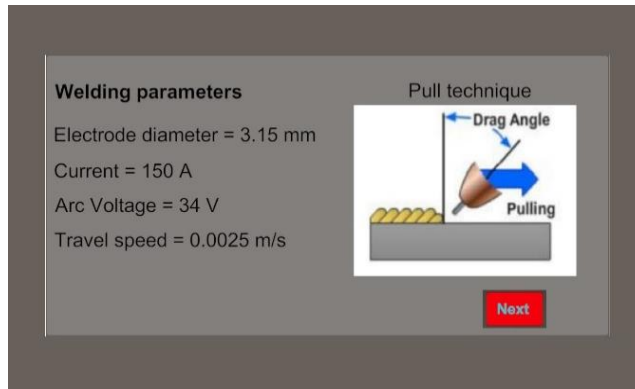
Fig. 3.5. Checking welding parameter values.

Step (3): Mounting the electrode in the electrode holder

A video is played to show the correct way to mount the electrode in the electrode holder and the correct way to weld a butt joint and a tee joint (Fig. 3.6).
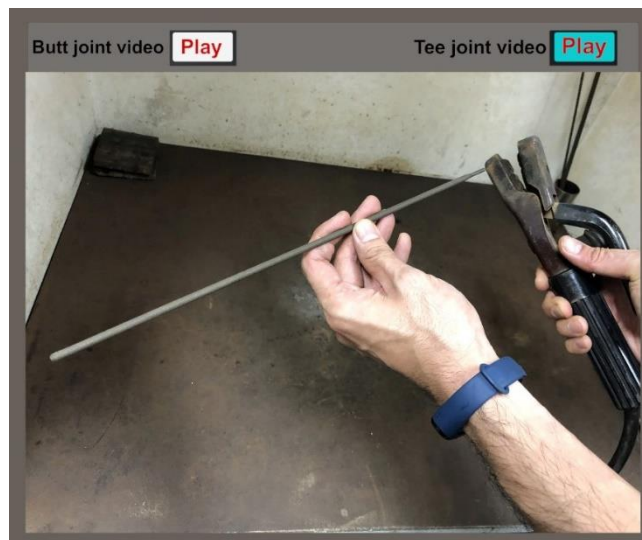
Fig. 3.6. Instructions for mounting the electrode in the electrode holder.
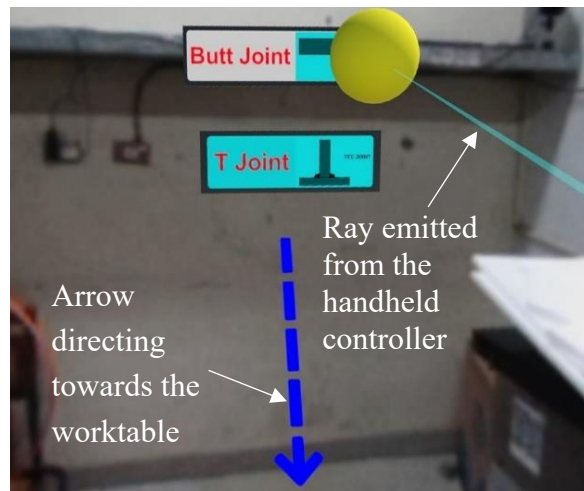
(a) Joint selection using the handheld controller.

(b) Real dummy plate (left) and workpiece in a fixture (right).
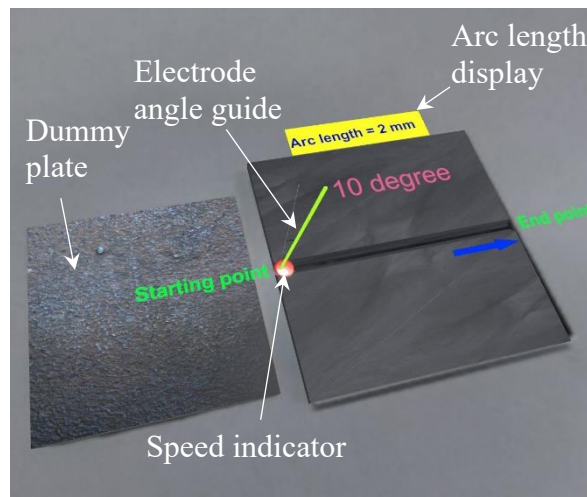
(c) A virtual butt joint augmented on a real workpiece.

Fig. 3.7. Joint selection.

60

Step (4): Placing the butt joint on the worktable

The butt joint icon is selected using a cyan ray emitted from the handheld controller, as shown in Fig. 3.7(a). A yellow sphere appears when the ray hits the UI element. When the UI button is selected, a blue arrow appears and points towards the worktable to guide users to place a real butt joint in a fixture (Fig. 3.7(b)). After that, a virtual joint and a virtual dummy plate are overlaid on the real ones (Fig. 3.7(c)). Visual aids and quantitative guidance, such as speed indicator, arc length, and electrode angle guide, are displayed to assist users to perform the welding.

Step (5): Holding the electrode holder in the right hand

Because one Vive tracker is mounted on the electrode holder, the spatial location of the electrode holder can be acquired. After placing the butt joint, a flickering red arrow appears and points towards the electrode holder, along with text instruction to guide users to hold the electrode holder in the right hand, as shown in Fig. 3.8.

Hold this in your right hand

Fig. 3.8. Holding the electrode holder.

Step (6): Switching on the power source

Users are guided to switch on the power source by dragging the UI slider from left to right using the cyan ray emitted from the handheld controller, as shown in Fig. 3.9.

61

Fig. 3.9. Switching on the welding power source.

Step (7): Holding the helmet in the left hand and placing it in front of the face

Due to the extreme brightness conditions in arc welding, a protective helmet is needed. However, even an experienced welder can hardly recognize the details of the welding components and the surrounding environment while using the protective helmet. Therefore, users are trained to hold a helmet in their left hand during the welding training, as shown in Fig. 3.10.
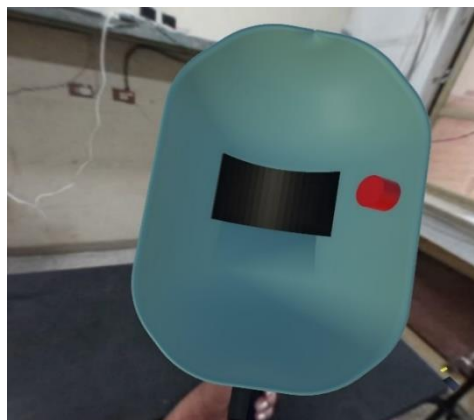
Fig. 3.10. Holding a helmet in the left hand.

Step (8): Scratching the dummy plate to initiate the electric arc

In order to initiate an electric arc, users have to scratch the dummy plate next to the workpiece, as shown in Fig. 3.11. After the arc is initiated, users need to maintain the arc

62

length in the range of 2 mm - 8 mm during the welding. In general, users are advised to maintain an arc length of 2 mm - 3 mm for a good quality weld.
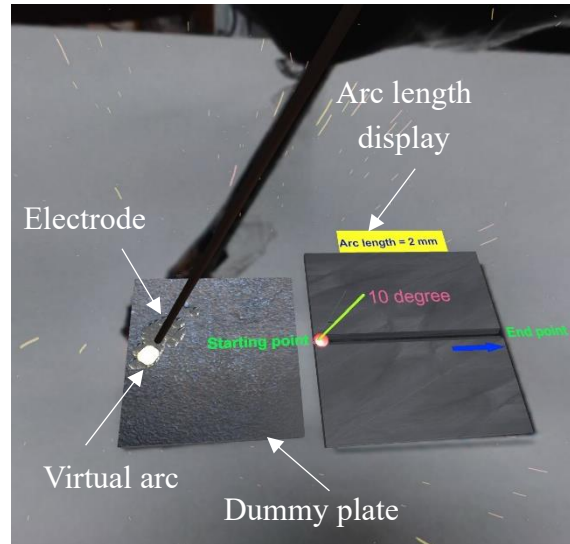
Fig. 3.11. Initiation of the electric arc by scratching the dummy plate.

Step (9): Welding the joint with a specified arc length, travel speed, and incline angle

In this step, users are instructed to perform welding by maintaining a constant arc length, travel speed, and electrode angle with the helmet in the left hand and the electrode holder in the right hand. Three cases are applied based on the arc length maintained by the users, as shown in Table 3.1. If the arc length is less than 2 mm, the simulated magnetic force will be enabled and the electrode will be stuck to the workpiece. In the meantime, thermal feedback and other visual and auditory feedback will be disabled to show the obstruction of the welding process. If the arc length is larger than 8 mm, all feedback will be disabled to show the stop of welding.

63

Table 3.1. Three different welding conditions.

	Case I (Arc length < 2 mm)	Case II (2 mm ≤ Arc length ≤ 8 mm)	Case III (Arc length > 8 mm)
Magnetic force feedback	Enabled	Disabled	Disabled
Thermal feedback	Disabled	Enabled	Disabled
Virtual arc generation	No	Yes	No
Auditory feedback	Disabled	Enabled	Disabled
Speed indicator	Stop	Move	Stop

64
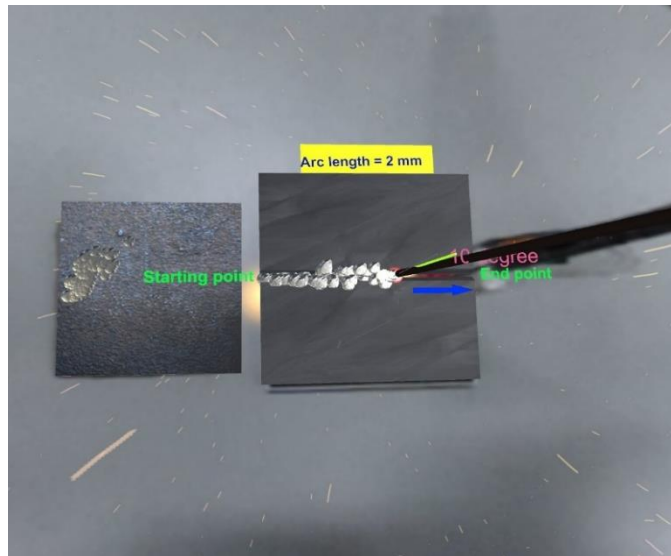
(a) First-person view of case II.

(b) Third-person view of case II.

Fig. 3.12. Practical welding training in MR environment.

If the arc length is kept between 2 mm and 8 mm, electric arc will be properly generated.

Users are guided to perform welding with a constant travel speed of 2.5 mm s^{-1} and a constant

electrode angle of 20°. In this case, magnetic force feedback is disabled, and thermal feedback,

auditory feedback, virtual arc, and speed indicator are enabled to show the continuation of

65

the welding process, as shown in Fig. 3.12. The angle guidance will move along with the speed indicator to guide users to correctly align the electrode throughout the welding.
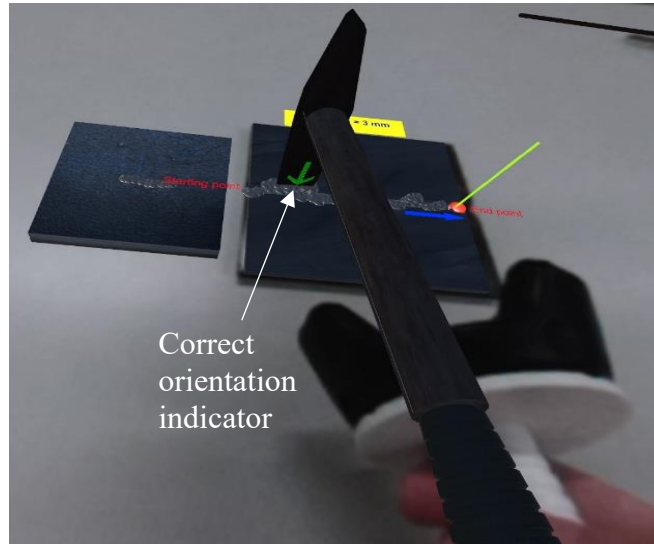
(a) First-person view of removing slag using a chipping hammer.

(b) A third-person view while removing slag

(b) Third-person view of removing slag using a chipping hammer.

Fig. 3.13. Removing slag from the welded joint using a chipping hammer.

Step (10): Removing solidified slag from the welded plates using a chipping hammer

After each pass of welding, users have to remove slag from the welded plates. Figs 3.13 (a) and (b) show a first-person view and a third-person view while removing slag. An arrow with green color is shown on the edge of the chipping hammer to guide users to remove slag in the correct orientation. This step helps users to remember to remove slag after each welding pass.

Step (11): Repeating the same welding procedure for the butt joint for three times

For a butt joint, in order to fill the gap between the two welding plates, at least three welding passes are required.

Step (12): Repeating the same welding procedure for the tee joint for two times

For a tee joint, in order to fill the gap between the two welding plates, at least two welding passes are required.

3.4 User test

A user test was conducted to evaluate the VHXR-based welding training system. Two groups of participants were recruited. The experimental group was trained using the VHXR-based welding training system as per the steps shown in Figs. 3.5 to 3.14 and the control group was trained using an educational video. The following general-purpose questionnaires were used to evaluate the training performance: NASA Task Load Index (NASA-TLX) was for assessing the workload, system usability scale (SUS) was for evaluating system usability, and presence questionnaire (PQ) was for measuring the sense of presence. In addition, a subjective questionnaire was designed and used to evaluate the system performance.

The sample size was calculated by using G*Power software, version 3.1.9.4. At least 30 participants were needed (effect size $d = 0.25$, $\alpha = 0.05$, power $P = 0.8$, correlation among

67

repeated measures = 0.5) (Cohen, 2013). Twenty male and 10 female participants between the ages of 20 to 40 (average = 27, *SD* = 4.23) were recruited from different engineering and science backgrounds without prior experience in MMAW. Participants were randomly divided into the VHXR group and the control group.

Fig. 3.14 is the flowchart of the user test. The VHXR group took 40 minutes to finish the training session. However, the control group took 15 minutes. The VHXR group took longer training time due to the hands-on practice in the MR environment. Participants of the both groups were asked to perform the real welding task in a workshop after twenty-four hours from completing the training sessions.

68
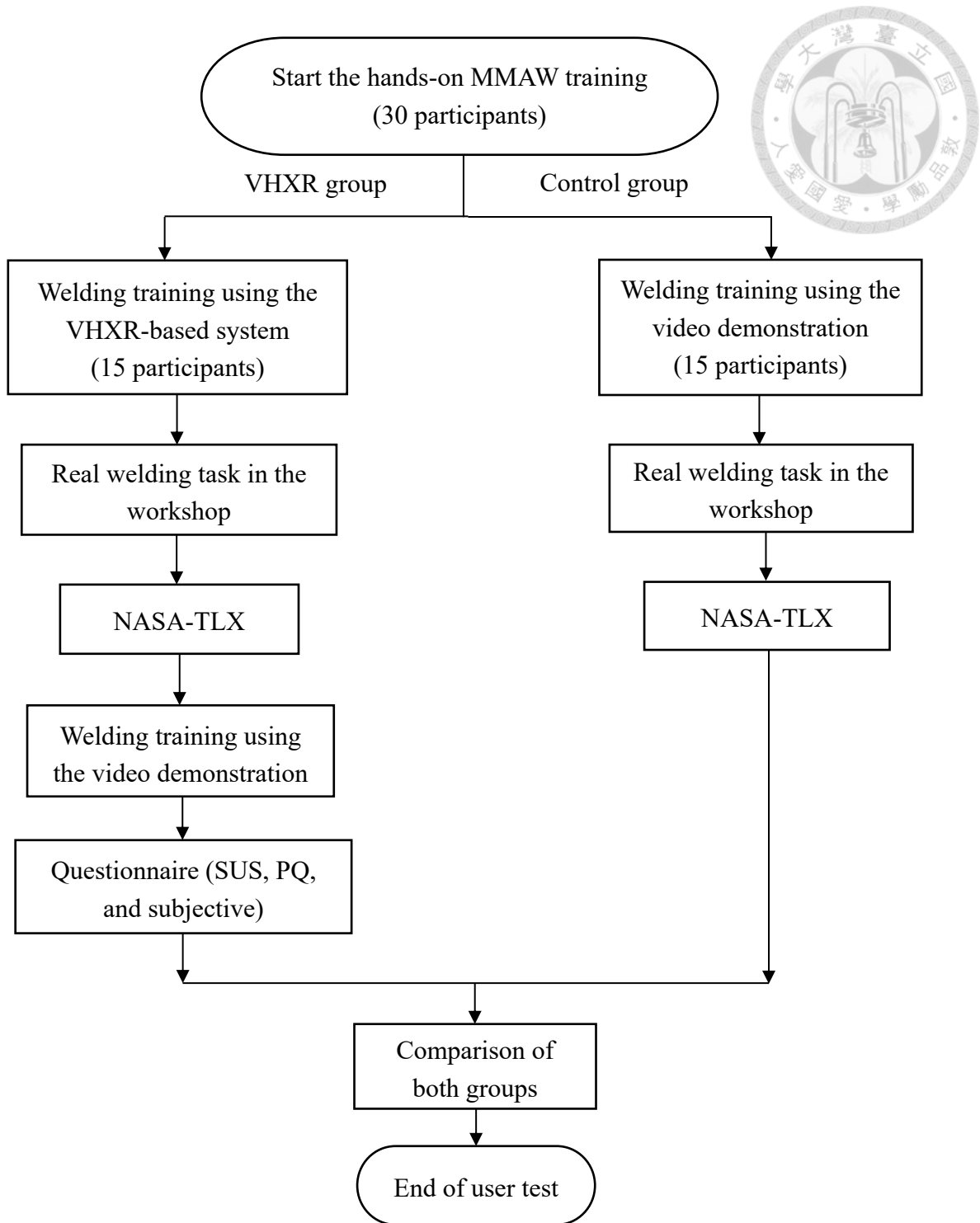
Fig. 3.14. Flowchart of the user test.

(a) Workpiece for butt joint
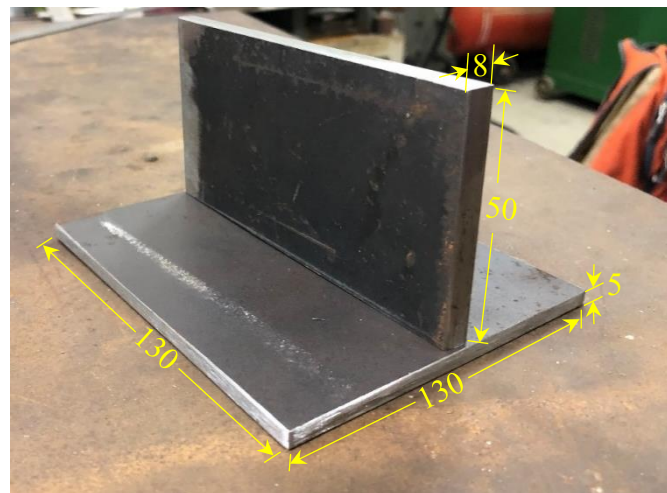
(b) Workpiece for tee joint

Fig. 3.15. Workpieces for the real welding task (all dimensions are in mm).

Participants were asked to follow the correct welding steps to conduct the real welding task. They were allowed to ask for help if they encountered any problems. Each participant was given SS41 low-carbon steel workpieces to weld the butt joint and tee joint, as shown in Figs. 15(a) and (b). An E6013 electrode with 300 mm in length and 3.15 mm in diameters was used. Figure 16(a) and (b) shows the participants from the VHXR group performing the real welding task and removing the slag from the welded joint using a chipping hammer, respectively.

Fig. 3.16 (a) Real welding task and (b) Chip removal

from the welded joint

After the real task, the welding performance of the two groups was compared. Both groups were asked to fill out the NASA-TLX questionnaire to assess the welding workload. After that, participants in the VHXR group also took the video training, and they were asked to fill out the SUS, UMUX, PQ, and subjective questionnaires to compare their experiences in both training environments.

3.5 Results

The training effectiveness was evaluated based on the welding performance and user's responses in the questionnaires.
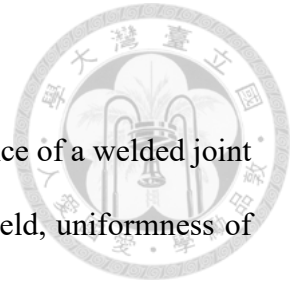
3.5.1 Real welding task

The welding quality was evaluated by a skilled welder. The appearance of a welded joint was given a score between 0 to 100, based on the straightness of the weld, uniformness of the filler material, uniformness of the bead width, and spatter around the weld (Kumar et al., 2018). The welding quality was also evaluated based on the appearance of the weld joints, number of hints, number of mistakes, number of arc extinctions, number of excess welding passes, and total welding time. Table 3.2 shows the best and worst butt joints and tee joints in both groups.

Table 3.2. The best and worse butt joint and tee joint in both groups.

		VHXR group	Control group
Best welding quality	Butt joint		
	Tee joint		
Worst welding quality	Butt joint		
	Tee joint		

72

An overall score $S_{overall}$ was computed to evaluate the performance of each participant using the appearance score (A), number of hints (H), number of mistakes (M), time spent spent on the welding task (T), number of arc extinctions (E), and excess number of passes (P), as shown in Eq. (3.1).

$$S_{overall} = A - (H + M + T + E + P) \tag{3.1}$$

To avoid a negative score, the overall score was normalized between 0 and 1 by applying Eq. (3.2).

$$S_{norm} = (S_{overall} - S_{min})/(S_{max} - S_{min}) \tag{3.2}$$

where S_{min} and S_{max} are the minimum and maximum scores among the participants, respectively. The results are shown in Table 3.3. The normality of the evaluation factors was checked by the Kolmogorov-Smirnov (KS) test using SPSS statistics software. It revealed that the number of mistakes *(M)*, time spent on welding task (*T*), number of arc extinctions (*E*) and excess number of passes (*P*) were not normally distributed, and thus, the Wilcoxon Rank Sum non-parametric tests were performed. In contrast, the appearance score *A* and normalized score S_{norm} were normally distributed, and thus, the *t*-tests were performed. The results revealed that the performance of the VHXR group was significantly better than the control group for most evaluation factors, except for the excess number of passes and the time spent to perform the welding tasks.

Table 3.3. Performance results of the welding task ($\alpha = 0.05$).

Evaluation factors	VHXR group		Control group		
	Mean	SD	Mean	SD	p value
Appearance score (A)	39.8	21.3	20.3	11.8	(**)
Hints given (H)	1.2	1.4	6.6	5.1	(**)
Number of mistakes (M)	1.8	1.8	10.2	5.2	(***)
Total time (s) to finish the welding on both joints (T)	1326	600	1281	543	(n.s.)
Number of arc extinction (A)	5.3	3.9	15.5	14.4	(**)
Number of excess passes (P)	3.2	1.8	8.3	12.3	(n.s.)
Normalized score ($Score_{norm}$)	0.8	0.15	0.5	0.2	(***)

Note: n.s. ($p > 0.05$), * ($p \leq 0.05$), ** ($p \leq 0.01$), *** ($p \leq 0.001$)

3.5.2 NASA-TLX

NASA-TLX assesses the overall workload based on six ratings: mental demand, physical demand, temporal demand, performance, effort, and frustration (Hart, 2006). The rating is between 0 and 100. A lower score implies a lower workload. In this study, NASA-TLX was used to evaluate the subjective workload of the VHXR group and control group in the real welding task. The evaluation results are represented in Table 3.4. The KS test results confirmed the normality of the six ratings. The t-test was performed to check the significance of the results. The results in Table 3.4 reveal that the overall workload of the control group in the real welding task was significantly higher than the VHXR group.

Table 3.4. NASA-TLX results for welding user test.
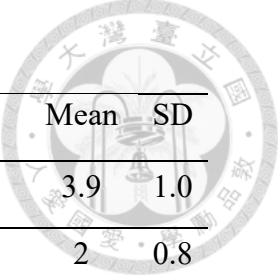
	VHXR group		Control group		
	Mean	SD	Mean	SD	*p* value
Mental demand	48	22.8	53.3	24.1	(n.s.)
Physical demand	48	27.9	66	22.2	(*)
Temporal demand	43.3	25.9	63.3	14.9	(**)
Performance	29.7	81.3	66.7	76.5	(***)
Effort	57	23.3	76	15.0	(**)
Frustration	28.6	19.4	54.6	37.1	(*)
Overall workload	42.4	11.2	57.7	8.4	(**)

3.5.3 System usability scale

Only the VHXR group took the SUS questionnaire. The SUS scale is a reliable tool to evaluate the usability of a system (Brooke, 1996). Scoring is based on a 5-point Likert scale, with 1 as "strongly disagree" and 5 as "strongly agree". Table 3.5 shows the SUS results of the VHXR-based welding training system. The overall SUS mean score is 72, which is higher than the average score of 70 (Borsci et al., 2015; Derisma, 2020).

The factor analysis with varimax rotation revealed three significant factors in the questionnaire. The factor loading of the statements is represented by Table 3.6, which indicates that statements 1, 2, 3, 5, and 6 are aligned with the first factor, statements 4, 7, and 10 with the second factor, and statements 8 and 9 with the third factor. The reliability test was conducted to determine the consistency of the SUS scale. The Cronbach alpha coefficient confirms sufficient reliability with a value of 0.71 above the threshold of 0.7, recommended by Lewis and Sauro (2009).

Table 3.5. SUS evaluation of welding task.

	SUS	Mean	SD
1	I think that I would like to use this system frequently.	3.9	1.0
2	I found the system unnecessarily complex.	2	0.8
3	I thought the system was easy to use.	4	0.8
4	I think that I would need the support of a technical person to be able to use this system.	3	0.9
5	I found the various functions in this system were well integrated.	3.8	0.7
6	I thought there was too much inconsistency in this system.	2.3	1.0
7	I would imagine that most people would learn to use this system very quickly.	4.2	0.8
8	I found the system very cumbersome to use.	1.8	0.7
9	I felt very confident using the system.	4.5	0.6
10	I needed to learn a lot of things before I could get going with this system.	2	0.7
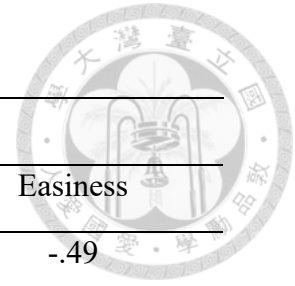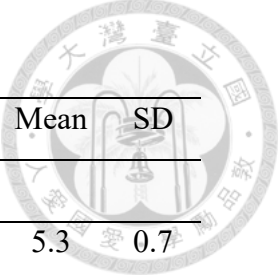
Table 3.6. Factor loading matrix for SUS.

Statement	Factors		
	Usability	Learnability	Easiness
1	**.71**	.34	-.49
2	**.70**	.45	.10
3	**.85**	-.27	-.04
4	-.10	**.83**	.17
5	**.62**	-.31	.45
6	**.68**	-.01	-.47
7	.48	**.54**	.33
8	-.11	.16	**.84**
9	.03	.06	**.85**
10	-.01	**.88**	-.08

Note: Bold values represent the highest correlation factor with the corresponding statement.

3.5.4   Presence questionnaire

The PQ analysis was designed to assess the sense of presence in a virtual environment (Witmer et al., 2005; Witmer and Singer, 1998). The scoring is based on a 7-point Likert scale, with 1 as "strongly disagree" and 7 as "strongly agree". PQ Version 3.0 was used in this study. The questionnaire was composed of four factors: involvement (items 1 to 13), sensory fidelity (items 14 to 17), adaptation/immersion (18 to 25), and interface quality (26 to 28). The PQ evaluation results are shown in Table 3.7. The reliability of the PQ questionnaire was confirmed with Cronbach alpha coefficient of 0.72.

Table 3.7. PQ evaluation results.

	PQ	Mean	SD
	Involvement		
1	How much were you able to control events?	5.3	0.7
2	How responsive was the environment to actions that you initiated (or performed)?	5.4	0.9
3	How natural did your interactions with the environment seem?	5.6	1.3
4	How much did the visual aspects of the environment involve you?	5.7	0.9
5	How natural was the mechanism which controlled movement through the environment?	4.9	1.0
6	How compelling was your sense of objects moving through space?	5.0	1.1
7	How much did your experiences in the virtual environment seem consistent with your real- world experiences?	5.1	1.3
8	How completely were you able to actively survey or search the environment using vision?	5.4	1.1
9	How compelling was your sense of moving around inside the virtual environment?	4.8	1.5
10	How well could you move or manipulate objects in the virtual environment?	5.8	1.0
11	How involved were you in the virtual environment experience?	5.9	0.9
12	Were you involved in the experimental task to the extent that you lost track of time?	5.7	1.3
13	How easy was it to identify objects through physical interaction, like touching an object, walking over a surface, or bumping into a wall or object?	6.0	1.0

78
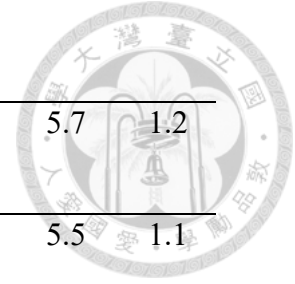
	Sensory fidelity		
14	How much did the auditory aspects of the environment involve you?	5.7	1.2
15	How well could you actively survey or search the virtual environment using touch?	5.5	1.1
16	How closely were you able to examine objects?	6	1.1
17	How well could you examine objects from multiple viewpoints?	5.6	1.1
	Adaptation/Immersion		
18	Were you able to anticipate what would happen next in response to the actions that you performed?	5.4	1.5
19	How quickly did you adjust to the virtual environment experience?	5.0	0.8
20	How proficient in moving and interacting with the virtual environment did you feel at the end of the experience?	5.6	1.0
21	How well could you concentrate on the assigned tasks or required activities rather than on the mechanisms used to perform those tasks or activities?	5.7	1.0
22	How completely were your senses engaged in this experience?	5.7	0.9
23	Were there moments during the virtual environment experience when you felt completely focused on the task or environment?	5.9	1.1
24	How easily did you adjust to the control devices used to interact with the virtual environment?	6.1	0.9
25	Was the information provided through different senses in the virtual environment (e.g., vision, hearing, touch) consistent?	6.0	1.1
	Interface quality		

26	How much delay did you experience between your actions and expected outcomes?	2.1	1.1
27	How much did the visual display quality interfere or distract you from performing assigned tasks or required activities?	3.4	1.8
28	How much did the control devices interfere with the performance of assigned tasks or with other activities?	4.4	1.6

3.5.5 Subjective questionnaire

The subjective questionnaire was designed and used to evaluate users' subjective experience of using the VHXR-based training system. A 5-point Likert scale was used, with 1 as "strongly disagree" and 5 as "strongly agree". Table 3.8 shows the results of the subjective questionnaire. Factor analysis revealed seven Eigenvalues from Cattell's scree plot. The results infer seven significant factors in the questionnaire. However, for better categorization of the statements in a concise way, only three factors were extracted in this study. The statement categorization is represented by the varimax rotation matrix of the factor loadings as shown in Table 3.9. The reliability of the questionnaire was validated with the Cronbach alpha coefficient of 0.83.

Table 3.8. Subjective questionnaire for VHXR welding training.

	Subjective	Mean	SD
1	The VHXR training for MMAW was not very useful for learning.	2.1	1.1
2	VHXR training system was easy to operate.	3.7	0.7
3	VHXR training system replicates the real welding process.	3.8	0.9
4	The welding process in the VHXR system looks very artificial.	3.2	1
5	The welding operation in the VHXR system was accurate.	3.4	0.8
6	The magnetic force at the tip of the electrode resembles the real force of attraction during welding.	3.6	1.2
7	The effect of the heat of the heat lamp makes the VHXR training more realistic.	3.2	1.3
8	The augmented instructions were adequate and intuitive for guidance.	4.1	0.9
9	The user interface was suitable for welding training.	3.8	0.7
10	The user interface was complex and difficult to interact.	2	0.8
11	The VHXR training was more useful than the video training.	4.4	0.7
12	The VHXR training was more interesting than the video training.	4.4	0.6
13	The graphic interface was complex and intrusive.	2.4	1
14	The VHXR training system rapidly enhanced my welding skill.	4	0.5
15	The VHXR training system was helpful for practicing to keep a constant speed of welding.	3.6	1.1
16	The VHXR training system was helpful for practicing to maintain the desired inclination angle of the electrode.	4.0	0.2

81

17	Incorporating the distance sensor in this training made it useful to maintain the desired gap between workpiece and electrode tip	3.7	0.7
18	It was useful to learn welding for the Butt joint and Tee joint.	4.3	0.9
19	It was difficult to understand the instructions to perform the correct welding operation.	1.8	0.7
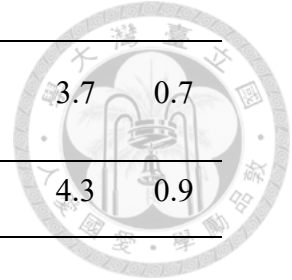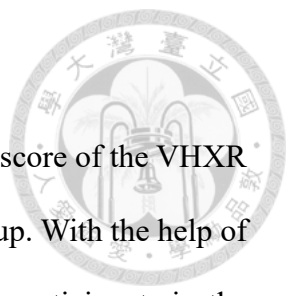
Table 3.9. Factor loadings for subjective questionnaire.

Statement	Factors		
	Usability	Learnability	Realism
1	-.14	.27	**.65**
2	**.94**	-.02	-.14
3	.07	.03	**.33**
4	.03	**.59**	-.02
5	**.58**	-.48	.41
6	**.51**	.18	-.70
7	**.78**	.17	-.15
8	**.81**	.31	.14
9	**.66**	.44	.21
10	.55	.00	**.66**
11	.13	**.66**	-.28
12	-.11	**.78**	.08
13	.26	**.83**	-.03
14	.31	**.73**	.25
15	**.67**	.37	.23
16	.09	**.52**	.04
17	**.73**	.01	.15
18	.32	**.59**	.45
19	.11	.03	**.57**

Note: Bold values represent the highest correlation factor with the corresponding statement.

3.5 Discussion

The results of the real welding task show that the overall normalized score of the VHXR group in the real welding task is significantly higher than the control group. With the help of quantitative guidance for arc length, travel speed, and electrode angle, participants in the VHXR group could practice how to make a uniform and straight welding joint during the training. Therefore, the VHXR group obtained a significantly higher appearance score than the control group in the real welding task. Using the natural welding operation behavior in the training also helped participants to remember the correct steps required in the real welding task. Therefore, significantly fewer hints and mistakes were recorded for the VHXR group than the control group. Moreover, hands-on welding practices under the influence of magnetic force helped participants to keep a proper arc length under a strong magnetic force in the real welding task. The retained muscle memory helped the VHXR group make significantly fewer number of arc extinctions than the control group. However, on the other hand, since the VHXR group paid more attention to controlling the arc length, travel speed, and electrode angle, they took more time in the real welding task, though the difference was not significant.

The NASA-TLX results show that the control group encountered significantly higher physical, temporal, effort, and frustration demands in the real welding task. Although no significant difference was found in the mental demand, the average metal demand of the VHXR group was still lower than the control group. Since the participants in the control group experienced the strong magnetic force and heat for the first time, some of them expressed fear during the real welding. However, since the participants in the VHXR group have already been aware of strong magnetic force and heat during the training, they showed

84

less workload in the real welding task. The performance of the VHXR group was also significantly better than the control group.

The SUS results indicate that the system's usability was appropriate and acceptable. In this study, the factor analysis reveals that the SUS questionnaire can be classified into three significant categories: usability, learnability, and easiness with satisfactory results. Despite the system having satisfactory usability, learnability, and easiness, it still requires further improvements to enhance the usability. For example, because most participants used the VHXR system for the first time, they showed a neutral response to the question that they needed the support of a technical person to be able to use the system. Therefore, clearer and more self-explanatory user interface is needed in the future.

In the PQ evaluation, all the questions in the involvement factor received positive responses with scores above 4. It indicates that providing natural welding user interface with haptic feedback and visual feedback enhanced participants' attention and involvement in the welding training. For the sensory fidelity factor, participants' responses indicate that realistic haptic, auditory, and visual feedback enabled them to sense different aspects of the VHXR environment. Participants could be better involved in the VHXR environment and examine the virtual objects. For the adaptation/immersion factor, participants agreed that they could quickly and easily be adapted to the VHXR environment, and they perceived themselves being immersed in the VHXR environment. Participants were able to acquire a continuous stream of experiences. They could proficiently conduct the welding task using a natural welding behavior and concentrate on the assigned tasks with the help of haptic, auditory, and visual effects. Finally, for the interface quality factor, participants' responses reveal that the training system was quick to respond to their actions. Participants could focus on the assigned

tasks without any distraction, and they could practice the welding technique in a natural way. However, question 28 reveals that the control devices slightly interfered with the performance of the assigned tasks. It might be because some of the participants did not correctly use the handheld controller to interact with the UI elements.
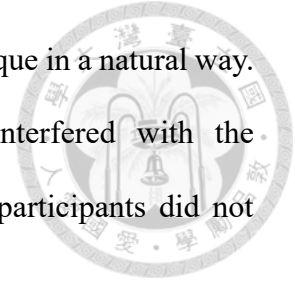
Based on the factor analysis results, the subjective questionnaire was categorized into three factors: usability, learnability, and realism. The factor analysis indicated the acceptable usability, learnability, and realism of the system. In addition to this, questions 3, 6, and 7 confirm that the electromagnetic force and heat lamp make the VHXR-based training more realistic. The natural user interface greatly enhances users' welding skills. However, some users found it difficult to operate the VHXR system, because the VHXR system was purposefully designed with several difficulties to make the users be familiar with the obstructions in the real welding environment. Although the magnetic force and the heat generated by the heat lamp in the VHXR environment were not as strong as in the real welding, participants still could learn the welding techniques in a similar interruptive way. The tracking of the virtual objects needs to be more accurate. The graphical representations need to be more realistic. In addition, a more precise and stable distance needs to be obtained to maintain a constant arc length.

Participants also provided some remarks as follows: "The welding training system was very useful to practice the steps required to perform in real welding.", "The magnitude of the magnetic force can be increased to make it exactly the same as the real welding", "The thermal feedback provided by the heat lamp built a natural welding environment, which helps me not to be afraid of heat during the real welding" and "The welding training system can be taken to the next level if the tracking accuracy can be improved".

86

3.6 Conclusion

Welding is a manufacturing process that needs highly manual skills. It requires a large amount of resources to train novice welders. In addition, the hazardous environment often frightens the users. This study developed an interactive VHXR-based training system with realistic haptic and visual feedback to train novice welders with correct welding steps in a safe and realistic environment. The system has been validated by a user study. The results show that the VHXR system significantly improved the performance of novice welders, and the natural user interface enabled them being well adapted to the real welding environment. Future work will focus on developing a more self-explanatory user interface, increasing the magnetic force feedback and thermal feedback, and the accuracy of the distance detection.
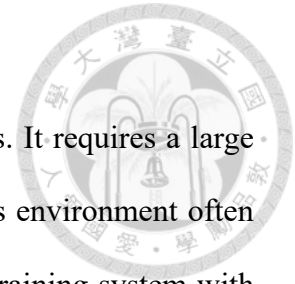
3.7 Appendix A

3.7.1 Calculation of magnetic force

To produce magnetic force in the electrode used in the AR system, insulated copper wire is winded around the electrode rod of medium carbon steel.

According to Ampere's law, the magnetic field can be obtained by using Eq. (A.1).

$$B = \mu_0 \left(\frac{N}{L} \right) I \tag{A.1}$$

Where N is the number of turns of the coil, L is the length of the coil and I is the current flowing through the coil. The current flowing through the coil is evaluated by using Ohm's law.
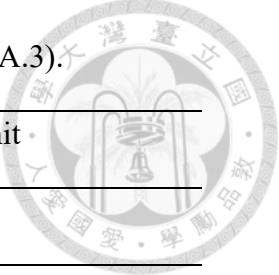
$$V = IR \tag{A.2}$$

The amount of current is increased by increasing the voltage capacity of batteries by using three batteries joined in series. The magnetic force on the tip of the electrode rod is evaluated by using Eq. (A.3).

$$F = \frac{\pi r^2 B^2}{2\mu_0} \left(\frac{\mu_m}{\mu_0} - 1 \right) \tag{A.3}$$

Where r is the radius of the electrode, μ_0 is the permeability of free space and μ_m is the permeability of electrode rod material.

Table A.1. Parameter values used in Eqs. (A.1), (A.2) and (A.3).

Parameters	Values	Unit
Number of turns (N)	610	-
Diameter of wire of coil (d)	0.405	mm
Diameter of electrode (core) rod	6	mm
Voltage of battery (V)	3.7	V
Number of batteries (i)	3	-
Permeability of free space (μ_0)	$4\pi\times10^{-7}$	N/A^2
Permeability of electrode rod material (μ_m)	1.26×10^{-4}	N/A^2
Resistivity of copper wire (ρ)	1.68×10^{-8}	Ω·m
Length of coil (L)	30	mm

Table A.2. Calculated results.

Calculated results	Values	Unit
Current in coil (I)	3.233	A
Magnetic field (B)	0.0825	Tesla
Magnetic force (F)	7.6	N

The magnitude of the induced magnetic force due to the electromagnet was $F = 7.6$ N

obtained from Eq. (A.3) and magnetic field $B = 0.0825$ T obtained from Eq. (A.1).

Kumar and Debroy (2003) computed the electromagnetic force components in x, y and z

directions in a workpiece of size 10 cm × 4 cm × 1 cm where the thickness of the workpiece

89

is represented in z direction:

$$F_x = 0.34 \text{ N/cm}^3, \ F_y = 0.35 \text{ N/cm}^3 \text{ and } F_z = 0.27 \text{ N/cm}^3$$

The electromagnetic force components for 40 cm³ volume of the workpiece are given as:

$$F_x = 13.6 \text{ N}, \ F_y = 14 \text{ N and } F_z = 10.8 \text{ N}$$

Therefore, the resultant electromagnetic force:

$$Fr \ = \ \sqrt{F_x^2 + F_y^2 + F_z^2} \ = 22.3 \text{ N}$$

90

Chapter 4 FEM visualization of manual metal arc welding process using an interactive mixed reality-based user interface
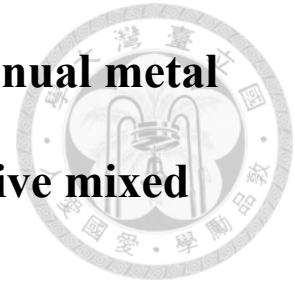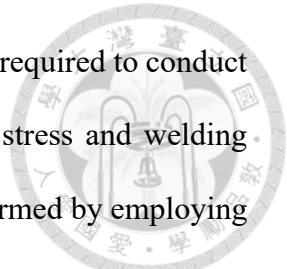
Welding is extensively used in manufacturing industries for various applications. However, due to the non-uniform temperature distribution on the welded plates during the welding process, residual stress is induced, which significantly affects the fatigue strength. In addition, the non-uniform expansion and contraction of the weld and surrounding base metal cause structural distortion. The distortion affects the final product quality due to a deformed shape resulting in reduced productivity. Therefore, the structural analysis of the welded component is critically important. In this work, an integrated simulation system is developed to predict and display the finite element analysis (FEA) results in a mixed reality (MR) environment in real time for the manual metal arc welding (MMAW) process. Since the numerical simulation of welding using FEM requires a large amount of computation time, the gradient boosted regression tree (GBRT) machine learning (ML) algorithm is employed to predict the FEA results. In order to train the GBRT model, a total number of 216 FEA simulations were performed with three input parameters (welding current, voltage, and travel speed) and two output variables (residual stress and deformation). The developed GBRT model is used to predict the residual stress and deformation results in real time. An interactive MR interface was developed to display the results for enhanced visualization and interpretation. The interactive MR interface can also help users to learn the relationship

between the welding parameters and the induced residual stress and deformation.

4.1 Introduction

Welding is one of the most preferred and widely used joining processes for the assembly and manufacturing of various types of components due to its versatility, simplicity, and reliability. Among the vast range of welding processes, manual metal arc welding (MMAW) is the most prevalent welding process that is used in several applications, for instance, maintenance, repair, construction of steel structures, and industrial fabrications. During the welding process, rapid thermal heating and cooling take place around the welded joint due to the movement of the heat source, which causes uneven temperature distribution in the weld plates. The thermal expansion around the welded joint is constrained by the low-temperature region away from the weld zones. As a result, residual stress and deformation are produced in the weld plates (Park et al., 2002). The residual stress can significantly affect fatigue behavior during cyclic loading (Barsoum and Barsoum, 2009). Besides residual stress, welding distortion is an undesirable phenomenon, which causes adverse effects on the accuracy of assembly, external appearance, and structural integrity (Maddox, 2000). The remedies for distortion require an additional cost and result in delays in schedules on the production line. Therefore, in light of the aforementioned reasons, predicting and controlling the residual stress and welding distortions are highly essential.
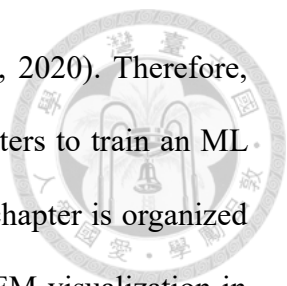
The quality of welded structure in terms of residual stress and analysis can be evaluated using two methods. First, the experimental measurement method, and second, the finite element method (FEM). The first method requires the real welding process to be performed in the workshop and experimentally measure the induced stress and deformation. On the contrary, the second method requires a numerical computation using FEM software (Smith

and Smith, 2009). The FEM analysis can save the expenditure and effort required to conduct the experiments for weld quality evaluation. Therefore, to predict the stress and welding distortions in welding, numerical computational analysis is usually performed by employing FEM (Deng and Murakawa, 2008; Pamnani et al., 2016). FEM plays a vital role in numerical computation and analysis of mathematical models of physical phenomena. Some of the notable software tools mostly used by professionals to perform FEM analysis include COMSOL Multiphysics, ABAQUS, and ANSYS.

The advances in mixed reality (MR) technology provide a more immersive environment to help users observe and visualize virtual content with an intuitive and interactive interface. The MR technology enhances users' perception of the real world with the superimposition of computer-generated digital information such as graphics, texts, and audio over the real world environment, and also allows the user to interact with and manipulate physical and virtual objects (Doolani et al., 2020). If finite element analysis (FEA) results can be overlaid on the corresponding real objects in real time, users could observe the changes in the residual stress and deformation in an MR environment. To evaluate the FEM results, an interactive MR interface can facilitate users to examine and comprehend the results with 3D visualization, and also allow them to examine the critical regions of the FEM results from different orientations.
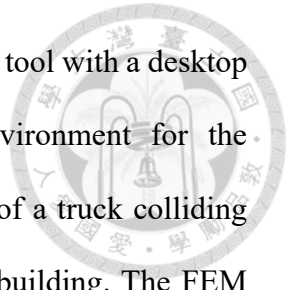
However, the large computations of the FEA simulations make it difficult to achieve real-time stress and deformation evaluations. The main objective of this study is to develop an MR-based user interface (UI) to examine and visualize the induced residual stress and deformation on the real weld plates in real time by employing a machine learning (ML) algorithm. The most influential controlling parameters of welding on residual stress and

deformation are welding current, voltage, and travel speed (Xie et al., 2020). Therefore, welding current, voltage, and travel speed are used as the input parameters to train an ML model and predict the residual stress and deformation. The rest of this chapter is organized as follows. Section 4.2 presents the reviews of the studies related to FEM visualization in extended reality (XR) and ML applications. Section 4.3 describes the system overview. Section 4.4 provides the details of FEM modeling of the MMAW process. Section 4.5 provides the development procedure of the prediction model. Section 4.6 describes the implementation of the MR interface with FEM results. Section 4.7 provides a discussion. Finally, the conclusion and future work are offered in Section 4.8.
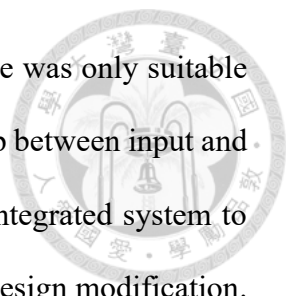
4.2 Related work

Different approaches have been developed to render FEA analysis results in an XR environment which includes virtual reality (VR), augmented reality (AR) and MR. For example, Ryken and Vance (2000) examined the challenges of applying VR techniques for analyzing FEA stress results of a tractor lift arm using a stereo projection to provide a 3D view of the assembly. Users could examine the resultant changes in the stresses by changing the shape of the part. The number of mesh elements was reduced by simplifying the geometric model to achieve the real-time results. Their study is limited to static structural analysis problems. Hambli et al. (2006) replaced FEM calculations by applying an artificial neural networks (ANN) to generate real-time deformations of a tennis ball and a racket during the impact. The predicted force feedback can be used to recreate the impact using a haptic glove in a VR environment. Torano et al. (2008) used FEM calculations, fuzzy logic, and neural networks (NN) to develop a numerical model to predict the static stress and displacement of a longwall coal mining installation against different operating conditions. The predicted

94

response is shown to the users using the VR modeling language (VRML) tool with a desktop computer screen. Lee and El-Tawil (2008) presented a virtual environment for the visualization of FEA results for two applications: the crash simulation of a truck colliding with a rigid wall, and the collapse simulation of a 8-story steel frame building. The FEM results were converted into a VRML geometric format to display in a virtual environment. However, the conversion required considerable amount of time, due to which, no real-time FEM results could be rendered in VR.
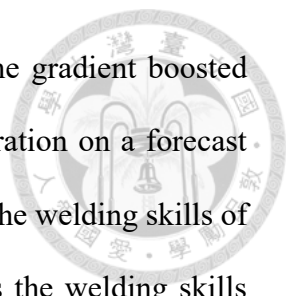
Besides applying VR technology in FEA analysis, some prior studies have also demonstrated the usage of AR for FEA results visualization in various applications. Yavuz Erkek et al. (2021) investigated the application of AR to provide in situ visualization of the modal analysis of an aluminum impeller. The FEA simulation results of the modal analysis were superimposed on the real impeller for enhanced comprehension. The AR application was implemented on a mobile phone screen. Huang et al. (2015) integrated a sensor measurement and a real-time FEA simulation of structural analysis of a step ladder by superimposing FEA results on real-world objects for enhanced user perception and data exploration in an AR-based environment. Their system is limited to stationary, linear and simple structural analysis problems. Fukuda et al. (2019) presented an AR-based methodology for intuitive visualization of indoor thermal distribution for building renovations. The real scene was augmented by the computational fluid dynamics (CFD) results to provide a better interpretation of the indoor thermal environment. However, it took time to change CFD parameters for visualization purpose. Turkan et al. (2017) introduced an AR-assisted pedagogy by using pre-calculated results using analytical equations for teaching structural analysis. The AR interface allowed students to interactively change loading

conditions and observed the reaction in real time. The proposed interface was only suitable for the basic problems of which the analytical equation of the relationship between input and output is known. Ong and Huang (2017) introduced an FEM and AR integrated system to allow users to apply virtual loads and add virtual structures to simulate design modification. Users could examine the critical regions with FEA results superimposed on the prototype. The proposed approach might lead to considerable time lag in dealing with complex and large scale models.

Prior studies have provided insight into the benefits of integrating FEM simulations with AR and VR. However, in these reported applications, no complex multiphysics FEA applications have been found. Examples of multiphysics problems include thermo-mechanical coupling, electric field structural coupling, thermal fluid structural coupling, and fluid flow mass transfer coupling. The numerical modeling of the welding process is a thermo-mechanical multiphysics problem that requires two types of physics modules namely, the heat transfer module and the solid mechanics module. Due to the drawbacks of FEA simulations, such as a large amount of data entry and longer execution time, real-time FEA result display in AR or VR for a multiphysics problem becomes impossible.
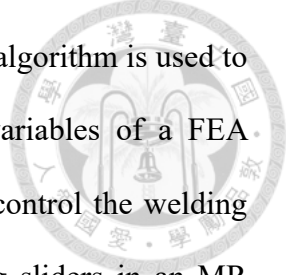
Apart from using ML methods for VR and FEA integration, many researchers have adopted ML approaches for data prediction in various applications. Ahmed et al. (2018) implemented an AI-based model to predict weld bead geometry in order to mitigate the efforts of professional welders and engineers to select input parameters by trial-and-error. Two different AI models were employed, namely multilayer perceptron NN (MLP-NN) and radial basis function NN (RBF-NN), for comparing their performance in terms of accuracy. Persson et al. (2017) applied a non-parametric ML approach to overcome the challenge of

96

optimally utilizing the weather-dependent renewable energy source. The gradient boosted regression tree (GBRT) model was trained to predict solar power generation on a forecast horizon of one to six hours. Kumar et al. (2018) utilized NN to evaluate the welding skills of trainee welders by acquiring the voltage during the welding process as the welding skills depend on the ability to maintain a constant arc length. The NN was used to grade the skills of welders based on arc length values maintained by welders. Sarkar et al. (2021) proposed an ML method to predict the transient temperature in the submerged arc welding process. A multi-linear regression (MLR) model was trained to predict the maximum temperature. Kostić and Vasović (2015) presented a prediction model using a three-layer back-propagation feed-forward ANN to predict the compressive strength of concrete.

The aforementioned literature reviews addressed the importance of integrating FEA in AR and VR. Although some of the studies applied ML to produce real-time FEA results in VR environments, they only applied for stationary and simple solid mechanics problems. Apart from this, the implementation of ML to predict FEA results in an AR environment is merely reported. In AR-FEA integrated studies, most of the applications are only restricted to stationary and linear structural analysis with simple and small-scale model geometry (Huang et al., 2015). Besides this, some studies applied ML for data prediction for a variety of applications, but no multiphysics analysis predictions have been reported. The finite element modeling of residual stress and deformation analysis in the welding process is a multiphysics problem, which is usually more complicated and time-consuming. So far, to the best of our knowledge, no literature has been found regarding FEA results predictions for multiphysics problems in AR or VR environments.

This research focuses on computing and displaying FEM analysis results of a

97
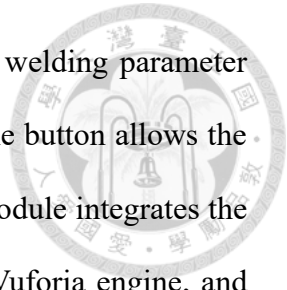
multiphysics problem in MR environments in real time. The GBRT ML algorithm is used to develop the interrelationship between input parameters and output variables of a FEA simulation. The main contribution of this chapter is to allow users to control the welding parameters including welding current, voltage, and travel speed, using sliders in an MR environment to visualize the FEA results overlaid on the real weld plate in real time and learn the relationship between the welding parameters and residual stress and deformation.

4.3 System overview

The system will allow users to vary welding parameters to visualize the induced residual stress and deformation on the real weld plate in an MR environment. To achieve this goal, the COMSOL Multiphysics version 4.4 finite element computation package is used with essential boundary conditions (BCs) and necessary input parameters. The pre-computed FEA results are used to train a GBRT model to produce output results in real time. The predicted residual stress and deformation from the GBRT model are superimposed on the real weld plate for enhanced comprehension and visualization in an immersive MR scene.

The MR system is developed using C# programming language on the Unity3D game engine and ran on a 3.00 GHz Intel Core i7-9700F processor, 64 GB RAM, and 6.0 dedicated GPU memory. The Microsoft Hololens 2 is used as a display device. To develop the MR scene, the Mixed Reality Toolkit (MRTK) and Vuforia engine are used.

The system architecture of the proposed MR system is illustrated in Fig. 4.1. The system is implemented in two parts: the MR module and the FEA pre-computation module. In the MR module, the real weld plate is captured by the front camera of HoloLens 2. The detection and tracking of the weld plate are established by utilizing the Vuforia model target. The user interaction module contains a virtual panel with various types of UI components including

98

slider, button, and text from MRTK. Users can continuously change a welding parameter value by moving a slider on a track by directly grabbing it. Likewise, the button allows the user to trigger an action by pressing it with bare hands. The rendering module integrates the virtual objects with the real-world scene with the help of MRTK and Vuforia engine, and subsequently, overlays FEA results on the real weld plates.

In the FEA pre-computation module, the FEM analysis module generates time-dependent residual stress and deformation results. Two physics namely, heat transfer and solid mechanics, are applied to compute the residual stress and deformation in the welding process. The input-output data from the FEA module is utilized to train the GBRT regression model to predict the residual stress and deformation results. To display the predicted FEA results in an MR environment based on the user-inputted welding parameters in real time, a Lookup Table is used, which is generated by the data produced by the GBRT model.
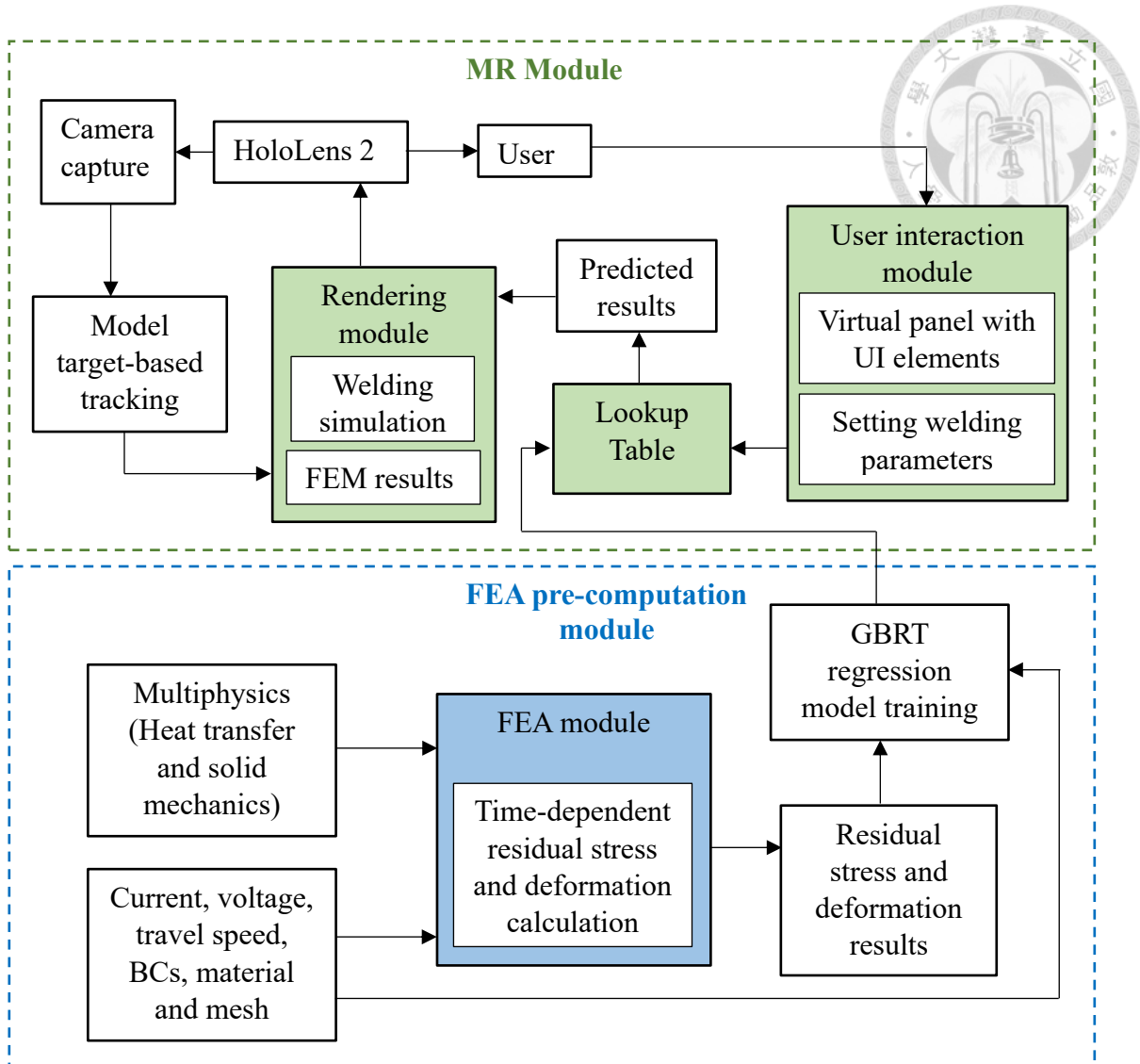
Fig. 4.1. System schematic.

4.4 Finite element modeling of the welding process

The quality of a welded structure is influenced by the induced residual stress and structural deformation, which negatively affect the fatigue strength as well as the final shape of the welded structure. FEM can be used to analyze different types of residual stress and structural deformation problems. For the FEM modeling of the MMAW process in COMSOL, the global system of equations obtained from the assembly of the elemental stiffness equations is represented by Eq. (4.1).

100

$$[K]\{d\}-\{F^t\}=0 \qquad (4.1)$$

where $[K]$ is the global stiffness matrix, $\{d\}$ is the global displacement vector, and $\{F^t\}$ is the global thermal load vector. $[K]$ and $\{F^t\}$ can be represented by $[K^e]$ and $\{F^e\}$, respectively.

$$[K]=\sum_{e=1}^{n}\left[K^e\right] \qquad (4.2)$$

$$\{F^t\}=\sum_{e=1}^{n}\{F^e\}^t \qquad (4.3)$$

where $[K^e]$ is the elemental stiffness matrix and $[F^e]$ is the elemental thermal load vector. Since the stress is proportional to the strain in the structure, the equivalent stress is calculated using the global displacement vector. The global displacement vector is computed by using Eq. (4.1).

In this study, the MMAW process is simulated in COMSOL software to analyze residual stress and deformation in a butt-welded plate made of ASTM A36 carbon steel. The dimension of the weld plate is 130 mm × 130 mm × 5 mm. The temperature-dependent thermo-mechanical properties of ASTM A36 carbon steel are detailed in Table 4.1 (Jeyakumar and Christopher, 2013), which is defined in the materials section of COMSOL. Since the welding process is carried out by supplying heat produced by the electric arc, the weld plate undergoes thermal expansion, that in turn induces thermal stress in the weld plate due to the non-uniform distribution of the temperature. Therefore, the finite element analysis is conducted by applying heat transfer and solid mechanics physics modules. Heat transfer analysis generates temperature distribution results on the weld plate, which is taken as an input for the solid mechanics analysis. Consequently, the residual stress and deformation results are obtained from the solid mechanics analysis.

Table 4.1. Temperature-dependent thermal and mechanical properties of the weld plate (Jeyakumar and Christopher, 2013).

	Thermal properties			Mechanical properties			
Temperature (K)	Specific heat (J/(kgK))	Thermal conductivity (W/(mK))	Density (kg/m³)	Young's modulus (GPa)	Poisson's ratio	Thermal expansion coefficient (10^{-6} /K)	Yield stress (MPa)
273	480	60	7880	210	0.280	1.10	380
373	500	50	7880	200	0.285	1.15	340
473	520	45	7800	200	0.290	1.20	315
673	650	38	7760	170	0.310	1.30	230
873	750	30	7600	80	0.330	1.42	110
1073	1000	25	7520	35	0.330	1.45	30
1473	1400	28	7300	15	0.360	1.45	20
1573	1600	37	7250	10	0.380	1.45	18
1823	1700	37	7180	10	0.390	1.45	15

4.4.1 Thermal analysis

In the finite element model, the moving heat source is applied perpendicular to the weld plate surface. The governing differential equation (Deng and Kiyoshima, 2012) for heat conduction in solids is given by Eq. (4.4).

$$\frac{\partial}{\partial x}\left(k\frac{\partial T}{\partial x}\right)+\frac{\partial}{\partial y}\left(k\frac{\partial T}{\partial y}\right)+\frac{\partial}{\partial z}\left(k\frac{\partial T}{\partial z}\right)+q=\rho c\frac{\partial T}{\partial t} \qquad (4.4)$$

Where k is the thermal conductivity [W/mK], T is the temperature [K], ρ is the density of material [kg/m³], c is the specific heat capacity [J/kgK], q is the heat generation rate supplied in welding [W/m³], x, y and z are the coordinates [m] and t is time [s]. The thermal conductivity and specific heat capacity are defined as per Table 4.1 during the FEM

simulation in COMSOL. The heat transfer module internally applies Eq. (4.4) which is a built-in equation in COMSOL. The heat generation rate is calculated by Eqs. (4.5) to (4.8), which are manually defined as an analytical function under the definitions section in COMSOL.
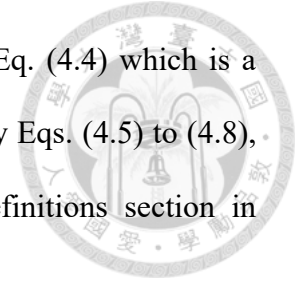
The heat source model is important in the heat transfer analysis of the welding process because it determines the reliability of calculated results. The double-ellipsoidal volumetric heat source model proposed by Goldak et al. (1984) is adopted for the modeling of the welding arc, where the width and depth of the penetration of weld beads are mapped with the major and minor axes of the ellipse, respectively. The analytical solution of the double-ellipsoidal heat source model is expressed as follows.

For the front heat source:

$$q_f = \frac{6\sqrt{3}Qf_f}{\pi\sqrt{\pi}a_f bc} e^{-3\left(\frac{x^2}{a_f^2}+\frac{y^2}{b^2}+\frac{z^2}{c^2}\right)} \tag{4.5}$$

For the rear heat source:

$$q_r = \frac{6\sqrt{3}Qf_r}{\pi\sqrt{\pi}a_r bc} e^{-3\left(\frac{x^2}{a_r^2}+\frac{y^2}{b^2}+\frac{z^2}{c^2}\right)} \tag{4.6}$$

$$f_f + f_r = 2 \tag{4.7}$$

$$f_f = \frac{2a_f}{a_f + a_r}, \quad f_r = \frac{2a_r}{a_f + a_r} \tag{4.8}$$

where q_f and q_r are the power density distributions inside the front and rear ellipsoids [W/m³], Q is the heat power [W], x, y, and z are the coordinates of the double-ellipsoid model aligned with the weld line [m], a_f, a_r, b and c are associated to the features of the welding heat source, which are mapped with length in the front and back halves of the weld the weld width, the weld width and depth of penetration [m]. f_f and f_r denote the fractions of the heat power deposited in the front and rear halves of ellipsoids. These parameters were obtained

103

from the experimental analysis conducted by Nezamdost et al. (2016). These parameters are

detailed in Table 4.2. The heat power Q is expressed in terms of welding current I [ampere],

voltage V [volt], and thermal efficiency η. It is defined in the parameters section of COMSOL.

$$Q = \eta IV \tag{4.9}$$

Heat loss due to convective heat transfer for all the surfaces of the weld plate is considered

in the thermal analysis using Newton's law as expressed in Eq. (4.10) and is inherent in the

heat transfer module of COMSOL. It is responsible for the cooling of the weld plate.

$$q_c = -h(T_{sur} - T_0) \tag{4.10}$$

where h is the heat transfer coefficient [W/m^{2}K], and T_{sur} and T_o are the current and initial

temperature of the weld plate. Eq. (4.10) is responsible for the cooling of the welded

structures due to the convective heat transfer.

Table 4.2. Goldak model parameters used in FEA analysis (Nezamdost et al. (2016).

a_f (mm)	a_r (mm)	b (mm)	c (mm)	f_f (mm)	f_r (mm)	η (mm)
5	23	5	5.5	1.64	0.36	0.65

4.4.2 Solid mechanics analysis

The temperature history calculated by the thermal analysis is used as input information

to conduct the mechanical analysis. During the actual welding process, the material

undergoes elastic, plastic, and thermal strain, which is represented by three components ε^e,

ε^p, and ε^{th}, respectively. The total strain is shown as follows.

$$\varepsilon^{total} = \varepsilon^e + \varepsilon^p + \varepsilon^{th} \tag{4.11}$$

The elastic strain is calculated by using Hooke's law with temperature-dependent

Young's modulus and Poisson's ratio. Thermal stain is modeled using the temperature-

104

dependent coefficient of thermal expansion. The plastic strain is calculated by employing von Mises yield criterion. These temperature-dependent properties are used by COMSOL from Table 4.1 to calculate residual stress and deformation. The boundary condition in the mechanical analysis is taken into consideration by assuming the welding zone to be fixed as shown in Fig. 4.2, which restricts the movement of the fixed surface in the x, y and z directions.
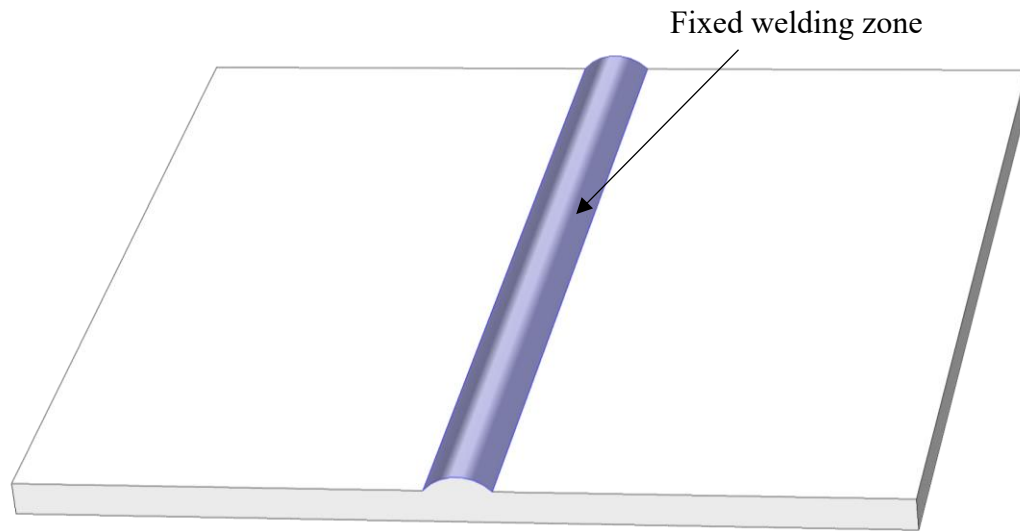
Fig. 4.2. Boundary condition for mechanical analysis.

The finite element mesh model is represented in Fig. 4.3, in which 3D tetrahedral elements with four nodes are used. A fine mesh division is adopted for the welding zone and its vicinity with a large temperature gradient, while gradually courser mesh division is adopted away from the welding zone to maintain accuracy and reduce the computation time. The mesh model comprises a total number of 8912 elements with 3346 triangular elements, 250 edge elements, 12 vertex elements, and 1783 nodes. In this study, the FEA simulations are carried out by considering the welding current range of 70 to 200 A, the voltage range of 20 to 35 V, and the travel speed range of 0.7 to 10 mm/s based on the prior research on

105

MMAW (Mahapatra et al., 2006; Nagesh and Datta, 2002; Saha and Mondal, 2017).
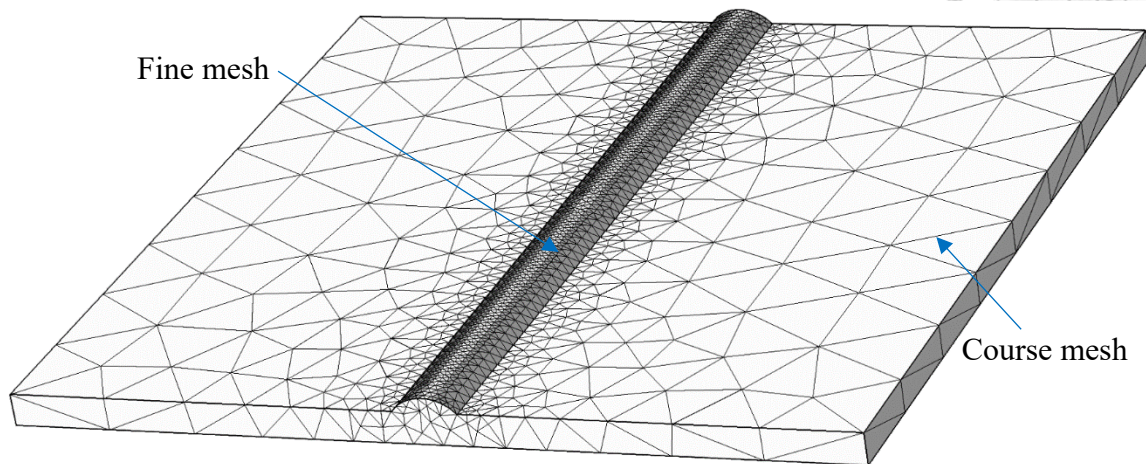
Fig. 4.3. The finite element mesh model.

4.4.3   FEM analysis results

The finite element computational procedure is developed by considering the real welding conditions. The MMAW process is simulated using FEM with three passes of welding, and the computation is continued after the third pass until the final temperature of the welded structure reaches the ambient temperature. For one combination of the input variables with the welding current of 122 A, the voltage of 26 V, and the travel speed of 0.7 mm/s, the results from FEM computation revealed that the induced von Mises residual stress and the distortion in the weld plate were 557 MPa and 0.36 mm. The maximum computational time required by the FEA simulation was 7 minutes and 12 seconds. The distortion of the weld plate is implied by the total displacement in the FEA. The residual stress and deformation results are shown in Figs. 4.4 and 4.5, respectively. The stress distribution is non-uniform with a large stress concentration in the welding region, which is attributed to the non-uniform temperature distribution. The non-uniform thermal expansion and contraction of the weld plate cause angular deformation in it, which is symmetrically distorted on both sides. Fig. 4.6 represents

106

the angular deformation of the weld plate along its length perpendicular to the welding direction.
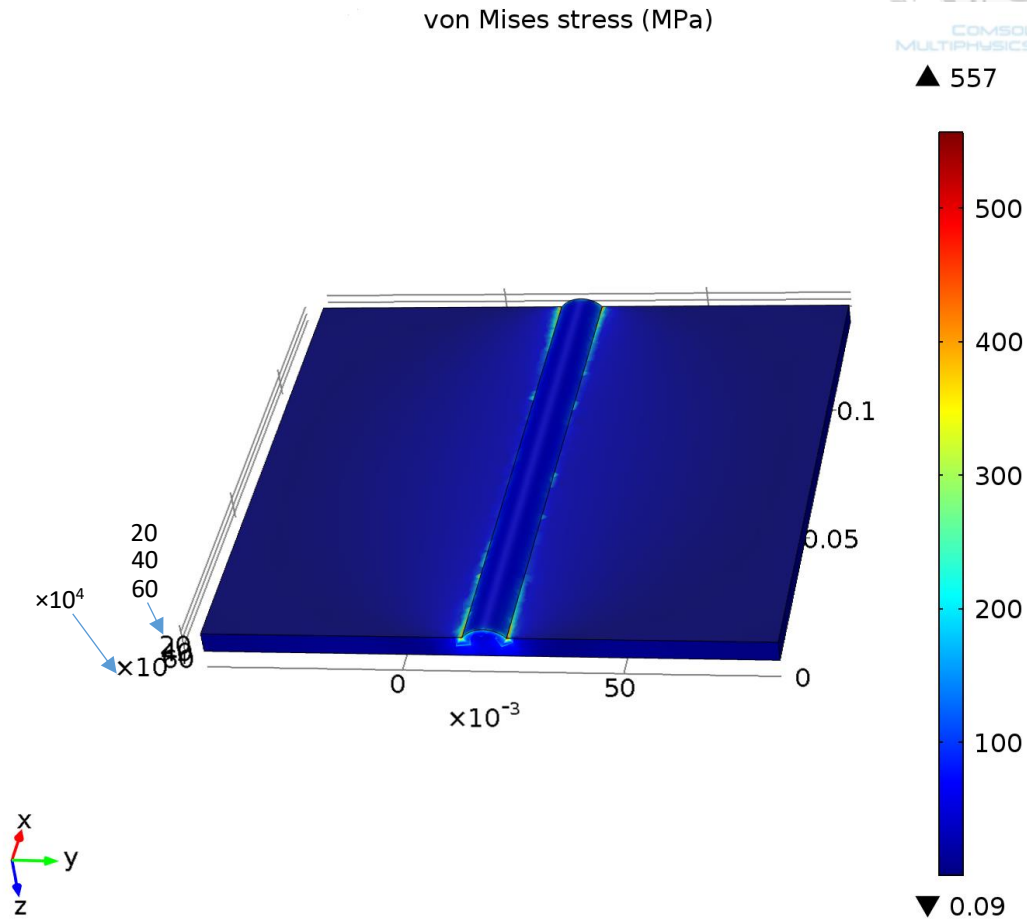
Fig. 4.4. Residual stress distribution on the weld plate.
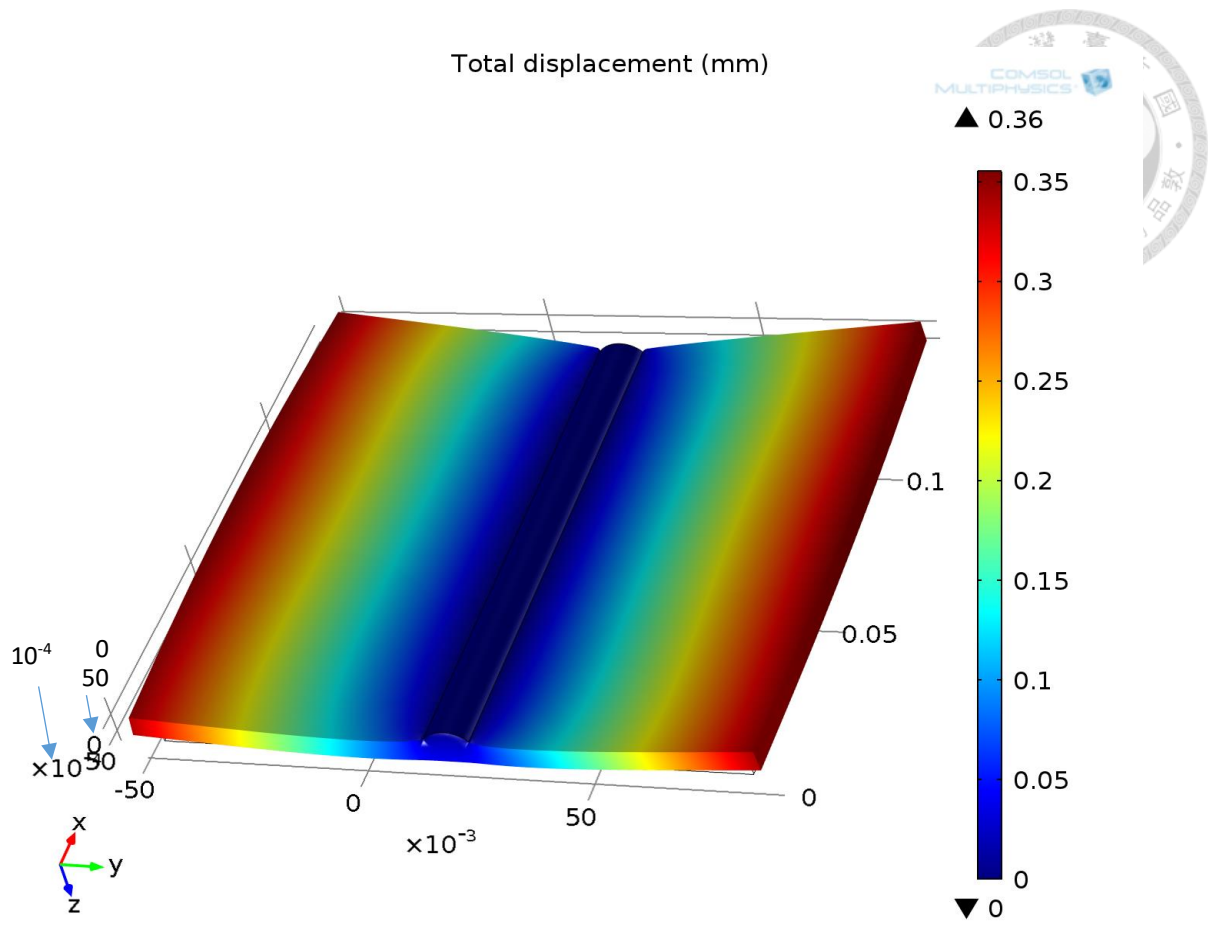
Fig. 4.5. Distortion in the weld plate after the welding.
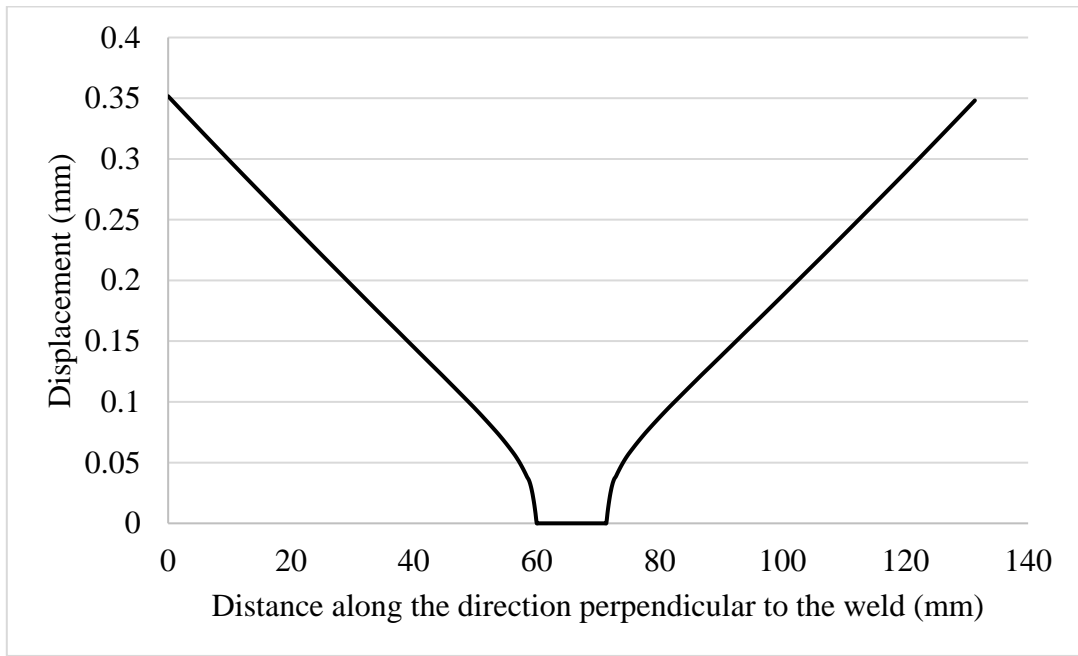
Fig. 4.6. Angular deformation of the weld plate.

108
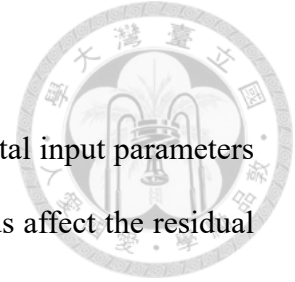
4.5 Development of the prediction model

It is noticeable that welding current, voltage, and travel speed are vital input parameters in the MMAW process to significantly affect the heat input rate and thus affect the residual stress and deformation. Therefore, it is essential to study the effects of the input welding parameters on weld quality. In this study, the working ranges of the selected input and output variables are shown in Table 4.3. The ranges of the input variables are divided into five intervals. The six-level full factorial design method is used to obtain the number of combinations for the FEM simulated results. With six levels and three parameters, a total number of 216 FEA simulations are conducted to obtain the residual stress and deformation results.

Table 4.3. Working range of the input and output variables.

Parameters	Units	Level 1	Level 2	Level 3	Level 4	Level 5	Level 6
Welding current	A	70	96	122	148	174	200
Voltage	V	20	23	26	29	32	35
Welding speed	mm/s	0.7	2.56	4.42	6.28	8.14	10
Residual stress	MPa	332	88	85.9	90.8	83.9	78
Displacement	mm	0.12	0.025	0.024	0.025	0.024	0.022

In the application of the ML algorithms for data prediction, the most essential step is to determine the interrelationship between the independent (input) and dependent (output) variables. The interrelationship between input-output variables can assist in choosing a suitable regression model. The scatter plots between input and output variables are used to determine the linearity of the data, which revealed that the travel speed is non-linearly

109

dependent on stress and deformation, while the welding current and voltage are linearly dependent on the response value as shown in Fig. 4.7. The MATLAB regression learner was used to determine the most suitable ML algorithm based on the prediction performance. The GBRT algorithm showed the best performance results among the other ML algorithms in terms of accuracy with the largest value of the coefficient of determination (R^2) and the least root mean square error (RMSE), as shown in Table 4.4. As a result, the prediction model for residual stress and deformation was developed using the GBRT algorithm. Another advantage of employing the GBRT algorithm is that it is more suitable for small datasets (Liang et al., 2020) and it can also avoid overfitting problem.
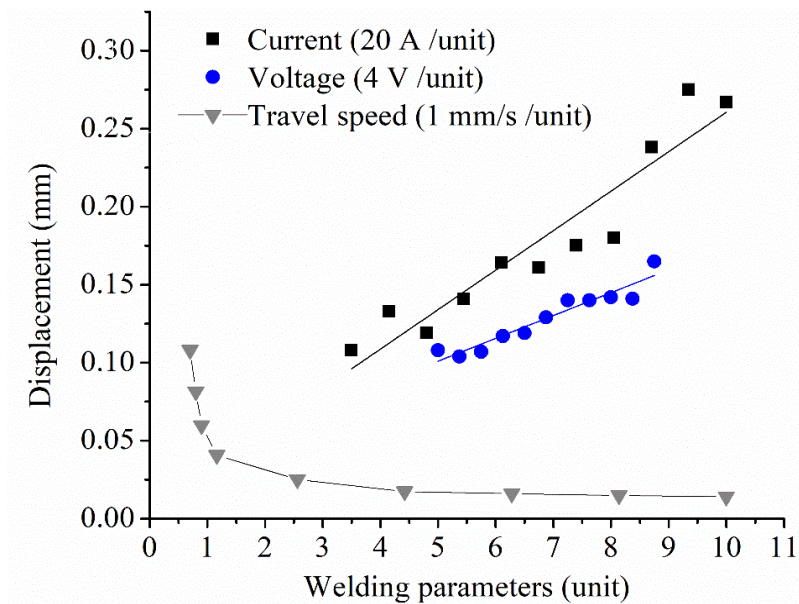
Fig. 4.7. The scatter plot between input variables and response

110

Table 4.4. Comparison of GBRT performance with different ML algorithms.

ML algorithms	R^2	RMSE
GBRT	0.95	1.93×10^{-5}
Linear regression	0.44	7.06×10^{-5}
Stepwise linear regression	0.46	6.93×10^{-5}
Fine tree	0.93	2.48×10^{-5}
Support vector machine	0.56	6.24×10^{-5}
Gaussian process regression	0.01	9.42×10^{-5}
Neural networks	-109.8	9.94×10^{-4}

4.5.1 Gradient boosted regression tree

The GBRT algorithm was initially developed by Friedman (2001). The GBRT technique is an enhanced form of the traditional decision tree approach, which combines the statistical technique called boosting aiming to improve model accuracy by aggregating a set of weak models to form a single strong model. In this study, the input variables are current, voltage and travel speed, and the output variables are residual stress and displacement. Since the residual stress is directly proportional to the displacement according to the FEM results, only displacement has been considered as an output variable while implementing the GBRT. The relationship between residual stress and displacement is expressed by Eq. (4.12).

$$s = 3 \times 10^6 d + 5.37 \tag{4.12}$$

Where s is the residual stress and d is the displacement obtained from the FEM simulation.

In the GBRT algorithm, the decision trees are sequentially built by minimizing the

residuals, which is the difference between the target displacement value and the predicted displacement value. Thus, the prediction is optimized by adding a new decision tree at each step to minimize the residual. The final predicted value of displacement is the weighted sum of predicted displacements given by previous models, which is implied by Eq. (4.13).

$$F(I)=F_1(I)+F_2(I)+...+F_m(I) \tag{4.13}$$

where $F(I)$ is the predicted displacement by the final regression model, which is the function of input variables. Three input variables are represented by I in Eq. (4.13). The GBRT method in the form of ensemble of decision trees is illustrated in Fig. 4.8. The training dataset is the collection of observations of the form (I, O), which is denoted by $\{(I_1, O_1), ..., (I_n, O_n)\}$. In this study, the input feature is denoted by vector $I = (u, v, w)$, where u, v and w represent the current, voltage and travel speed, respectively, while the output feature is denoted by vector $O = (d)$. The number of observations (samples) of the training data is $n = 216$.

With the given training data set, the model is initialized by considering the mean of target displacement values in the first iteration. In the next step, the residual is calculated with the initial predicted displacement value from the first iteration. After this, a decision tree (weak learner) is built, which predicts the displacement value by learning simple decision rules inferred from the dataset in the second iteration. The internal nodes of the decision tree contain an if clause of input variables to make the decision and the leaf nodes contain the predicted values. Furthermore, the new residual is calculated by subtracting the predicted value obtained by the current decision tree from the target displacement value. from the prediction results from the previous decision tree. The iterations are continued until the number of iterations matches the number of estimators (number of decision trees) specified by the hyperparameter, which eventually minimizes the residual error. The final regression

112

model provides the prediction results of displacement, which is the aggregation of predictions provided by weak models. To avoid the overfitting problem, the predicted value given by the previous decision tree is multiplied by the learning rate η.

Training data set
$\{I_i, O_i\}_{i=1}^n$ $(n = 216)$

Voltage	Current	Speed	Displacement

I_i
(Input columns)

O_i
(Output column)

Model M_1

Iteration 1 [ ] Initial prediction
$\hat{O}_1 = F_1(I)$

Residual $= O - \hat{O}_1$

Model M_2

Iteration 2 [ ] +

$\hat{O}_2 = F_2(I)$

Residual $= O - (\hat{O}_1 + \eta\hat{O}_2)$

Model M_3

Iteration 3 [ ] + +

$\hat{O}_3 = F_3(I)$

Residual $= O - (\hat{O}_1 + \eta\hat{O}_2 + \eta\hat{O}_3)$

Iteration m Model M_m

[ ] + + + $\cdots$ +

Ensemble prediction $\hat{O} = (\hat{O}_1 + \eta\hat{O}_2 + \eta\hat{O}_3 + \cdots + \eta\hat{O}_m)$
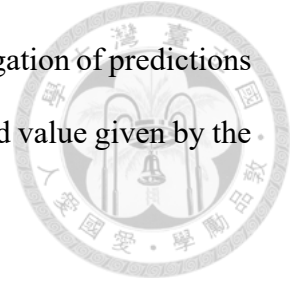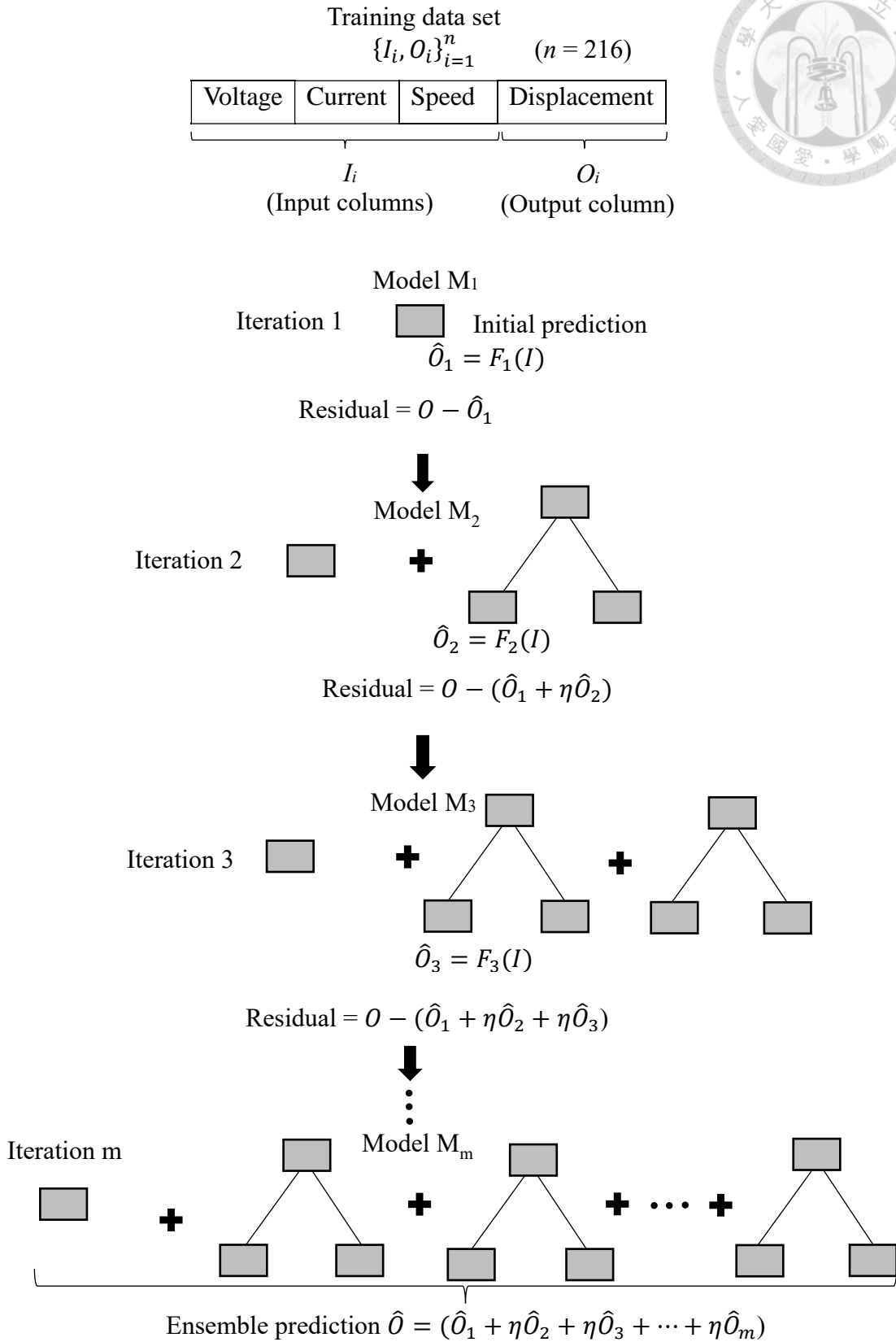
Fig. 4.8. Visual representation of GBRT algorithm.
114

During data analysis for ML, it is important to evaluate the correlation among the variables of the training data set. The data with non-correlated input variables can provide faster learning of the algorithm and high interpretability (Gupta and Singh, 2021). Thus, the Pearson correlations are used to determine which parameter has the highest impact on each other. The correlation between all parameters is illustrated in Table 4.5. The correlation coefficient value from 0 to 1 or -1 represents how strongly the variables are correlated with each other (Schober et al., 2018). It is confirmed by the Pearson correlation matrix that the input parameters, welding current, voltage, and travel speed are not correlated with each other. However, the input parameters are correlated with stress and displacement.

Table 4.5. Pearson correlation between the parameters employed in the GBRT model.

	Current	Voltage	Travel speed	Displacement	Residual stress
Current	1	0.00	-0.00	0.17	0.17
Voltage	0.00	1	-0.00	0.09	0.09
Travel speed	-0.00	-0.00	1	-0.65	-0.65
Displacement	0.17	0.09	-0.65	1	1
Residual stress	0.17	0.09	-0.65	1	1

The training data with 216 samples were split into 70% of the training dataset and 30% of the testing dataset. Furthermore, choosing the best hyperparameters for the GBRT model is also necessary. The hyperparameters of the GBRT model such as the number of estimators (number of trees), maximum depth, and learning rate are responsible for the model performance (Yang et al., 2020). The optimal hyperparameters are determined by validating the GBRT model with the range of 1-200 for the number of estimators, 2-8 for maximum

115

depth, and 0.01-0.9 for the learning rate. Subsequently, the optimal value for the number of estimators was 30, the maximum depth was 8, and the learning rate was 0.1. For these hyperparameters, the GBRT model was able to predict FEA results in real time. However, if the number of estimators and the maximum depth is increased, the GBRT model takes longer time to predict the results.

4.5.2 Model performance evaluation

The performance of the developed GBRT model in terms of accuracy of the estimated predictions is evaluated by using statistical metrics, namely normalized root mean square error (NRMSE) and R^2 which are shown in Eqs. (4.14) to (4.16).

$$NRMSE = \frac{RMSE}{\hat{O}_{max} - \hat{O}_{min}} \tag{4.14}$$

$$R^2 = 1 - \frac{\sum_{i=1}^{n}(O_i - \hat{O}_i)^2}{\sum_{i=1}^{n}(O_i - \bar{O}_i)^2} \tag{4.15}$$

where,

$$RMSE = \sqrt{\frac{1}{n}\sum_{i=1}^{n}(O_i - \hat{O}_i)^2} \tag{4.16}$$

where n is the number of samples, O_i is the ith observed value, $\hat{O}_i$ is the ith predicted value, $\bar{O}_i$ is the mean of observed values, $\hat{O}_{max}$ is the maximum predicted value and $\hat{O}_{min}$ is the minimum predicted value. RMSE is the standard deviation of the prediction error which characterizes the deviation of prediction errors from the line of best fit. The RMSE is normalized by using NRMSE, which facilitates the comparison between datasets with different scales. The R^2 value indicates the proportion of variance in the response explained

116

by the regression model. The higher value of R^2 represents a better fit of data with the model. Ideally, the R^2 value should be as close as possible to 100%. The performance evaluation metrics for residual stress and displacement prediction have been illustrated in Table 4.6. The prediction results using the GBRT model for residual stress and total displacement versus observed data are shown in Fig. 4.9(a) and (b) where x axes represent the observed stress and displacement values while y axes represent predicted stress and displacement values.

(a)
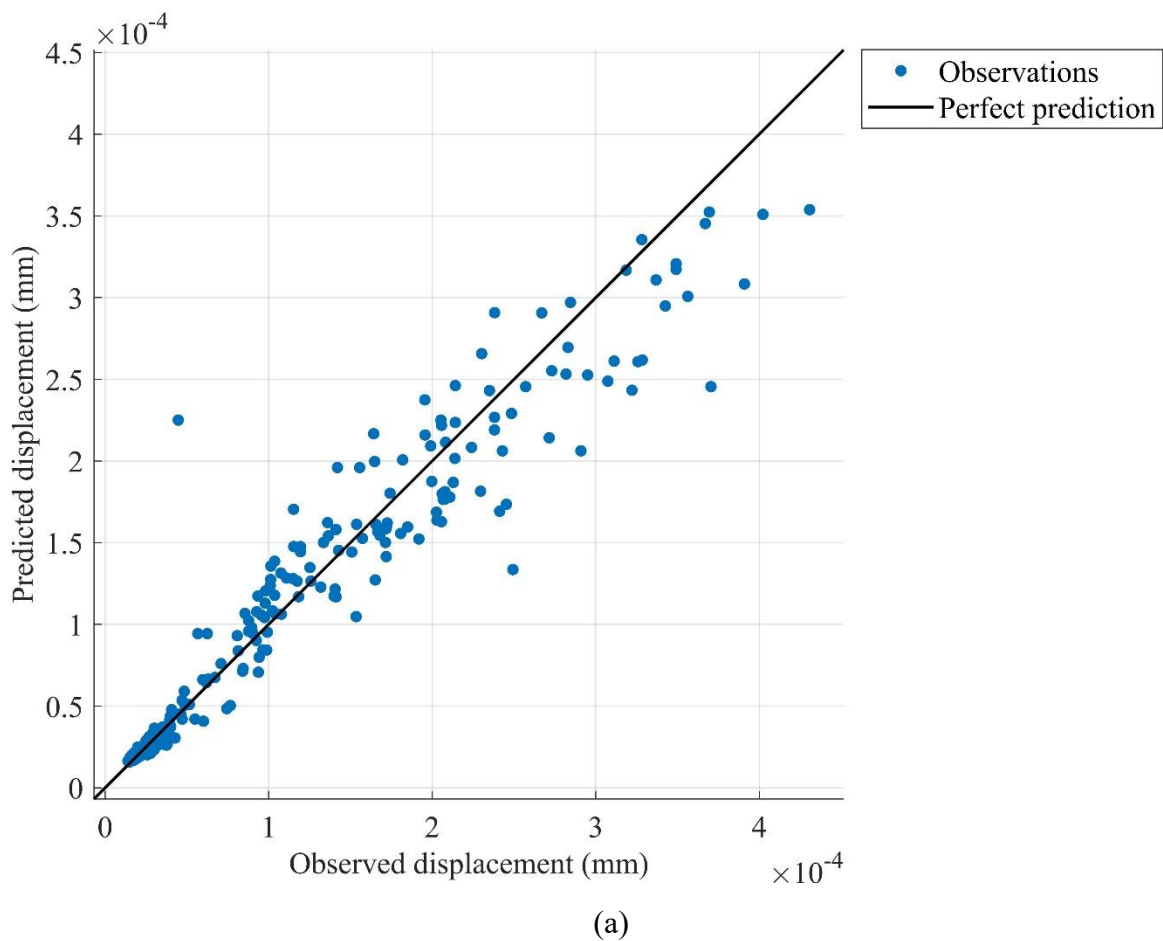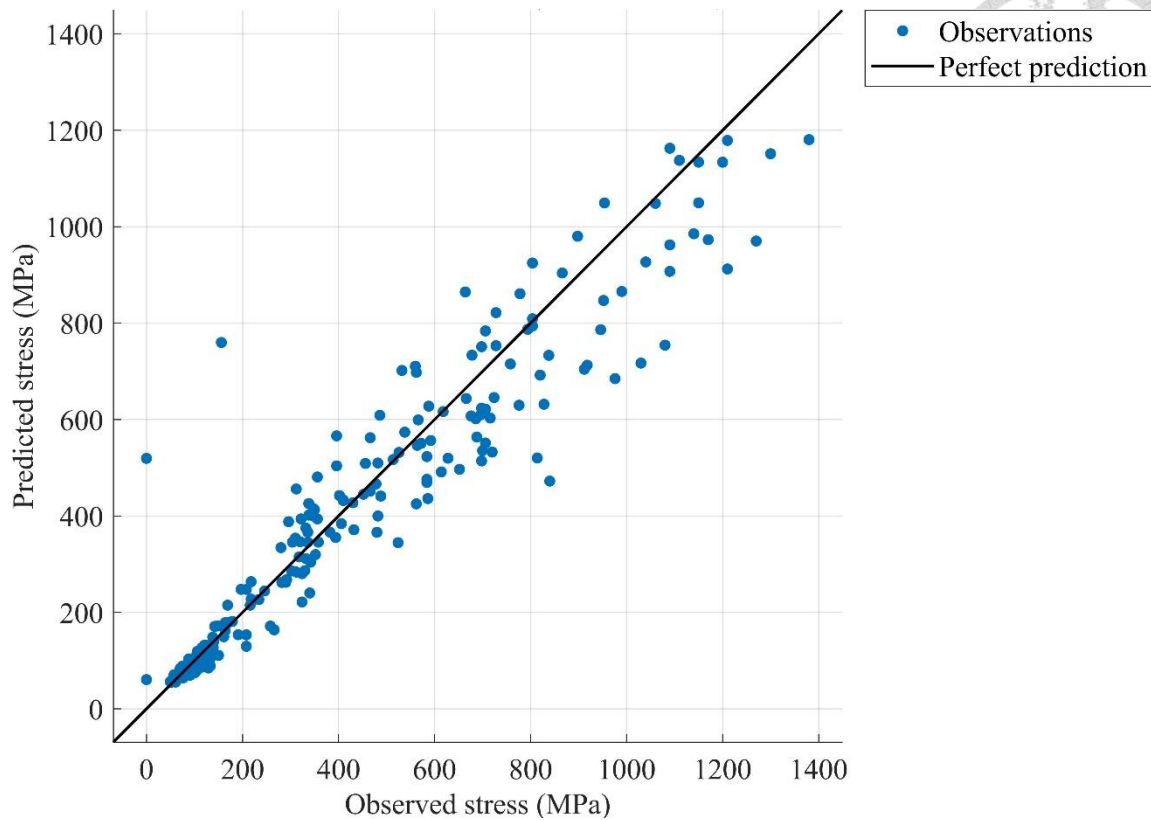
(b)

Fig. 4.9. GBRT model prediction results for (a) displacement and (b) stress.

Table 4.6. Performance metric of residual stress and displacement prediction.

	Residual stress (MPa)	Total displacement (mm)
NRMSE	7.69×10^{-2}	7.62×10^{-2}
R^2	0.95	0.95

4.5.3 GBRT implementation in Unity3D

For scientific computing, data science, and ML, Python is the most preferred programming language, which includes a large number of useful add-on libraries (Raschka, 2015; Raschka et al., 2020). However, this study uses C# programming language to implement the GBRT algorithm in order to develop an MR user interface and display the

118

predicted results in an immersive environment using the Unity3D platform. To access the ML algorithms, the ML.NET cross-platform ML framework was used. The .NET libraries and required plugins were imported from the NuGet package manager. The C# code was written by importing all required ML libraries and plugins to the Unity3D assets. The GBRT regression model was generated as a Simulink model with MDL file format. This developed code was able to predict residual stress and deformation results on the Unity3D platform in VR environments.

The User interface for FEA results visualization in VR is shown in Fig. 4.10. The user can set the welding process parameters using the virtual sliders and can visualize the FEA results immediately produced by the GBRT regression model. However, the MDL format was not supported in Hololens 2. Therefore, in order to provide an interactive and intuitive MR user interface in Holoens2 for FEA results visualization, a Lookup Table was used to produce the FEA results in the MR environment. The Lookup Table was built by generating output data using GBRT model. The input variables were divided into 10 intervals and total number of 1331 output data were produced from GBRT model with 11 levels of input variables. Thus, the Lookup Table consists of 1331 rows of corresponding known input and output data with displacement values in the output colum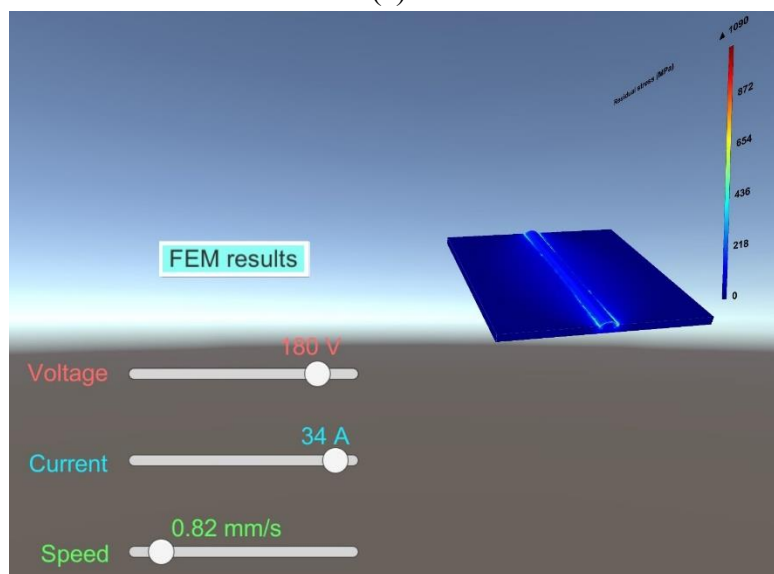n. To estimate the displacement values lying between the known data points of the output column, a trilinear interpolation method was adopted to map the input values to output values. The Lookup Table used for trilinear interpolation is represented by three input and one output column as shown in Table 4.7.

119
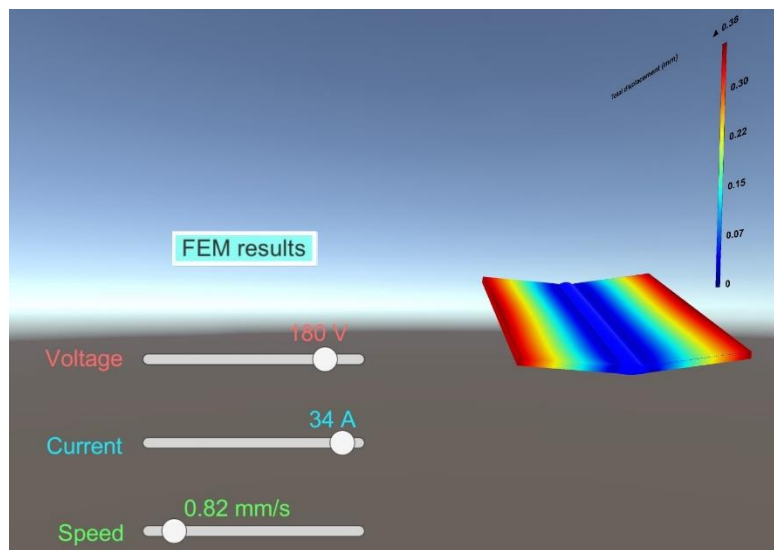
(a)

(b)

Fig. 4.10. Visualizing (a) deformation and (b) residual stress results in a VR environment.

Table 4.7. Lookup Table for trilinear interpolation.

	Input		Output
u	v	w	p
u_1	v_1	w_1	p_{111}
u_2	v_2	w_2	p_{222}
u_3	v_3	w_3	p_{333}
.	.	.	.
.	.	.	.
.	.	.	.
u_i	v_j	w_k	p_{ijk}

In this Lookup Table, $i = 1\ldots11$, $j = 1\ldots11$ and $k = 1\ldots11$ because the training data has been created by dividing the range of input variables into 11 levels. If the input values u, v, w lying between u_i and u_{i+1}, v_j and v_{j+1}, w_k and w_{k+1}, respectively, a trilinear interpolation method is employed to predict the displacement $p(u, v, w)$ as follows. A function of three input variables $p(u, v, w)$ to be determined is expressed as follows.

$$p(u,v,w) = c_0 + c_1\Delta u + c_2\Delta v + c_3\Delta w + c_4\Delta u\Delta v + c_5\Delta v\Delta w + c_6\Delta w\Delta u + c_7\Delta u\Delta v\Delta w \quad (4.17)$$

where Δu, Δv, and Δw is represented as follows.

$$\Delta u = \frac{u - u_i}{u_{i+1} - u_i}; \quad \Delta v = \frac{v - v_j}{v_{j+1} - v_j}; \quad \Delta w = \frac{w - w_k}{w_{k+1} - w_k}; \quad (4.18)$$

where u_i and u_{i+1} are the two consecutive values of the first input variable (current), v_j and v_{j+1} are the two consecutive values of the second input variable (voltage), and, w_k and w_{k+1} are the two consecutive values of the third input variable (travel speed) from the Lookup

121

Table. In this study, the user is allowed to set three welding process parameters simultaneously. Therefore, if the user sets three different values of parameters lying between any two consecutive values of three different input variables from the Lookup Table, the value of the output variable (displacement) will be obtained by applying the trilinear interpolation. In this method, the displacement value is represented as $p(u, v, w)$. The coefficients c_i are determined by using the output values corresponding to the consecutive input values as expressed by Eq. (4.19).
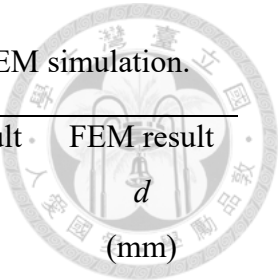
$$
\begin{aligned}
c_0 &= p_{i,j,k}; \\
c_1 &= (p_{i+1,j,k} - p_{i,j,k}); \\
c_2 &= (p_{i,j+1,k} - p_{i,j,k}); \\
c_3 &= (p_{i,j,k+1} - p_{i,j,k}); \\
c_4 &= (p_{i+1,j+1,k} - p_{i,j+1,k} - p_{i+1,j,k} + p_{i,j,k}); \\
c_5 &= (p_{i,j+1,k+1} - p_{i,j,k+1} - p_{i,j+1,k} + p_{i,j,k}); \\
c_6 &= (p_{i+1,j,k+1} - p_{i,j,k+1} - p_{i+1,j,k} + p_{i,j,k}); \\
c_7 &= (p_{i+1,j+1,k+1} - p_{i,j+1,k+1} - p_{i+1,j,k+1} - p_{i+1,j+1,k} + p_{i+1,j,k} + p_{i,j,k+1} + p_{i,j+1,k} - p_{i,j,k});
\end{aligned}
\tag{4.19}
$$

Thus, the interpolated value of the displacement $p(u, v, w)$ can be obtained from Eq. 4.17. Using this method, the displacement values are displayed to the user in the MR environment. For 10 samples of input variables, the output results using interpolation, GBRT and FEM simulation have been illustrated in Table 4.8 and compared using percent error in Table 4.9. The percent error is calculated using Eq. (4.20). The percent error between interpolation and GBRT, GBRT and FEM, and interpolation and FEM is represented by δ_1, δ_2 and δ_3, respectively.

$$
\% \text{ error } \delta = \frac{|d_{osb} - d_e|}{d_e} \times 100
\tag{4.20}
$$

where d_{obs} is the actual value observed and d_e is the expected value.

122

Table 4.8. Displacement results using the interpolation, GBRT and FEM simulation.

Current u (A)	Voltage v (V)	Travel speed w (mm/s)	Interpolation result p (mm)	GBRT result $\hat{d}$ (mm)	FEM result d (mm)
100	24.5	7.1	0.0179	0.0176	0.0172
117.5	33.2	9.1	0.0188	0.0189	0.0204
133.2	24.6	3.8	0.0255	0.0256	0.0285
162.3	21.8	7.5	0.0211	0.0202	0.0225
188	25.3	5.0	0.0256	0.0267	0.0248
87	33.4	6.8	0.0189	0.0190	0.0191
192	30.4	2.4	0.0674	0.0596	0.0643
153.4	30.2	3.5	0.0321	0.0310	0.0357
136.8	27.8	9.1	0.0198	0.0199	0.0196
80	21	0.9	0.0775	0.0703	0.074

Table 4.9. Comparison between interpolation and GBRT, FEM and GBRT, and FEM and interpolation results.

Interpolation and GBRT (δ_1)	GBRT and FEM (δ_2)	Interpolation and FEM (δ_3)
1.8	2.5	4.4
0.9	6.8	6.8
0.5	10.0	10.5
4.2	10.1	6.2
4.1	7.7	3.3
0.5	0.1	0.2
12.9	7.1	4.8
3.6	13.1	10.0
0.4	1.8	1.8
10.1	4.8	10.2
Average = 3.9	Average = 6.4	Average = 5.8

4.6 FEM results in MR

The designed MR-based UI for the FEM results exploration includes a virtual panel with a customized menu to control the welding process parameters, virtual welding animation on a real weld plate, and FEM results overlaid on the real weld plate after the welding animation.

4.6.1 Tracking

In order to display the welding animation and FEM results on the real weld plate, the AR tracking is accomplished using the Vuforia software development kit (SDK). This study focuses on using model targets to implement the tracking instead of choosing image targets.

124

Model target-based tracking detects and tracks a physical object in the real environment based on the shape of that particular object. Since the shape of the real weld plate is too simple to be distinguished from other objects in the environment, a complex geometry was used as a model target as per the suggestion provided by the Vuforia developer library (PTC, 2021). The physical object of the model target was created using a 3D printer. The model target is generated using the Model Target Generator (MTG) in Vuforia, which takes the 3D model of the object to be tracked as the input and saves the model target in the Vuforia database. Fig. 4.11(a) shows a real weld plate placed on a model target to be detected and tracked. Fig. 4.11(b) shows a virtual content overlaid on it.

125
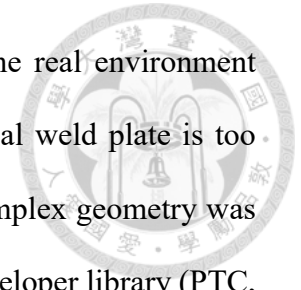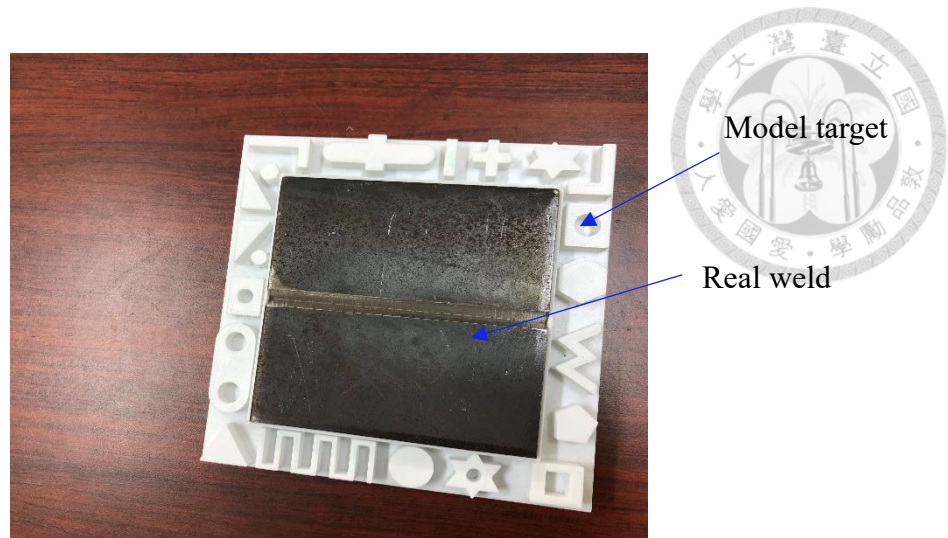
(a) Real weld plate placed on a model target.
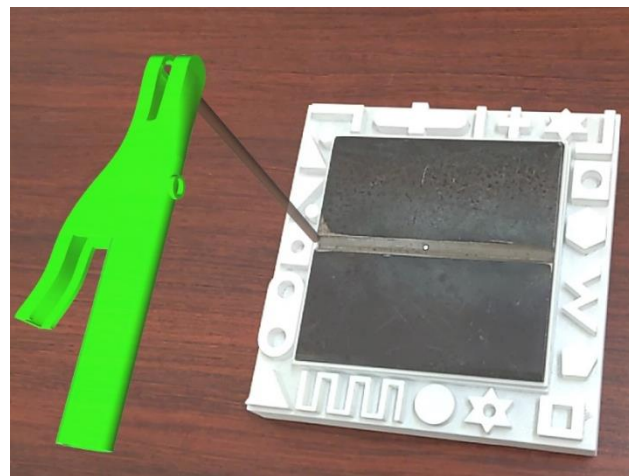
(b) Virtual electrode holder and electrode.

Fig. 4.11. Model target for tracking the real weld plate.

4.6.2 User interface

One experiment has been conducted to demonstrate the effects of the MMAW process on it including the weld bead geometry and, residual stress and displacement.

Users are instructed through the text to set the welding parameters, which can be adjusted simultaneously by dragging sliders from left to right with bare hands using natural hand gestures as shown in Fig. 4.12(a). Fig. 4.12(b) shows a third-person view of the user interacting with the sliders using a Hololens 2 HMD. The welding animation can be seen in

126

which a continuous weld bead is formed as the electrode moves with the set travel speed from left to right with virtual sparkling particles and electric arc (Fig. 4.13(a)). After the completion of the welding animation, the weld bead geometry can be observed with certain bead width and depth of penetration for a particular value of set parameters as demonstrated by Shankhwar and Smith (2022) (Fig. 4.13(b)). After the animation, the FEM results overlaid on the real weld plate are displayed with predicted values in color legend as shown in Fig. 4.14(a) and (b) for a perspective and side view, respectively. Similarly, the residual stress results are displayed, as shown in Fig. 4.15. The higher value of stress and displacement is achieved when the welding current and voltage are set to a large value and travel speed to a small value. On the other hand, the lower value of stress and displacement is obtained for a smaller value of the welding current and voltage, and a larger value of travel speed. Thus, the user can learn the relationship between welding process parameters with the induced stress and deformation results using the UI. To achieve this, first, the heat map (Fig. 4.14(a)) of the FEM results produced by the COMSOL software is incorporated into the MR system using the Unity3D platform. Second, the numerical values of the FEM results are produced by the Lookup Table according to the set welding parameters and displayed in the color legend next to the heat map of FEM results.

127
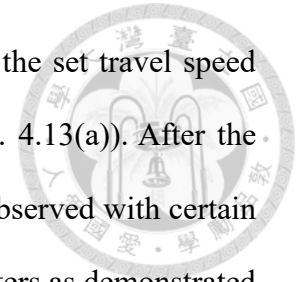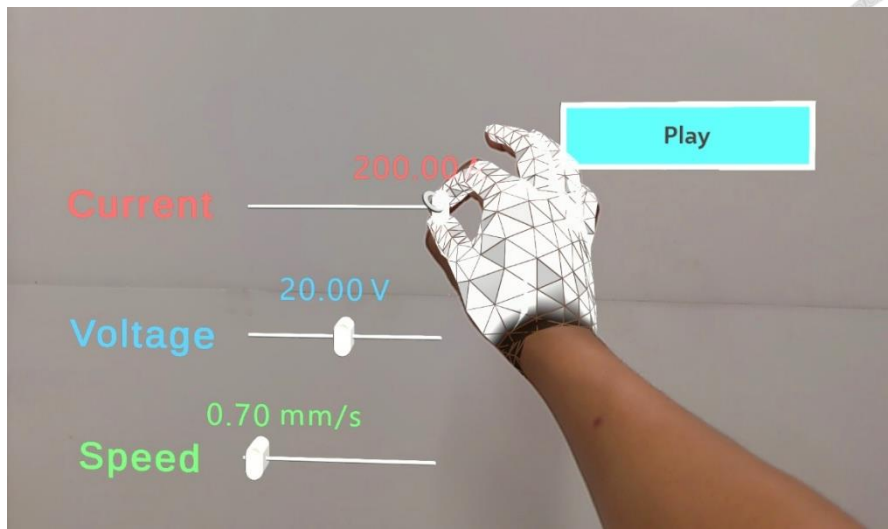
(a) First person view
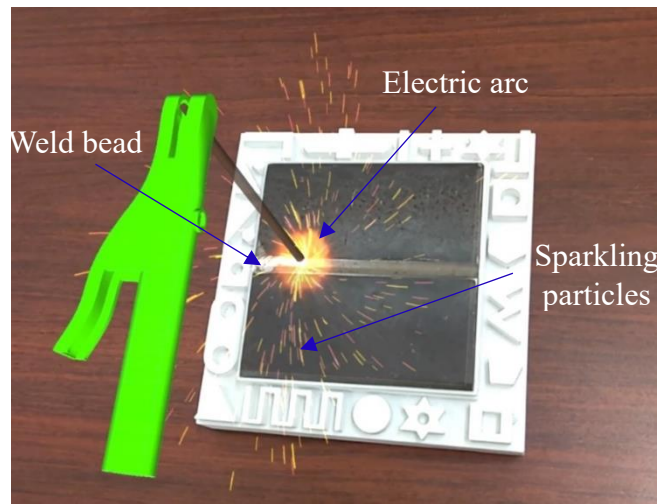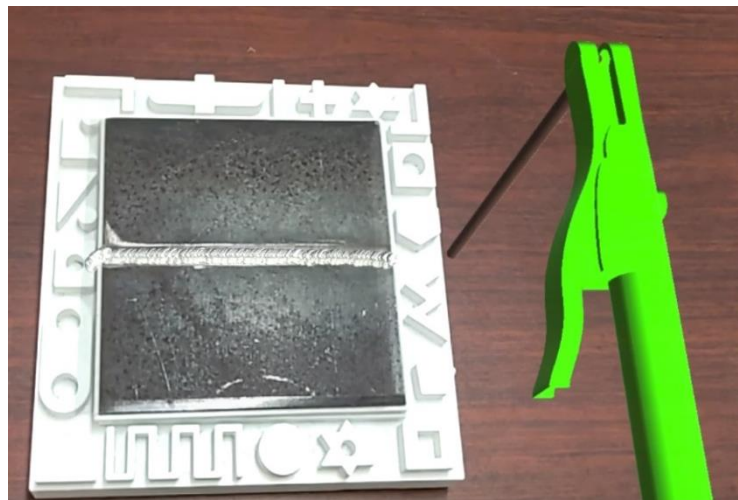

(b) Third person view

Fig. 4.12. Interacting with the slider to select the welding parameters.

(a) Welding animation in MR environment

(b) weld bead geometry after finishing the welding animation

Fig. 13 Observing the welding animation and weld bead geometry.

129
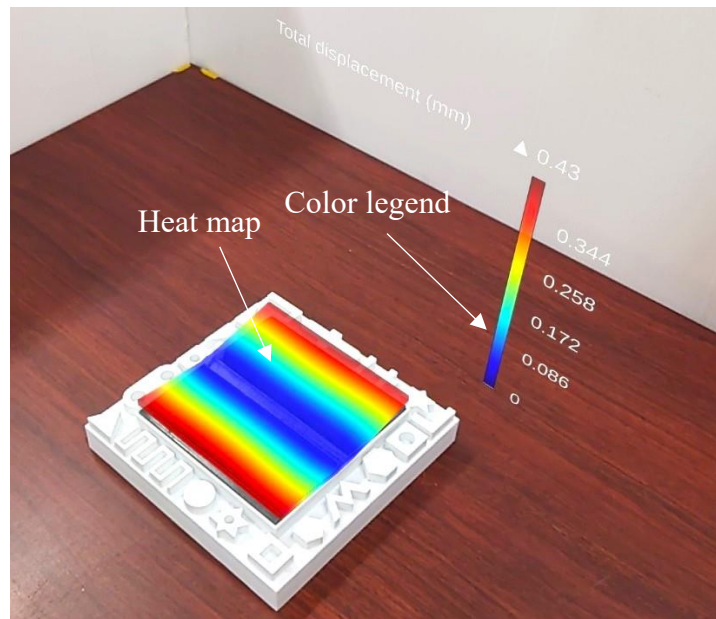
(a) Perspective view
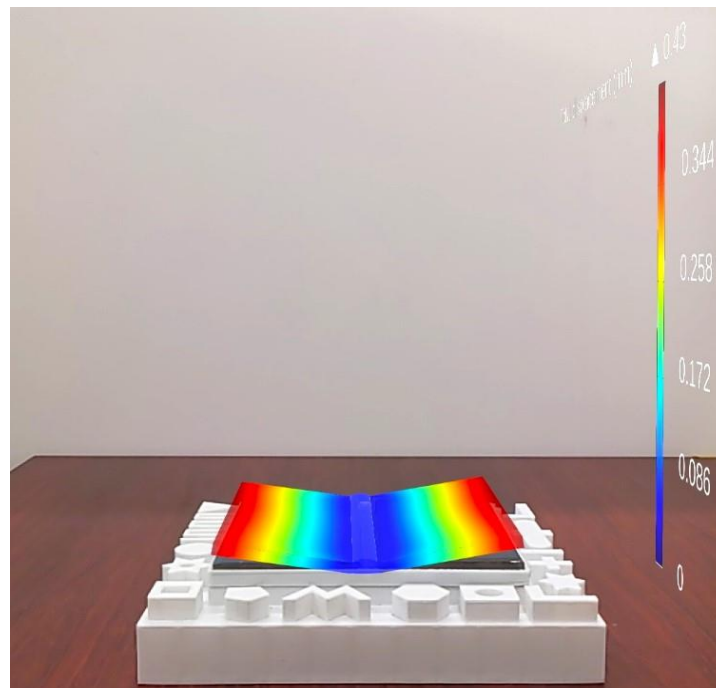
(b) Side view

Fig. 4.14. Visualizing the deformation of weld plate after welding.

130
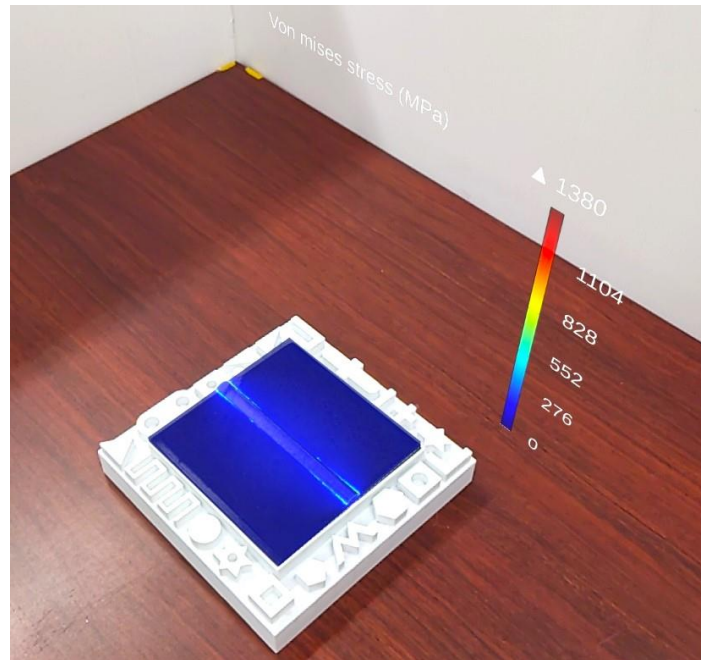
Fig. 4.15. Visualizing the residual stress induced in weld plate.

4.7 Discussion

This research investigates the feasibility of using the ML method to predict FEA results in the MR environment for the MMAW process. The MR-FEA integrated system reduces the effort of the user to perform the FEA simulation and allows users to observe the MMAW process with enhanced visualization and comprehension of the FEA results. In addition, this UI facilitates users to learn the relationship between the input parameters and the output results. Users can change the welding process parameters directly by using virtual sliders with their natural hand gestures. The MR-FEA system can immediately generate the residual stress and deformation results overlaid on the weld plate for any given welding process parameters. Moreover, the welding animation and FEA results are overlaid accurately on the physical weld plate by implementing a model target-based tracking, which recognizes and tracks a particular object based on its shape. Besides this, the application of Hololens 2 provides a remarkable experience of MR with a holistic perspective of the MR content and

131

allows users to engage thoroughly with their surroundings.

According to Fig. 4.14, the color legend indicates the maximum value of the total displacement that occurred in the weld plate in red color while the minimum value of the total displacement in blue color. It can be noticed that the weld plate deflects the most at the edges parallel to the welding line. Such deflection is known as an angular deformation which appears uniform in the direction parallel to the weld line. The reason behind the angular deformation is that particularly in butt joints, the weld tends to be wider at the top than at the bottom which causes more shrinkage due to solidification and thermal contraction. The shrinkage moment acts on the weld plate and leads to angular deformation (Park et al., 2002).

It is observed that a higher amount of stress and deformation is produced in the weld plate with a large value of the current and voltage, and a small value of the travel speed and vice versa. This happens because the heat input rate increases with high voltage and current, and with low travel speed. Which in turn produces a large amount of thermal stress due to a larger temperature gradient, resulting in larger deformation.

It can be noted that the application of the Lookup Table in MR environment for FEA results prediction reduces the significant amount of computation time from the average of 5 minutes and 38 seconds using COMSOL to about 0.01 seconds. Residual stress modeling in welding is a highly complex task due to several associated phenomena which require multiphysics analysis. Moreover, the numerical analysis using FEM simulation requires various types of information, this system allows the user to sequentially observe the MMAW process, the effect of welding process parameters on the weld bead geometry, and the effect of welding process parameters on induced residual stress and deformation on weld plate in an interactive and immersive environment without requiring a large data entry and

132

fundamental knowledge of FEM and FEM software packages.

4.8 Conclusions

Multiphysics FEM analysis for welding is extremely time-consuming due to large computations. Therefore, it is difficult to render a real-time FEA simulation in an MR environment for welding training. This study uses the ML method to integrate FEM with an MR-based environment. A GBRT model is developed by using the welding current, voltage, and travel speed as the input variables and the simulated residual stress and deformation results of the FEM analysis as the output variables. The accuracy of the prediction for displacement measured by NRMSE and R^2 were 7.62×10^{-2} and 0.95 respectively. Hoever, to display the real-time FEA results in HoloLens 2, a trilinear Lookup Table is employed which is generated by using GBRT model. Integrating FEA with the MR-based environment allows users to visualize the FEA results superimposed on the real weld plate which are readily updated based on the input parameters. The MR interface also facilitates users to learn the relationship between the welding process parameters, and the residual stress and displacement.

The current MR-FEA system only provides the FEA results of the time-dependent study for the last time step, which implies the FEA results after the cooling of weld plate. An interesting continuation of the current study is to update the FEA results during the welding animation in the MR environment, which is able to imitate the actual FEA simulation. In addition to this, further analyses such as thermal fatigue analysis and microstructure characterization of the heat-affected zone in various types of welding processes can be considered to be integrated with the MR environment for enhanced comprehension and scientific visualization.
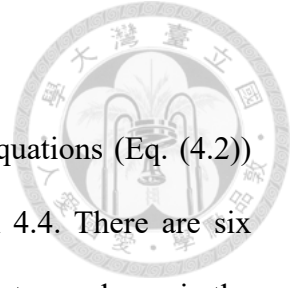
4.9 Appendix B

This section elaborates the method to solve the global system of equations (Eq. (4.2)) obtained from the assembly of element stiffness equations in Section 4.4. There are six components of stress and strain in three dimensions. The stress components are shown in the Fig. B.1 and the corresponding six strain components can be interpreted from this. The expressions for various strain components in three dimensions will be obtained as:

$$
\begin{aligned}
\varepsilon_x &= \frac{\partial u}{\partial x} \\
\varepsilon_y &= \frac{\partial v}{\partial y} \\
\varepsilon_z &= \frac{\partial w}{\partial z} \\
\gamma_{xy} &= \frac{\partial u}{\partial y} + \frac{\partial v}{\partial x} \\
\gamma_{yz} &= \frac{\partial v}{\partial z} + \frac{\partial w}{\partial y} \\
\gamma_{zx} &= \frac{\partial u}{\partial z} + \frac{\partial w}{\partial x}
\end{aligned}
\tag{B.1}
$$
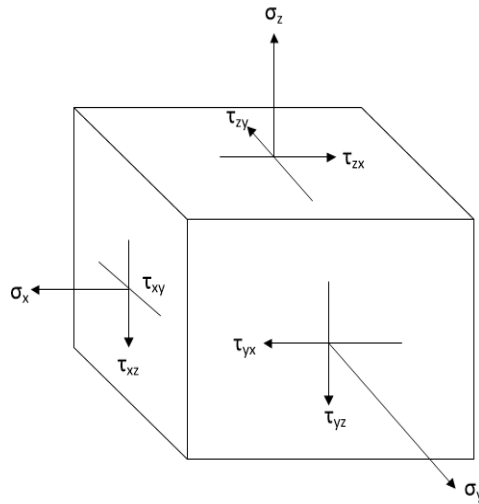
Fig. B.1. Representation of stress and strain components.

134

4.9.1 Stress-strain relationship

The six stress components are related to corresponding strains as follows.

$$\varepsilon_x = \frac{\sigma_x}{E} - v\frac{\sigma_y}{E} - v\frac{\sigma_z}{E}$$

$$\varepsilon_y = -v\frac{\sigma_x}{E} + \frac{\sigma_y}{E} - v\frac{\sigma_z}{E}$$

$$\varepsilon_z = -v\frac{\sigma_x}{E} - v\frac{\sigma_y}{E} + \frac{\sigma_z}{E}$$

$$\gamma_{xy} = \frac{\tau_{xy}}{G} = \tau_{xy}.\frac{2(1+v)}{E}$$

$$\gamma_{yz} = \tau_{yz}.\frac{2(1+v)}{E}$$

$$\gamma_{zx} = \tau_{zx}.\frac{2(1+v)}{E}$$

(B.2)

Where E, G and v are Young's modulus, Shear modulus and Poisson's ratio,

respectively. Considering the first three of these equations and writing in matrix form.

$$\begin{Bmatrix} \varepsilon_x \\ \varepsilon_y \\ \varepsilon_z \end{Bmatrix} = \frac{1}{E}\begin{bmatrix} 1 & -v & -v \\ -v & 1 & -v \\ -v & -v & 1 \end{bmatrix}\begin{Bmatrix} \sigma_x \\ \sigma_y \\ \sigma_z \end{Bmatrix}$$

(B.3)

On inverting Eq. (B.3),

$$\begin{Bmatrix} \sigma_x \\ \sigma_y \\ \sigma_z \end{Bmatrix} = \frac{E}{(1+v)(1-2v)}\begin{bmatrix} 1-v & v & v \\ v & 1-v & v \\ v & v & 1-v \end{bmatrix}\begin{Bmatrix} \varepsilon_x \\ \varepsilon_y \\ \varepsilon_z \end{Bmatrix}$$

(B.4)

By adding shear strain equations from Eq. (B.2) with Eq. (B.4), the following equation is

obtained.

135

$$\begin{Bmatrix} \sigma_x \\ \sigma_y \\ \sigma_z \\ \gamma_{xy} \\ \gamma_{yz} \\ \gamma_{zx} \end{Bmatrix} = \frac{E}{(1+\nu)(1-2\nu)} \begin{bmatrix} 1-\nu & \nu & \nu & 0 & 0 & 0 \\ \nu & 1-\nu & \nu & 0 & 0 & 0 \\ \nu & \nu & 1-\nu & 0 & 0 & 0 \\ 0 & 0 & 0 & \frac{1-2\nu}{2} & 0 & 0 \\ 0 & 0 & 0 & 0 & \frac{1-2\nu}{2} & 0 \\ 0 & 0 & 0 & 0 & 0 & \frac{1-2\nu}{2} \end{bmatrix} \begin{Bmatrix} \varepsilon_x \\ \varepsilon_y \\ \varepsilon_z \\ \gamma_{xy} \\ \gamma_{yz} \\ \gamma_{zx} \end{Bmatrix} \quad (B.5)$$

Where elasticity matric $[D]$ is represented as follows.

$$[D] = \frac{E}{(1+\nu)(1-2\nu)} \begin{bmatrix} 1-\nu & \nu & \nu & 0 & 0 & 0 \\ \nu & 1-\nu & \nu & 0 & 0 & 0 \\ \nu & \nu & 1-\nu & 0 & 0 & 0 \\ 0 & 0 & 0 & \frac{1-2\nu}{2} & 0 & 0 \\ 0 & 0 & 0 & 0 & \frac{1-2\nu}{2} & 0 \\ 0 & 0 & 0 & 0 & 0 & \frac{1-2\nu}{2} \end{bmatrix} \quad (B.6)$$

4.9.2 Shape function

The shape function provides information regarding the piecewise continuous approximating polynomial. For 4-noded tetrahedral element, the derivation of expressions for nodal displacement is given as

$$\begin{aligned} u &= \frac{1}{6V} \left[a_1 u_1 + a_2 u_2 + a_3 u_3 + a_4 u_4 + b_1 u_1 x + b_2 u_2 x + b_3 u_3 x + b_4 u_4 x + c_1 u_1 y + \ldots + e_1 u_1 z + \ldots \right] \\ &= N_1 u_1 + N_2 u_2 + N_3 u_3 + N_4 u_4 \end{aligned} \quad (B.7)$$

where N_1 represents $(a_1 + b_1 x + c_1 y + e_1 z)/6$ and N_2, N_3, N_4 are represented by similar expressions obtained by changing the suffixes.

136
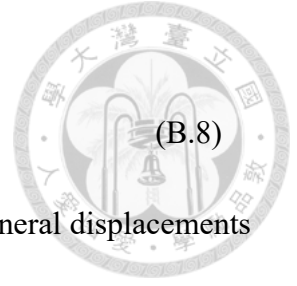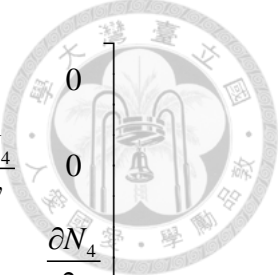
$$\{d\} = [N]\{d_e\} \tag{B.8}$$

where $\{d\}$ and $\{d_e\}$ are the displacement vectors representing the general displacements and nodal displacements, respectively within the element.

$$\{d\} = \begin{Bmatrix} u \\ v \\ w \end{Bmatrix} = \begin{bmatrix} N_1 & 0 & 0 & N_2 & 0 & 0 & N_3 & 0 & 0 & N_4 & 0 & 0 \\ 0 & N_1 & 0 & 0 & N_2 & 0 & 0 & N_3 & 0 & 0 & N_4 & 0 \\ 0 & 0 & N_1 & 0 & 0 & N_2 & 0 & 0 & N_3 & 0 & 0 & N_4 \end{bmatrix} \begin{Bmatrix} u_1 \\ v_1 \\ w_1 \\ . \\ . \\ . \\ u_4 \\ v_4 \\ w_4 \end{Bmatrix} \tag{B.9}$$

Since $B = LN$

$$\{B\} = \begin{bmatrix} \dfrac{\partial}{\partial x} & 0 & 0 \\ 0 & \dfrac{\partial}{\partial y} & 0 \\ 0 & 0 & \dfrac{\partial}{\partial z} \\ \dfrac{\partial}{\partial y} & \dfrac{\partial}{\partial x} & 0 \\ 0 & \dfrac{\partial}{\partial z} & \dfrac{\partial}{\partial y} \\ \dfrac{\partial}{\partial z} & 0 & \dfrac{\partial}{\partial x} \end{bmatrix} \begin{bmatrix} N_1 & 0 & 0 & N_2 & 0 & 0 & N_3 & 0 & 0 & N_4 & 0 & 0 \\ 0 & N_1 & 0 & 0 & N_2 & 0 & 0 & N_3 & 0 & 0 & N_4 & 0 \\ 0 & 0 & N_1 & 0 & 0 & N_2 & 0 & 0 & N_3 & 0 & 0 & N_4 \end{bmatrix}$$

137

$$
= \begin{bmatrix}
\dfrac{\partial N_1}{\partial x} & 0 & 0 & \dfrac{\partial N_2}{\partial x} & 0 & 0 & \dfrac{\partial N_3}{\partial x} & 0 & 0 & \dfrac{\partial N_4}{\partial x} & 0 & 0 \\[2ex]
0 & \dfrac{\partial N_1}{\partial y} & 0 & 0 & \dfrac{\partial N_2}{\partial y} & 0 & 0 & \dfrac{\partial N_3}{\partial y} & 0 & 0 & \dfrac{\partial N_4}{\partial y} & 0 \\[2ex]
0 & 0 & \dfrac{\partial N_1}{\partial z} & 0 & 0 & \dfrac{\partial N_2}{\partial z} & 0 & 0 & \dfrac{\partial N_3}{\partial z} & 0 & 0 & \dfrac{\partial N_4}{\partial z} \\[2ex]
\dfrac{\partial N_1}{\partial y} & \dfrac{\partial N_1}{\partial x} & 0 & \dfrac{\partial N_2}{\partial y} & \dfrac{\partial N_2}{\partial x} & 0 & \dfrac{\partial N_3}{\partial y} & \dfrac{\partial N_3}{\partial x} & 0 & \dfrac{\partial N_4}{\partial y} & \dfrac{\partial N_4}{\partial x} & 0 \\[2ex]
0 & \dfrac{\partial N_1}{\partial z} & \dfrac{\partial N_1}{\partial y} & 0 & \dfrac{\partial N_2}{\partial z} & \dfrac{\partial N_2}{\partial y} & 0 & \dfrac{\partial N_3}{\partial z} & \dfrac{\partial N_3}{\partial y} & 0 & \dfrac{\partial N_4}{\partial z} & \dfrac{\partial N_4}{\partial y} \\[2ex]
\dfrac{\partial N_1}{\partial z} & 0 & \dfrac{\partial N_1}{\partial x} & \dfrac{\partial N_2}{\partial z} & 0 & \dfrac{\partial N_2}{\partial x} & \dfrac{\partial N_3}{\partial z} & 0 & \dfrac{\partial N_3}{\partial x} & \dfrac{\partial N_4}{\partial z} & 0 & \dfrac{\partial N_4}{\partial x}
\end{bmatrix}
\tag{B.10}
$$

Where L is differential operator matrix, B is strain displacement gradient matrix and N is shape function matrix.

$$
k_e = \int_{V_e} B^T DB \, dV = \iiint_{-1}^{1} [B]^T [D][B] |J| \, \partial \xi \partial \psi \partial \eta
\tag{B.11}
$$

$$
|J| \partial \xi \partial \psi \partial \eta = dxdydz
$$

where matrix $|J|$ is called the Jacobian matrix of transformation and ξ, ψ and η are the natural coordinates.
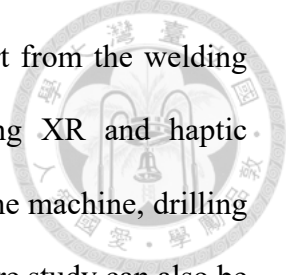
138

Chapter 5　　　　Conclusions

This dissertation is dedicated to exploring the application of XR technologies in the welding process. The research work has been conducted in three sections. In the first section, an XR-based welding tutorial system for fundaments of welding science and technology, and hands-on practice was successfully developed. The developed system was validated by the user study, which revealed that the user from the XR group could perform significantly better than the user from the control group in terms of the written test, SUS, NASA-TLX, and subjective questionnaire evaluation results. However, the developed system has certain limitations such as the user needing to perform the hands-on welding task in a standing position which leads to a higher physical load. Additionally, the UI of the system can be improved with more intelligent and intuitive features to allow users to interactively ask questions and receive relevant answers from the XR system.

The second section was the extended version of the first research work, which solely focused on providing welding training by adding haptic feedback in the XR system with a natural user interface. The user could practice welding tasks using XR-system with a natural operational behavior as if they were performing real welding in the real world. The haptic feedback included magnetic force feedback at the tip of the electrode and thermal feedback to replicate the real welding process. The XR system for welding training was validated by a user study and the results deduced that the user from the XR group performed significantly better than the control group in terms of weld quality, fewer number of hints required, and fewer mistakes. Despite, the magnetic force and thermal feedback were not as strong as

139

experienced during real welding, the user could still practice and learn welding in a similar obstructive way to the real task.

The third section of this dissertation aimed to address the challenges of induced residual stress and structural deformation due to the welding process by developing an MR-based user interface to facilitate the design engineers with interactive FEM result visualization and comprehension. In order to reduce the computation time of the complex FEM analysis, the GBRT ML algorithm was used to predict the FEM analysis results in the MR environment. The current study only considered three welding parameters to observe their effect on residual stress and deformation, which can be further extended by considering additional parameters such as Goldak model parameters, the diameter of the electrode, the thickness of the weld plate, etc.

The aforementioned study implies the successful implementation of an XR-based welding training system employing XR technologies with few limitations such as, less magnitude of the simulated magnetic force and thermal feedback compared to the actual magnetic force and heat, the requirement of a more stable distance sensor, improved tracking and more realistic graphical representation. According to the satisfactory result outcomes in terms of improved performance and skills using the XR system, it is obvious that the XR-based tutorial and training system can be competent for exploring the various field of education and manufacturing operation training. On the one hand, XR technologies can be employed for building virtual tutorial systems for various labs and workshop tasks of the mechanical engineering program, which can reduce the resources and energy required in performing real experiments. It also has the potential to replace the presence of an instructor for explaining the experiment with artificial intelligence-assisted XR systems for a more

140
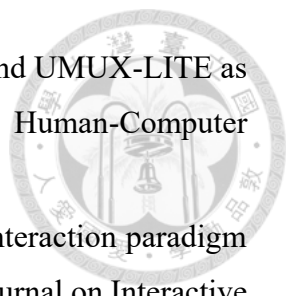
interactive and self-explanatory user interface. On the other hand, apart from the welding training, customized training systems can be developed by applying XR and haptic technologies for various manufacturing operations such as operating lathe machine, drilling machine, shaper machine, gear hobbing machine, laser cutting, etc. Future study can also be extended to develop an MR-FEM integrated ML-based system for enhanced visualization and interpretation of FEM results for various practical applications with linear, non-linear, stationary, and time-dependent multiphysics phenomena.
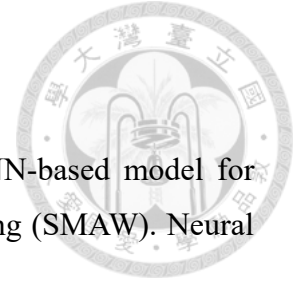
References

Ahmed A. N., Noor C., Allawi M. F., El-Shafie A. (2018). RBF-NN-based model for prediction of weld bead geometry in Shielded Metal Arc Welding (SMAW). Neural Computing and Applications. 29:889-899.

Aiteanu D., Hillers B., Graser A. (2003). A step forward in manual welding: demonstration of augmented reality helmet. In: The Second IEEE and ACM International Symposium on Mixed and Augmented Reality, Tokyo, Japan, pp.309-310.

Akçayır M., Akçayır G., Pektaş H. M., Ocak M. A. (2016). Augmented reality in science laboratories: The effects of augmented reality on university students' laboratory skills and attitudes toward science laboratories. Computers in Human Behavior. 57:334-342.

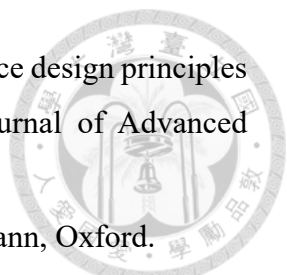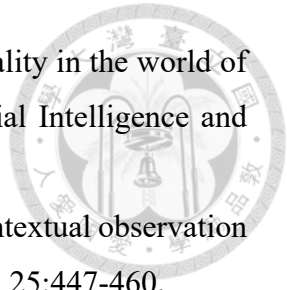Andrews C., Southworth M. K., Silva J. N., Silva J. R. (2019). Extended reality in medical practice. Current Treatment Options in Cardiovascular Medicine. 21:1-12.

Ansaripour N., Heidari A., Eftekhari S. A. (2020). Multi-objective optimization of residual stresses and distortion in submerged arc welding process using Genetic Algorithm and Harmony Search. Proceedings of the Institution of Mechanical Engineers, Part C: Journal of Mechanical Engineering Science. 234:862-871.

Arvanitis T. N., Petrou A., Knight J. F., Savas S., Sotiriou S., Gargalakos M., Gialouri E. (2009). Human factors and qualitative pedagogical evaluation of a mobile augmented reality system for science education used by learners with physical disabilities. Personal and Ubiquitous Computing. 13:243-250.

Barsoum Z., Barsoum I. (2009). Residual stress effects on fatigue life of welded structures using LEFM. Engineering Failure Analysis. 16:449-467.

Berg L. P., Vance J. M. (2017). Industry use of virtual reality in product design and manufacturing: a survey. Virtual Reality. 21:1-17.

Boob A. N., Gattani G. (2013). Study on effect of manual metal Arc welding process parameters on width of heat affected zone (HAZ) for Ms 1005 steel. International Journal of Modern Engineering Research (IJMER). 3:1493-1500.

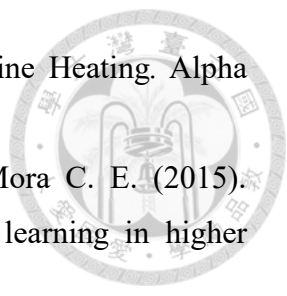Borsci S., Federici S., Bacci S., Gnaldi M., Bartolucci F. (2015). Assessing user satisfaction

in the era of user experience: Comparison of the SUS, UMUX, and UMUX-LITE as a function of product experience. International Journal of Human-Computer Interaction. 31:484-495.

Bottecchia S., Cieutat J. M., Merlo C., Jessel J. P. (2009). A new AR interaction paradigm for collaborative teleassistance system: the POA. International Journal on Interactive Design and Manufacturing (IJIDeM). 3:35-40.

Brooke J. (1996). Usability Evaluation in Industry. CRC Press, London.

Byrd A., Anderson R., Stone R. (2015). The use of virtual welding simulators to evaluate experienced welders. Welding Journal. 94:389.

Calvert J., Abadia R. (2020). Impact of immersing university and high school students in educational linear narratives using virtual reality technology. Computers & Education. 159:104005.

Cardoso O. I. H., Kus A., Unver E., Aslan R., Dawood M., Kofoglu M., Ivanov V. (2019). A design-based approach to enhancing technical drawing skills in design and engineering education using VR and AR tools. In: 14th International Joint Conference on Computer Vision, Imaging and Computer Graphics Theory and Applications, pp.306-313. Science and Technology Publications, Lda.

Chen Y., Yang Z. (2004). Haptic rendering based on spatial run-length encoding. Robotics and Computer-Integrated Manufacturing. 20:237-246.

Chigarev V. V., Shchetinina V. I., Shthetinin S. V. (2016). Magnetic field in electric arc welding. Welding International. 30:319-324.

Clark J. (1985). Manual metal arc weld modelling: Part 1 Effect of process parameters on dimensions of weld bead and heat-affected zone. Materials Science and Technology. 1:1069-1080.

Cohen J. (1988). Statistical Power Analysis for the Behavioral Sciences. Routledge, London.

Cohen J. (2013). Statistical Power Analysis for the Behavioral Sciences. Academic Press, New York.

Cosco F., Garre C., Bruno F., Muzzupappa M., Otaduy M. A. (2012). Visuo-haptic mixed reality with unobstructed tool-hand integration. IEEE Transactions on Visualization and Computer Graphics. 19:159-172.
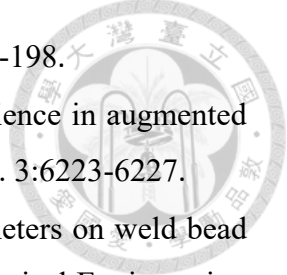
Crison F., Lécuyer A., d'Huart D. M., Burkhardt J.-M., Michel G., Dautin J.-L. (2005). Virtual technical trainer: Learning how to use milling machines with multi-sensory feedback in virtual reality. In: IEEE Proceedings. VR 2005. Virtual Reality, Bonn, Germany, pp.139-145.

Davies R. (2015). Industry 4.0 Digitalisation for productivity and growth. Available at: https://www.europarl.europa.eu/thinktank/en/document.html?reference=EPRS_BRI%282015%29568337 (accessed 19 May 2021).

Deng D., Kiyoshima S. (2012). Numerical simulation of welding temperature field, residual stress and deformation induced by electro slag welding. Computational Materials Science. 62:23-34.

Deng D., Murakawa H. (2008). Prediction of welding distortion and residual stress in a thin plate butt-welded joint. Computational Materials Science. 43:353-365.

Derisma D. (2020). The usability analysis online learning site for supporting computer programming course using system usability scale (SUS) in a university. International Journal of Interactive Mobile Technologies. 14:182-195.

Di Natale A. F., Repetto C., Riva G., Villani D. (2020). Immersive virtual reality in K-12 and higher education: A 10-year systematic review of empirical research. British Journal of Educational Technology. 51:2006-2033.

Doolani S., Wessels C., Kanal V., Sevastopoulos C., Jaiswal A., Nambiappan H., Makedon F. (2020). A review of extended reality (XR) technologies for manufacturing training. Technologies. 8:77.

Doshi A., Smith R. T., Thomas B. H., Bouras C. (2017). Use of projector based augmented reality to improve manual spot-welding precision and accuracy for automotive manufacturing. The International Journal of Advanced Manufacturing Technology. 89:1279-1293.

Eck U., Pankratz F., Sandor C., Klinker G., Laga H. (2015). Precise haptic device co-location for visuo-haptic augmented reality. IEEE Transactions on Visualization and Computer Graphics. 21:1427-1441.

Egger J., Masood T. (2020). Augmented reality in support of intelligent manufacturing – A systematic literature review. Computers & Industrial Engineering. 140:106195.

Ejaz A., Ali S. A., Ejaz M. Y., Siddiqui F. A. (2019). Graphic user interface design principles for designing augmented reality applications. International Journal of Advanced Computer Science and Applications (IJACSA). 10:209-216.

Eyres D. J., Bruce G. J. (2012). Ship Construction. Butterworth-Heinemann, Oxford.

Feier A. I., Banciu F. V. (2021). Ergonomic aspects of real and virtual welding tools. ACTA Technica Napocensis, Series: Applied Mathematics, Mechanics, and Engineering 64:117-126.

Fletcher C., Ritchie J., Lim T., Sung R. (2013). The development of an integrated haptic VR machining environment for the automatic generation of process plans. Computers in Industry. 64:1045-1060.

Friedman J. H. (2001). Greedy function approximation: a gradient boosting machine. Annals of Statistics.1189-1232.

Fukuda T., Yokoi K., Yabuki N., Motamedi A. (2019). An indoor thermal environment design system for renovation using augmented reality. Journal of Computational Design and Engineering. 6:179-188.

Goldak J., Chakravarti A., Bibby M. (1984). A new finite element model for welding heat sources. Metallurgical Transactions B. 15:299-305.

Gonzalez-Franco M., Pizarro R., Cermeron J., Li K., Thorn J., Hutabarat W., Tiwari A., Bermell-Garcia P. (2017). Immersive mixed reality for manufacturing training. Frontiers in Robotics and AI. 4:3.

Gupta P., Singh A. (2021) Phishing Website Detection Using Machine Learning. ICT Analysis and Applications. Springer, pp.183-192.

Hambli R., Chamekh A., Salah H. B. H. (2006). Real-time deformation of structure using finite element and neural networks in virtual reality applications. Finite Elements in Analysis and Design. 42:985-991.

Hart S. G. (2006). Nasa-task load index (NASA-TLX); 20 years later. Proceedings of the Human Factors and Ergonomics Society Annual Meeting. 50:904-908.

He X., Chen Y. (2006). A haptic virtual turning operation system. In: International Conference on Mechatronics and Automation, Luoyang, China, pp.435-440. IEEE.

Heirman J., Selleri S., De Vleeschauwer T., Hamesse C., Bellemans M., Schoofs E.,

145

Haelterman R. (2020). Exploring the possibilities of extended reality in the world of firefighting. In: 2020 IEEE International Conference on Artificial Intelligence and Virtual Reality (AIVR), pp.266-273.

Howie S., Gilardi M. (2021). Virtual Observations: a software tool for contextual observation and assessment of user's actions in virtual reality. Virtual Reality. 25:447-460.

Huang J., Ong S. K., Nee A. Y. (2015). Real-time finite element structural analysis in augmented reality. Advances in Engineering Software. 87:43-56.

Huang T. K., Yang C. H., Hsieh Y. H., Wang J. C., Hung C. C. (2018). Augmented reality (AR) and virtual reality (VR) applied in dentistry. The Kaohsiung Journal of Medical Sciences 34:243-248.

Jeffus L. (2020). Welding: Principles and Applications. Cengage Learning

Jeyakumar M., Christopher T. (2013). Influence of residual stresses on failure pressure of cylindrical pressure vessels. Chinese Journal of Aeronautics. 26:1415-1421.

Kaplan A. D., Cruit J., Endsley M., Beers S. M., Sawyer B. D., Hancock P. (2020). The Effects of Virtual Reality, Augmented Reality, and Mixed Reality as Training Enhancement Methods: A Meta-Analysis. Human Factors. 63:706-726.

Karadeniz E., Ozsarac U., Yildiz C. (2007). The effect of process parameters on penetration in gas metal arc welding processes. Materials & Design. 28:649-656.

Kostić S., Vasović D. (2015). Prediction model for compressive strength of basic concrete mixture using artificial neural networks. Neural Computing and Applications. 26:1005-1024.

Kumar A., DebRoy T. (2003). Calculation of three-dimensional electromagnetic force field during arc welding. Journal of Applied Physics. 94:1267-1277.

Kumar V., Albert S., Chandrasekhar N., Jayapandian J. (2018). Evaluation of welding skill using probability density distributions and neural network analysis. Measurement. 116:114-121.

Lavrentieva O., Arkhypov I., Kuchma O., Uchitel A. (2020). Use of simulators together with virtual and augmented reality in the system of welders' vocational training: past, present, and future. In: Proceedings of the 2nd International Workshop on Augmented Reality in Education, Kryvyi Rih, Ukraine, pp.201-216. Arnold E. Kiv, Mariya P.
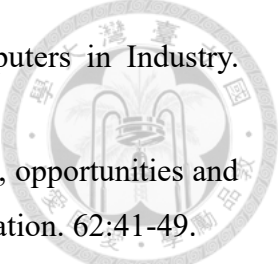
146

Shyshkina.

Lee E. J., El Tawil S. (2008). FEMvrml: An interactive virtual environment for visualization of finite element simulation results. Advances in Engineering Software. 39:737-742.

Lenin N., Sivakumar M., Vigneshkumar D. (2010). Process parameter optimization in arc welding of dissimilar metals. Science & Technology Asia.1-7.

Lewis J. R., Sauro J. (2009). The factor structure of the system usability scale. In: International conference on human centered design, pp.94-103. Springer.

Liang W., Luo S., Zhao G., Wu H. (2020). Predicting hard rock pillar stability using GBDT, XGBoost, and LightGBM algorithms. Mathematics. 8:765.

Liu Y., Zhang Y. (2015). Super welder in augmented reality welder training system: A predictive control approach. In: 2015 IEEE 24th International Symposium on Industrial Electronics (ISIE), Buzios, Brazil, pp.131-136.

Loureiro S. M. C., Bilro R. G., De Aires Angelino F. J. (2021). Virtual reality and gamification in marketing higher education: a review and research agenda. Spanish Journal of Marketing-ESIC. 25:179-215.

Maas M. J., Hughes J. M. (2020). Virtual, augmented and mixed reality in K–12 education: a review of the literature. Technology, Pedagogy and Education 29:231-249.

Macariu C., Iftene A., Gîfu D. (2020). Learn chemistry with augmented reality. Procedia Computer Science. 176:2133-2142.

MacCargar B. (2006). Watts, heat and light: Measuring the heat output of different lamps. https://www.reptileuvinfo.com/html/watts-heat-lights-lamp-heat-output.html. (accessed 05 November 2021).

Maddox S. J. (2000). Fatigue design rules for welded structures. Progress in Structural Engineering and Materials. 2:102-109.

Mahapatra M., Datta G., Pradhan B. (2006). Three-dimensional finite element analysis to predict the effects of shielded metal arc welding process parameters on temperature distributions and weldment zones in butt and one-sided fillet welds. Proceedings of the Institution of Mechanical Engineers, Part B: Journal of Engineering Manufacture. 220:837-845.

Mandal N. R. (2001). Aluminum Welding. Woodhead Publishing, Sawston.

Mandal N. R. (2009). Welding Techniques, Distortion Control and Line Heating. Alpha Science International Limited, Oxford.

Martín-Gutiérrez J., Fabiani P., Benesova W., Meneses M. D., Mora C. E. (2015). Augmented reality to promote collaborative and autonomous learning in higher education. Computers in Human Behavior. 51:752-761.

Masood T., Egger J. (2019). Augmented reality in support of Industry 4.0—Implementation challenges and success factors. Robotics and Computer-Integrated Manufacturing. 58:181-195.

Matsas E., Vosniakos G. C., Batras D. (2018). Prototyping proactive and adaptive techniques for human-robot collaboration in manufacturing using virtual reality. Robotics and Computer-Integrated Manufacturing 50:168-180.

Mavrikios D., Karabatsou V., Fragos D., Chryssolouris G. (2006). A prototype virtual reality-based demonstrator for immersive and interactive simulation of welding processes. International Journal of Computer Integrated Manufacturing. 19:294-300.

Milovanovic J., Moreau G., Siret D., Miguet F. (2017). Virtual and augmented reality in architectural design and education. In: 17th International Conference, CAAD Futures 2017.

Mourtzis D. (2018). Development of skills and competences in manufacturing towards Education 4.0: A teaching factory approach. In: Proceedings of 3rd International Conference on the Industry 4.0 model for Advanced Manufacturing, AMP 2018. Lecture Notes in Mechanical Engineering. Springer, Cham. (ed Ni J. MV, Djurdjanovic D.), pp.194-210. Springerr, Cham.

Nagesh D., Datta G. (2002). Prediction of weld bead geometry and penetration in shielded metal-arc welding using artificial neural networks. Journal of Materials Processing Technology. 123:303-312.

Nezamdost M., Esfahani M., Hashemi S., Mirbozorgi S. (2016). Investigation of temperature and residual stresses field of submerged arc welding by finite element method and experiments. The International Journal of Advanced Manufacturing Technology. 87:615-624.

Ni D., Yew A., Ong S., Nee A. (2017). Haptic and visual augmented reality interface for

programming welding robots. Advances in Manufacturing. 5:191-198.

Okimoto M. L. L., Okimoto P. C., Goldbach C. E. (2015). User experience in augmented reality applied to the welding education. Procedia Manufacturing. 3:6223-6227.

Omajene J. E., Martikainen J., Kah P. (2014). Effect of welding parameters on weld bead shape for welds done underwater. International Journal of Mechanical Engineeering and Applications. 2:128-134.

Ong S., Huang J. (2017). Structure design and analysis with integrated AR-FEA. CIRP Annals. 66:149-152.

Ong S., Yew A., Thanigaivel N., Nee A. (2020). Augmented reality-assisted robot programming system for industrial applications. Robotics and Computer-Integrated Manufacturing. 61:101820.

Pamnani R., Vasudevan M., Jayakumar T., Vasantharaja P., Ganesh K. (2016). Numerical simulation and experimental validation of arc welding of DMR-249A steel. Defence Technology. 12:305-315.

Park J. U., Lee H. W., Bang H. S. (2002). Effects of mechanical constraints on angular distortion of welding joints. Science and Technology of Welding and Joining. 7:232-239.

Persson C., Bacher P., Shiga T., Madsen H. (2017). Multi-site solar power forecasting using gradient boosted regression trees. Solar Energy. 150:423-436.

Pomerantz J. (2019). Teaching and learning with extended reality technology. Information and Technology Transforming Lives: Connection, Interaction, Inovation.137-157.

PTC. (2021). Model Targets Supported Objects & CAD Model Best Practices. Available at: https://library.vuforia.com/model-targets/model-targets-supported-objects-cad-model-best-practices (accessed 21 July 2022).

Raschka S. (2015). Python Machine Learning. Packt publishing ltd,

Raschka S., Patterson J., Nolet C. (2020). Machine learning in python: Main developments and technology trends in data science, machine learning, and artificial intelligence. Information. 11:193.

Regazzoni D., Rizzi C., Vitali A. (2018). Virtual reality applications: guidelines to design natural user interface. In: International Design Engineering Technical Conferences

and Computers and Information in Engineering Conference. American Society of Mechanical Engineers.

Roldán J. J., Crespo E., Martín-Barrio A., Peña-Tapia E., Barrientos A. (2019). A training system for industry 4.0 operators in complex assemblies based on virtual reality and process mining. Robotics and Computer-Integrated Manufacturing. 59:305-316.

Ryken M. J., Vance J. M. (2000). Applying virtual reality techniques to the interactive stress analysis of a tractor lift arm. Finite Elements in Analysis and Design. 35:141-155.

Saha A., Mondal S. C. (2017). Multi-objective optimization of manual metal arc welding process parameters for nano-structured hardfacing material using hybrid approach. Measurement. 102:80-89.

Sarkar S. S., Das A., Paul S., Mali K., Ghosh A., Sarkar R., Kumar A. (2021). Machine learning method to predict and analyse transient temperature in submerged arc welding. Measurement. 170:108713.

Schober P., Boer C., Schwarte L. A. (2018). Correlation coefficients: appropriate use and interpretation. Anesthesia & Analgesia. 126:1763-1768.

Shankhwar K., Chuang T. J., Tsai Y. Y., Smith S. (2022). A visuo-haptic extended reality–based training system for hands-on manual metal arc welding training. The International Journal of Advanced Manufacturing Technology.1-17.

Shankhwar K., Smith S. (2022). An interactive extended reality-based tutorial system for fundamental manual metal arc welding training. Virtual Reality. 26:1173-1192.

Smith M., Smith A. (2009). NeT bead-on-plate round robin: Comparison of residual stress predictions and measurements. International Journal of Pressure Vessels and Piping. 86:79-95.

Sung R., Ritchie J. M., Lim T., Dewar R., Weston N. (2011). Knowledge capture inside a haptic soldering environment. In: Proceedings of the 6th International Conference on Virtual Learning, CLUJ-NAPOCA, Romania, pp.38-44.

Taggart R., Architects S. o. N., Engineers M. (1980). Ship Design and Construction. Society of Naval Architects and Marine Engineers, New Jersey.

Tang Y. M., Chau K. Y., Kwok A. P. K., Zhu T., Ma X. (2021a). A systematic review of immersive technology applications for medical practice and education-Trends,

application areas, recipients, teaching contents, evaluation methods, and performance. Educational Research Review 100429.

Tang Y. M., Ng G. W. Y., Chia N. H., So E. H. K., Wu C. H., Ip W. H. (2021b). Application of virtual reality (VR) technology for medical practitioners in type and screen (T&S) training. Journal of Computer Assisted Learning. 37:359-369.

Tewari S., Gupta A., Prakash J. (2010). Effect of welding parameters on the weldability of material. International Journal of Engineering Science and Technology. 2:512-516.

Thomas P., David W. (1992). Augmented reality: An application of heads-up display technology to manual manufacturing processes. In: Hawaii International Conference on System Sciences, pp.659-669.

Torano J., Diego I., Menéndez M., Gent M. (2008). A finite element method (FEM)–Fuzzy logic (Soft Computing)–virtual reality model approach in a coalface longwall mining simulation. Automation in Construction. 17:413-424.

Tschirner P., Hillers B., Graser A. (2002). A concept for the application of augmented reality in manual gas metal arc welding. In: International Symposium on Mixed and Augmented Reality, Darmstadt, Germany, pp.257-258. IEEE.

Turkan Y., Radkowski R., Karabulut-Ilgu A., Behzadan A. H., Chen A. (2017). Mobile augmented reality for teaching structural analysis. Advanced Engineering Informatics. 34:90-100.

Uva A. E., Gattullo M., Manghisi V. M., Spagnulo D., Cascella G. L., Fiorentino M. J. T. I. J. o. A. M. T. (2018). Evaluating the effectiveness of spatial augmented reality in smart manufacturing: a solution for manual working stations. The International Journal of Advanced Manufacturing Technology 94:509-521.

Van Lopik K., Sinclair M., Sharpe R., Conway P., West A. (2020). Developing augmented reality capabilities for industry 4.0 small enterprises: Lessons learnt from a content authoring case study. Computers in Industry. 117:103208.

Witmer B. G., Jerome C. J., Singer M. J. (2005). The factor structure of the presence questionnaire. Presence (Camb). 14:298-312.

Witmer B. G., Singer M. J. (1998). Measuring presence in virtual environments: A presence questionnaire. Presence. 7:225-240.

Wu C. (1992). Microcomputer-based welder training simulator. Computers in Industry. 20:321-325.

Wu H. K., Lee S. W. Y., Chang H. Y., Liang J. C. (2013). Current status, opportunities and challenges of augmented reality in education. Computers & Education. 62:41-49.

Xie Y., Zhuang J., Huang B., Chen Q., Li G. (2020). Effect of different welding parameters on residual stress and deformation of 20/0Cr18Ni9 dissimilar metal arc-welding joint. Journal of Adhesion Science and Technology. 34:1628-1652.

Yang F., Wang D., Xu F., Huang Z., Tsui K. L. (2020). Lifespan prediction of lithium-ion batteries based on various extracted features and gradient boosting regression tree model. Journal of Power Sources. 476:228654.

Yavuz Erkek M., Erkek S., Jamei E., Seyedmahmoudian M., Stojcevski A., Horan B. (2021). Augmented reality visualization of modal analysis using the finite element method. Applied Sciences. 11:1310.